2019

Experimental Characterization of Hydraulic System Sound

Ben Kolb
Michigan Technological University, bskolb@mtu.edu

EXPERIMENTAL CHARACTERIZATION OF HYDRAULIC SYSTEM SOUND

By

Ben S. Kolb

A THESIS

Submitted in partial fulfillment of the requirements for the degree of

MASTER OF SCIENCE

In Mechanical Engineering

MICHIGAN TECHNOLOGICAL UNIVERSITY

2019

This thesis has been approved in partial fulfillment of the requirements for the Degree of MASTER OF SCIENCE in Mechanical Engineering.

Department of Mechanical Engineering-Engineering Mechanics

Thesis Advisor:	*Andrew Barnard*
Committee Member:	*Jason Blough*
Committee Member:	*James DeClerck*
Department Chair:	*William W. Predebon*

Disclaimer

The views and opinions expressed in this article are those of the author and do not necessarily reflect the policies, views or positions of Caterpillar Inc. or its affiliates. Assumptions and conclusions made within the analysis may not be reflective of the position of Caterpillar Inc. or any of its affiliates.

Table of Contents

List of figures

List of tables

Acknowledgments

I would like to thank my advisor, Dr. Andrew Barnard, for his confidence in my ability to deliver results and for his continuous guidance through this project and my graduate school experience as a whole. The research would not have been possible without the expertise provided by Pravin Sondkar, Rich Romick, and Joe Bobchick. Additional sincere thanks go to Mike Johnson and the entire Caterpillar Global Sound Solutions team for their welcome, training, and sharing of countless valuable experiences during my time with the group. Lastly, I would like to thank my family and Taylor Franklin for their love, support, and patience while I worked to complete this project.

List of abbreviations

FBN	Fluidborne Noise
SBN	Structureborne Noise
ABN	Airborne Noise
FSI	Fluid-Structure Interaction
DOF	Degree-of-Freedom
FRF	Frequency Response Function
FFT	Fast Fourier Transform
ODS	Operational Deflection Shape
EMA	Experimental Modal Analysis
OMA	Operational Modal Analysis
OBMA	Order Based Operational Modal Analysis
LCFD	Least-Squares Complex Frequency Domain
MAC	Modal Assurance Criterion
CSAC	Cross Signature Assurance Criterion
FRFSF	Frequency Response Function Scale Factor
SEREP	System Equivalent Reduction Expansion Process
CPSS	Constant Pressure Speed Sweep
SS	Steady-State
LV	Load Valve
DOE	Design of Experiments

Abstract

The purpose of this research was to establish test methods for characterizing the interaction between the hydraulic fluid and hydraulic hose at clipping points in mobile heavy equipment hydraulic systems. A simple hydraulic circuit test bench was developed and the laboratory axial piston pump was characterized using ISO 10767-1. A direct relationship between the fluidborne noise and structureborne noise present at each hose clip location was observed for a specific operating condition using operating deflection shapes and structureborne noise measurements. This result shows that optimal hose clip placement can be a viable solution to structureborne noise reduction. Additionally, a modal superposition method for predicting pressure ripple at any point in the pump outlet hose was established using order-based modal analysis. The fluidborne noise in the circuit was balanced in a power flow approach and compared to fluidborne noise predictions at the mounts.

1 Introduction

Hydraulic systems are used in mobile heavy equipment for their high power density. This means that a well-designed hydraulic circuit can produce more power for its size than any other available actuation system. The hydraulic engineer needs to direct this power from the pump to the actuator which results in a complex hydraulic network of hoses, control valves, cylinders, and various branching junctions. The need to maximize the power available from a given pump has driven designers to use smaller hydraulic lines and higher pressures. This solution comes at a cost in the form of increased vibrational energy in the hydraulic fluid which exists as periodic fluctuations in pressure and flow. Although the fluid itself may be a poor acoustic radiator, the hydraulic fluid and hose interaction can transmit the fluid energy into the frame at any hose clip attachment location. Unlike industrial hydraulics where hoses can be routed to massive foundational structures, mobile heavy equipment manufacturers must route all hydraulic lines to frame members or compliant enclosure assemblies. If the fluid energy exists at frequencies near the structural resonances, significant vibration or audible noise issues can result. These issues have the potential to affect the sale of the machine, the reliability of the machine and, in some circumstances as indicated by certain occupational noise exposure research, the health of the operator [1].

There is a need for lab-based experimental studies on real heavy equipment circuits to help understand fluid vibrational energy flow from the pump to each clipping point. This will help validate models and create design tools for hydraulic hose routing. Background information is provided on hydraulic noise mechanisms and existing experimental fluid-

structure interaction research for hydraulic piping systems. A test bench is developed at Michigan Technological University to analyze the fluidborne to structure-borne energy transmission at hose clip locations based on a reference hydraulic circuit. The noise energy in the hydraulic pump, hydraulic fluid, and hose structure is characterized using test methods to show that optimized hose clip location can be a viable solution to structureborne noise reduction. The measurements were formulated into energy assessment metrics and a method was developed to balance the fluidborne energy from the pump through the outlet hose using a power flow approach.

1.1 Motivation

Hydraulic noise is a significant issue in the development of heavy equipment machines. The hydraulic noise can contribute to the overall noise level potentially harming the hearing of the operator or exist as an annoyance that may lead to negative perceptions of the machine quality. The job of a machine operator is stressful due to high demand for productivity over long shifts on construction and mine sites. High vibration or uncomfortable noise in the machine cab will contribute to operator fatigue and, according to some research, may affect the operator's ability to make safe decisions while at work in certain circumstances [2].

The hydraulic noise originates at the pump outlet and passes through the system as FBN energy. This FBN energy interacts with the hose wall where it is transferred into the frame of the machine at any hose clip attachment location. If the fluid or hydraulic hose resonances exist near the resonances of the attachment structure, significant SBN issues

could result. There is currently no test method to characterize the FBN transmission through a hose for quantifying the FBN to SBN energy transfer. This project seeks to develop a method for obtaining the fluid and line resonances of a simple hydraulic system to understand SBN contributors. The results should confirm that placement of hose clips away from high FBN locations is a viable solution to SBN reduction.

Caterpillar provided funding to Michigan Tech to develop a test bench to measure and evaluate hose clip locations on simple hydraulic circuits. The results and developed test methods gained through this work will go towards updating design tools and guidelines for hydraulic line routing. The data sets collected on the test bench will be used for model validation and correlation efforts. The first phase of this project is focused on establishing test methods in a laboratory environment. The laboratory test bench will allow MTU to conduct future hydraulic noise research.

1.2 Background

Background information is provided on the primary noise mechanisms in the design of hydraulics for heavy equipment and the governing physics of hydraulic piping system fluid-structure interaction (FSI). Existing FSI test benches and test methods for hydraulic clipping point assessment are explored.

1.2.1 Noise Mechanisms in Heavy Equipment Hydraulic Systems

There are three noise mechanisms in hydraulic systems that can couple together to produce significant design challenges. These mechanisms are FBN, SBN, and ABN.

1.2.1.1 Fluid-borne Noise

The fluid energy responsible for fluid-borne noise can be broken up into two source categories, pump pulsations, and valve noise.

1.2.1.1.1 Pump Pulsations

Real pumps generate an unsteady pressure and flow. In an axial piston pump, the incoming volume of fluid is divided and drawn into cylinders on the suction stroke and then pressurized and expelled on the delivery stroke. An ideal pump is timed so that the piston is over pressurized by 2% before being exposed to the discharge port. This ensures that there is no backflow into the cylinder before the targeted pressure is reached [3]. The timing of the fluid discharge is based on the location of the discharge port on the port plate. Perfect timing can only be achieved for a specific operating condition and therefore backflow occurs at all other working conditions. The backflow generated produces an oscillating flow pulsation on top of the mean flow referred to as 'flow ripple'. Reflections of the flow ripple wave at any fluid obstruction produce pressure oscillations known as 'pressure ripple'. The flow and pressure ripple occur at harmonics of the product of the pump shaft frequency and the number of pistons in the pump. If the hydraulic system is linear then the pressure and flow ripple levels can be assumed directly proportional [4]. Examples of commercially available software for the analysis of FBN are PRASP and DSH plus [5, 6].

In the engineering of hydraulic pumps, port timing is the most effective pump design parameter to optimize for reduction of these ripples. The noise control components for FBN reduction once the pulsations enter into the hydraulic circuit can be reduced with

suppressors [7]. Tuning cables are a type of suppression device used in the automotive industry to reduce the amplitude of the pressure ripples [8]. This solution may not be effective in heavy equipment circuits due to the stiff hoses needed for the high-pressure requirements. One possible suppression type for these systems is gas loaded pass through filters [9]. These tube-in-tube systems are designed to suppress specific frequencies based on the tunable pressure of an enclosed gas. These suppressor systems add weight, cost, and require additional space in the design of the circuit. A review of hydraulic fluid-borne noise reduction methods has been developed by Kevin Edge through many years of significant contribution to hydraulic noise control at the University of Bath [4].

1.2.1.1.2 Valve Noise

Additional noise generation mechanisms associated with the hydraulic fluid are cavitation, valve excitation, and waterhammer. These mechanisms are related to the interaction of the fluid and a control component. Cavitation is the implosion of small entrained air bubbles often produced at the pump. These air bubble implosions can create broadband FBN, unwanted growling ABN and cause reduced pump life [10]. Waterhammer is the hydraulic equivalent to a shock in structural dynamics. This type of excitation exists as a high-amplitude pressure wave in the fluid that can occur after a sudden valve closing. Valve excitation is the unstable oscillation of a valve internal components that typically produces a high-frequency tonal sound. This is a sound quality issue that may affect the customer's perception of the machine.

1.2.1.2 Structure-borne Noise

Oscillating internal forces and moments in the axial piston pump generate imbalances that transmit energy through the pumping cylinder connections and into the pump casing [11]. The forcing function for this excitation exists at pumping frequencies or larger broadband ranges in the case of impacts. Pump designers will often try to use less material in the pump casing to reduce weight and dissipate heat. This can increase the acoustic radiation efficiency of the casing. The pump casing vibration can transfer through the mounts or the outlet hose and excite resonances in the rest of the hydraulic circuit. Additionally, the FBN energy in the hose can excite hose resonances causing high vibration levels at any attached frame structure. Hydraulic circuit network SBN responses have been modeled with finite element methods [12]. Numerous experimental test methods have been developed and compared for experimentally determining SBN sound power at mounting points [13]. These methods use a combination of measured force and velocity to produce a transmitted SBN metric.

1.2.1.3 Airborne Noise

It is helpful to consider ABN in mobile heavy equipment hydraulic circuits with respect to the source-path-receiver paradigm. The pump is the noise generation source producing FBN, the FBN energy can transfer into the structure through multiple paths depending on the circuit layout. The receivers are the operators and bystanders. ABN issues can result if excited structures can efficiently transform vibrational energy into audible noise. If the audible hydraulic noise is tonal or has an excessive whine, the perceived quality of the machine could be affected. The audible noise levels from the hydraulic circuit

will add to the overall noise level of the machine which is strictly regulated in many countries that have high population densities [14]. According to some research, if audible noise levels exceed 85 dBA in the cab of the machine or in surrounding work areas, the health and safety of the operators and bystanders could be affected [1].

Isolation of the pump and hoses from the frame members and supports is a commonly proposed solution. Isolation with rubber compounds can work well for a specific design frequency but may suffer in broad frequency range applications or in attenuating low-frequency amplitudes. Noise issues can sometimes be reduced through design modifications such as mass and rigidity changes. Overall ABN sound levels will be measured using field tests during product development. Finite element and boundary element methods have been used successfully in combination to simulate SBN and FBN energy generating ABN and predicting the radiated sound field [15, 16].

1.2.2 Fluid-Structure Interaction

The piping system fluid-structure interaction (FSI) research field is described through its origins, governing physics and mechanisms and then explored through existing experimental applications and model validation methods.

1.2.2.1 Origins, Governing Physics, and Mechanisms

Researchers have been devoted to understanding the FSI phenomena in piping systems since a foundational study in 1876 [17]. Early FSI studies specific to piping systems were aimed at understanding waterhammer shock excitation. This was followed by an increase in studies related to periodic fluid flow and pressure ripple excitation. The

study of FSI is important because the analysis of the fluid and structural responses independently may not accurately represent the behavior of the system as a whole. Incorrect representation of the governing physics could lead to poorly correlated results to validation experiments. Simply adding the fluid mass to the pipe wall does not work for all design cases [18]. In 1987, Wiggert et. al. published 14 governing differential equations to describe a 1-dimensional hydraulic piping system's FSI [19]. Of the 14 equations, 12 of the equations represent the axial, torsional and flexural vibrations in the structure and 2 equations represent flow and velocity in the fluid. The relative importance of each FSI model degree of freedom was determined experimentally by evaluating the transmitted power through a pipe for a given axial velocity, lateral velocity, bending angular velocity, torsional angular velocity and pressure input [20]. It was found that the most significant structural input to structural wave transmission through the hose wall is the hose axial force. Tijsseling and Wiggert provide a complete review of the development and applications of the flexible piping system FSI model until 2001 [21]. Li and Ferrás have extended this work to create single sources for a more current state-of-the-art [22, 23].

Fluid-structure interaction can be divided into three mechanisms: friction coupling, Poisson coupling, and junction coupling. Friction coupling comes from the shear stress at the interaction of the hose or pipe wall and the fluid. Poisson coupling comes from the radial deflection of the hose which causes a pressure wave to transmit axially through its length. The Poisson coupling mechanism occurs most efficiently when the breathing modes of the hose wall are excited. The junction coupling mechanism is often the biggest FSI

contributor and occurs at pipe bends and restrictions that produce unbalanced forces or sudden changes in the fluid momentum [24].

1.2.2.2 Existing Experimental Test Setups and Methods for Mount Assessment

A 2015 review of FSI research in pipeline systems points out that less than 20% of their presented literature contained experimental validations [21]. The designs for existing experimental test setups are explored, followed by existing methods for hydraulic clipping point assessment. A detailed list of current laboratories with experimental piping system FSI setups is provided by Ferrás [20]. The development of a hydraulic circuit FSI test bench requires three primary design considerations: fluid excitation mechanism, boundary conditions, and measurement devices.

1.2.2.2.1 Fluid Excitation Mechanism

Validations focused on analyzing waterhammer shock waves commonly use solid rods or impact hammers to excite the fluid in a pipe system. For validation of hydraulic circuits with flow and pressure pulsations, a rotary valve is commonly used. This method provides precise control of the excitation frequency. In this configuration type, the mean fluid flow is provided by a hydraulic pump. A long length of hose or a suppression device attenuates the pump source ripples before a rotary valve reintroduces a target ripple level to the system. This type of excitation is shown in Figure 1 [25]. A real hydraulic pump system can also be used for analysis as shown in the setup in Figure 2 [26]. This ensures that all pumping dynamics are conserved. This type of system requires that the pump source flow ripple and source impedance are characterized by either the secondary source method

or two pressures/two systems method [27, 28]. A detailed comparison of the strengths and shortcomings of each method has been provided by the University of Bath where the secondary source method was developed [29].

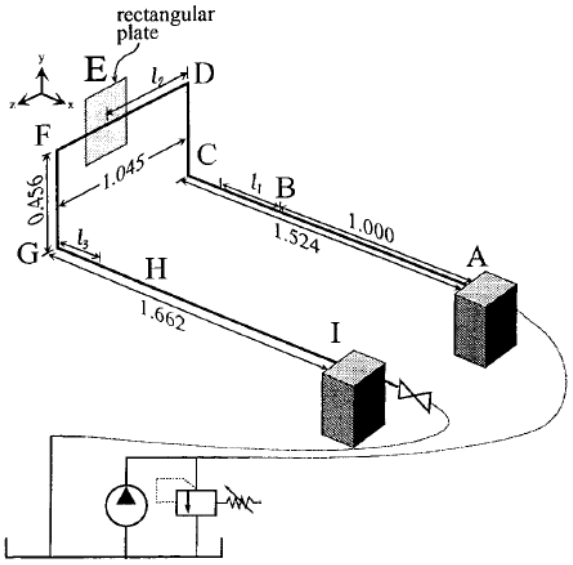

Figure 1: Pipe Clamp Vibration Reduction Test Rig

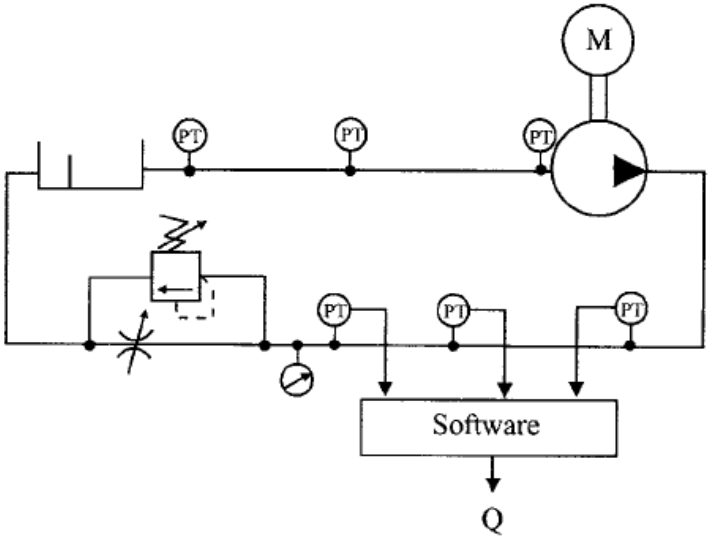

Figure 2: Pump Pressure Pulsations Test Rig

1.2.2.2.2 Boundary Conditions

Understanding the boundary condition variables in an experimental test configuration requires a consideration of the rig shape and hose mounting types. Suspension systems for hoses and pipe mounting have been used to minimize the structural energy losses from the hydraulic systems [30]. Massive anchor blocks have been used at pipe ends or intermediate locations to dissipate vibrational energy into the ground [31]. Configurations with straight pipelines or hoses are common in wave transmission tests in order to minimize junction coupling variables. Single bend and U-bend configurations have been used successfully in correlation studies since high vibration amplitudes are generated at the elbows due to junction coupling [25]. Real aircraft systems with in situ boundary conditions have been studied successfully with consideration of FSI using experimental modal analysis [32].

1.2.2.2.3 Measurement Transducers

Typical transducers used for FSI model correlation are dynamic pressure transducers, accelerometers, and microphones. Intensity probes have been used for transfer path analysis of a simple gear pump – pipe – load valve system [33]. Force transducers and accelerometers were used together to successfully expand the transfer matrix of a hose using axial hose wall force and axial hose wall motion in addition to the fluid pressure and flow measurements [34]. The combination of a microphone and a modally dense metal plate was used as shown in Figure 1 to measure the SBN to ABN efficiency at a hydraulic clipping point [25].

1.2.2.3 Existing Methods for Hydraulic Mount Assessment

A reconfiguration of the hydraulic hose clipping points to reduce the transmission of FBN energy into the structure is the lowest weight and most cost-effective noise control solution because it does not add any additional components to the circuit. It also has no effect on hydraulic performance because it does not alter the fluid pressure or flow. Isolation can be an effective noise control solution for hose clip designs but it is most suitable for higher frequencies [35]. This approach is also used when designing mounts for the machine cabs [36]. The primary interest of this project, however, is the location of the hose attachment and not the attachment type or design. It has been shown using transfer matrix methods that periodically placed supports on hydraulic piping systems can reduce overall pipe vibration in certain frequency bands [37]. This was verified using a fluid-filled fixed-fixed pipe excited by an impact hammer with pipe clip response vibration levels measured with an accelerometer. Numerical modal analysis approaches have been used to validate predicted boundary conditions of intermediate supports on long hydraulic pipelines [31, 38]. Experimental modal analysis of an aircraft hydraulic system was used to evaluate the effect of hose curvature and friction on hose natural frequencies [32]. It is claimed that most of the vibrational energy in the aircraft piping system is lost through the first mount and that hose clip locations producing long segments will reduce hose natural frequencies to within normal pump operating ranges. Genetic algorithms have been used to determine the best and worst clipping point locations [25]. Significant improvements between best and worst clip location were only observed in the first harmonic and the reduced amplitudes occurred over wide frequency bands. The optimization results correlated with moving away from the pipe bends as expected based on junction coupling.

The optimization parameter used was the FRF between the predicted force at the mount and pressure ripple at the pump outlet. The test setup for this study is shown in Figure 1. An attempt at a simulation tool for the aircraft industry to optimize clipping points and suppressor locations was completed at the Hamburg University of Technology. The 14 FSI equations were added to FBN results from commercially available software. The results were not strongly correlated to experimental validations, however, it is claimed that the solution could help minimize iterative test efforts to find the optimal clip locations [39].

1.3 Project Milestones and Scope

1.3.1 Project Milestones

The primary project milestones that will define the success of this project are as follows.

1. A test bench is developed in Michigan Tech's hydraulic laboratory that produces data that correlates to field data collected on a reference hydraulic circuit.
2. The test bench pump source flow ripple is characterized using ISO 10767-1.
3. Test methods are established to determine the fluid and line resonances.
4. Test metrics are developed to evaluate SBN at mount clipping points and measurements show that optimal hose clip placement can be a viable solution to SBN reduction.
5. A predictive power flow approach is developed that quantifies the fluidborne energy at any location in the pump outlet hose based on measurements and modal parameters.

1.3.2 Scope

The results of this project will come from a generalized mobile equipment hydraulic circuit that will replicate hydraulic noise issues for a variety of line configurations. The resonances of the fluid, hydraulic line and attaching structures are all within the scope of this project. The hydraulic components used in the design of the hydraulic circuit-under-test will include a pump, filter and loading valve with the focus being from the pump outlet to the first fluid restriction. All other hydraulic components are considered out of scope for this phase of the project. The structural parameters that will be considered controlled variables for the study of FBN to SBN transfer are the number of hose mounts, the location of hose mounts and bending in the hose. The ABN energy lost from the system is considered negligible for the energy balance techniques, however, ABN generated will be criteria used to evaluate the results generated from this project in future tests. The pump casing SBN is another known hydraulic noise contributor that is not within the scope of this project. It is assumed that the damping provided by the outlet hose will eliminate the SBN contribution to measured hose mount SBN.

2 Theory

This section provides background on methods used to collect, analyze and interpret the test bench data. The theory is categorized by hydraulic system sizing for test bench development, structural dynamics characterization, and hydraulic energy characterization.

2.1 Hydraulic System Sizing

The correct sizing of a hydraulic system is important for maximized performance, long-term durability, and operator safety. The following empirical equations for flow rate, power, and torque are shown in equations 1-3 respectively and are used for sizing the hydraulic pump and motor to circuit design parameters.

$$Q_{GPM} = \frac{\omega_{RPM} \cdot V_{in^3}}{231} \tag{1}$$

$$P_{HP} = \frac{Q_{GPM} \cdot p_{psi}}{1714 \cdot \eta} \tag{2}$$

$$T = \frac{P_{psi} \cdot V_{in^3}}{2\pi} = \frac{P_{HP} \cdot 63025}{\omega_{RPM}} \tag{3}$$

The flow rate, Q, rotational frequency, ω, volume, V, power, P, pressure, p, mechanical efficiency, η, and torque, T should be converted to the units denoted in the subscript of each variable.

2.2 Structural Dynamics Characterization

Analytical background to structural dynamics characterization is provided before describing alternative experimental techniques using measured and unmeasured force inputs.

2.2.1 Analytical Characterization Methods

The simplest vibrating system can be described by the mass, stiffness, and damping of an SDOF system excited by a force, F. If the system is linear and time-invariant, the model can be expanded to multiple degrees of freedom through the use of symmetric matrices where the off-diagonal terms show the coupling of each DOF to another DOF. The system is defined by its equation of motion which is a second order linear differential equation with constant coefficients shown in the time domain in equation (4) and transformed to the frequency domain in equation (5). This equation describes the motion of the system in physical space where $[M]$ is the mass matrix, $[C]$ is the damping matrix and $[K]$ is the stiffness matrix.

$$[M]\ddot{x}(t) + [C]\dot{x}(t) + [K]x(t) = f(t) \tag{4}$$

$$[M]\ddot{x}(\omega) + [C]\dot{x}(\omega) + [K]x(\omega) = f(\omega) \tag{5}$$

The relationship between the displacement response and the forcing function is known as the system's compliance FRF denoted $H(\omega)$. This is a slice of the system transfer function at $j\omega$ and is shown diagrammatically in Figure 3 and formulated for each DOF in the FRF matrix shown in equation (6). The response of the structure can be characterized by its modes of vibration which depend on the systems mass, stiffness, damping and boundary conditions. The number of modes in the system is equal to the number of poles in the transfer function. There are an infinite number of modes in real systems, each of which can be described by a unique natural frequency, modal damping value and mode

shape. These modal parameters are independent of the forcing function acting on the system.

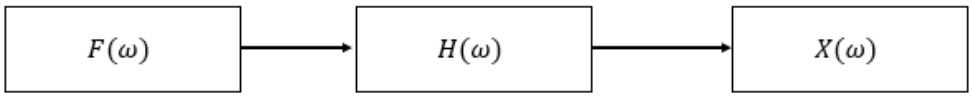

Figure 3: Analytical Compliance Block Diagram

$$[H(\omega)] = \left[-\omega^2[M] + j\omega[C] + [K]\right]^{-1} \tag{6}$$

Each FRF in the multiple DOF FRF matrix shown in equation (6) can also be expressed in partial fraction form shown in equation (7) where it is described by system poles, λ_n, and residues, A_n. The poles of the system are the roots of the denominator of the transfer function and the residues are the roots of the numerator. The poles are defined using damped natural frequency, ω_d, and damping factor, σ, as shown in equation (8). The residues are defined by the mode shape vector, $\{v\}$ and a participation scale factor, q_n, shown in equation (9).

$$H(\omega) = \sum_{n=1}^{\infty} \frac{A_n(\omega)}{j\omega - \lambda_n} + \frac{A_n^*(\omega)}{j\omega - \lambda_n^*} \tag{7}$$

$$\lambda_n = -\sigma \pm j\omega_d \tag{8}$$

$$A_n = q_n \cdot \{v\} \cdot \{v\}^T \tag{9}$$

In an analytical model, the systems mode shapes and natural frequencies can be found from the solution of the eigenvalue problem shown in equation (10) where the

resulting eigenvalue matrix, λ, is a diagonal matrix of squared natural frequencies and the eigenvectors are a matrix of the associated mode shapes, $[U]$. Solving the eigenvalue problem assumes that the stiffness and mass relationships of all DOF's are known. It is typical in analytical models for the modal damping to be estimated or assumed negligible for mechanical systems.

$$([K] - \lambda[M]) \cdot \bar{X}(\omega) = \bar{0} \tag{10}$$

The physical space FRF shown in equation (6) can be transformed with the eigenvector matrix to modal space notation, $q(\omega)$, using equation (7). Modal space notation uncouples all DOFs to produce SDOF FRF's for the contribution of each mode to the overall response of the system.

$$[U]^T[M][U]\ddot{q}(\omega) + [U]^T[C][U]\dot{q}(\omega) + [U]^T[K][U]q(\omega) = [U]^T F(\omega) \tag{11}$$

Both the modal space representation and the pole-residue form of the FRF explicitly show that the overall response of any DOF can be described by the sum of the response of each mode. This is known as modal superposition. In real systems, the mass, stiffness and damping relationships between each DOF cannot be measured for the above analytical methods to be applied. Experimental techniques to extract modal parameters from measured data must be used.

2.2.2 Experimental Characterization Methods with Measured Inputs

Moving from an analytical to signal processing notation, the FRF in Figure 3 can be represented where $F(\omega)$ is the measured input spectrum and $x(\omega)$ is the measured output

spectrum. In the case of real measurements, there will be noise on both the output and input channels. The data is often collected in the time domain and transformed to the frequency domain using an FFT. The H1 formulation shown in equation (12) uses the crosspower between the input and output signals, $G_{xF}(j\omega)$ in the numerator and the autopower of the input, $G_{FF}(j\omega)$ in the denominator. The * denotes the complex conjugate of the measured spectrum. This FRF formulation minimizes all signal content in the output signal that is uncorrelated with the input signal.

$$H_1(j\omega) = \frac{x(j\omega) \cdot F^*(j\omega)}{F(j\omega) \cdot F^*(j\omega)} = \frac{G_{xF}(j\omega)}{G_{FF}(j\omega)} \tag{12}$$

The output signal from any transducer on a structure is measuring the overall response of the system at a specific measurement location to the given excitation input. The response can be measured throughout a spatial domain to produce a shape known as an operational deflection shape (ODS). It is assumed that if modal density is low and the forcing frequency of the input signal is at or near a mode of the system, the ODS will be dominated by the shape of the excited mode. It is not possible to extract modal parameters from ODS but it can be done through an established test method known as experimental modal analysis (EMA).

EMA requires that the structure being analyzed is linear and time-invariant. A mode must be excited by the input forcing function to be evaluated using EMA. It is typical to use an impact hammer to produce an impulse response or a shaker with a white noise spectrum to excite a broad frequency range. In both cases, the input signal and response signal are measured and an FRF is produced using equation (12) and then curve fit to obtain

an estimate for the modal parameters of each mode. There are many methods for curve fitting a measured FRF. One such method for extracting natural frequency, damping and participation factor is the PolyMAX method [40]. In this method, poles are selected from a stabilization diagram which is created by evaluating the pole-residue form of the FRF in equation (7) with increasing model order. A stable pole is determined when model order no longer changes the estimated natural frequency and modal damping. The shape of the mode is extracted from the residues using least squares complex frequency domain (LCFD) method [41]. Since EMA is only evaluating a finite number of modes based on input excitation, the effect of modes outside of the frequency range of interest can be accounted for with upper and lower residuals where the lower residual is represented as a stiffness line and the upper residual is represented as a mass line.

The estimated modal parameters can be validated by synthesizing the FRF using a finite number of modes, the upper residual, UR, and the lower residual, LR, using equation (13). If all modes that significantly contribute to the overall response at the DOF of interest are represented in the synthesis, the FRF will look identical to the measured DOF. The least squared error shown in equation (14) can be used to quantify the difference between the synthesized FRF, H_{synth}, and the measured FRF, H_{meas} .

$$H(\omega) = LR + \sum_{n=1}^{N} \frac{A_n(\omega)}{j\omega - \lambda_n} + \frac{A_n^*(\omega)}{j\omega - \lambda_n^*} + UR \tag{13}$$

$$LS_{error} = \frac{\sum(H_{synth}(\omega) - H_{meas}(\omega)) \times (H_{synth}(\omega) - H_{meas}(\omega))^*}{\sum(H_{meas}(\omega) - H_{meas}(\omega))} \tag{14}$$

All mode shapes that describe a system are unique. The modal assurance criterion (MAC) shown in equation (15) is used to determine the relationship between any two extracted mode shapes, n and m, and quantify similarity.

$$MAC(n,m) = \frac{|\{v_n\}^T\{v_m\}^*|^2}{(\{v_n\}^T\{v_n\}^*)\cdot(\{v_m\}^T\{v_m\}^*)} \tag{15}$$

Methods based on MAC have been developed to analyze the similarity between two FRFs without the need for a complete set of EMA data [42]. The cross signature assurance criterion (CSAC) shown in equation (16) quantifies the shape differences of two FRFs and an FRF scaling factor (FRFSF) shown in equation (17) compares the amplitude differences.

$$CSAC = \frac{\left|\{H_{synth}(\omega)\}^T\{H_{meas}(\omega)\}^*\right|^2}{\left(\{H_{synth}(\omega)\}^T\{H_{synth}(\omega)\}^*\right)\cdot(\{H_{meas}(\omega)\}^T\{H_{meas}(\omega)\}^*)} \tag{16}$$

$$FRFSF = \frac{\sum_{i=1}^{L}|H_{synth}(\omega_L)|}{\sum_{i=1}^{L}|H_{meas}(\omega_L)|} \tag{17}$$

Techniques have been developed for taking modal parameters from an EMA and expanding the information to analytical DOF [43]. These expansion processes require a transformation matrix to relate each measured DOF to an analytical DOF. In the case of the system equivalent reduction expansion process (SEREP), the transformation matrix, $[T_u]$, is the product of the mode shapes for all DOF's, $[U_n]$, and the generalized inverse of only the measured DOF shape vectors, $[U_a]$, as shown in equation (18). The SEREP expansion can then be performed for all DOF's, $\{x_n\}$, using equation (19).

$$[T_u] = [U_n][U_a]^g \tag{18}$$

$$\{x_n\} = \begin{Bmatrix}\{x_a\}\\ \{x_d\}\end{Bmatrix} = [T_u] \cdot \{x_a\} \tag{19}$$

2.2.3 Experimental Characterization Methods with Unmeasured Inputs

A subset of EMA known as operational modal analysis (OMA) has been developed to be applied to systems where measuring the input force is not possible or practical [44]. OMA uses measured responses from ODS data to estimate modal parameters with modified EMA curve fitting techniques. The assumption of a linear time-invariant system and broadband excitation over the entire frequency range of interest should still be valid. Instead of participation factors, complex reference factors are used to represent modal contribution.

A unique challenge in OMA arises for the case of rotating machinery. The fundamental excitation frequency for components kinematically connected to a rotating shaft is known as an order. The frequency of an order can be determined using equation (20). Stationary rotating operating conditions will excite orders with frequencies that are deterministic and typical operation conditions produce time-varying excitation frequencies which negates the necessary assumptions for modal analysis to be performed. In addition, OMA techniques with rotating components can produce false peaks at the end of orders that do not relate to the system's dynamics. An experimental method that combines the tracking of orders and OMA known as order-based modal analysis (OBMA) has been developed to solve these problems [45].

$$f_o = \frac{\omega_{RPM}}{60} \cdot Events\ per\ cycle \tag{20}$$

The tracking of orders allows for analyzing the contribution of a subcomponent to the overall measured vibration level. The simplest order tracking method is known as FFT order tracking. In this method, a vibration response time history and pulse train signal from a tachometer on a reference shaft are recorded simultaneously using a fixed sampling rate and block size. The reference shaft speed is extracted from the tachometer signal and a vibration response spectrum is generated using FFT. The frequency of the order is determined from the average operating speed during the measurement period and paired with the amplitude of the related frequency bins in the measured response spectrum. Integration over an order bandwidth (constant frequency or constant order) is desired to account for variations in order frequency over the measurement period. It is important that windows are used to minimize leakage since the frequency resolution is independent of the order frequency. Slow sweep rates will improve the accuracy of a tracked order since the amplitude of the order is an average over the measurement period. Advanced order tracking techniques have been developed to overcome the limitations due to fixed sampling rates [46].

Rotating component data is best visualized using colormaps made of incremental vibration response measurements over a speed sweep of the rotating reference shaft. In this display type, excited orders are easily identified by diagonal lines of high amplitude. The resonances in the system appear as vertical lines since their excitation frequency is independent of operating speed. Observing the speed sweep colormap will also help

determine what bandwidth type and size is necessary to capture all of the energy in the order.

The foundational assumption of OBMA is that broadband excitation is achieved with run up or run down speed sweeps of the rotating reference shaft. The OBMA technique assumes that the input is a multiple sine sweep excitation defined by two correlated inputs of rotating shaft imbalance equal in amplitude having a 90° phase difference [45]. Each force input has a corresponding FRF for each order contributing. The output order, $Y(\omega)$, is extracted from measured operational speed sweep response data using order tracking. Operational PolyMAX curve fitting techniques can be applied to the orders to estimate natural frequencies, modal damping and residuals and LCFD can be applied to get mode shapes and reference factors, $< g_i >$ [45]. The extracted modal parameters from OBMA can be validated by order synthesis using each mode, N, and equation (21). The synthesized results can then be compared to the measured order sections [47].

$$Y(j\omega) = (j\omega)^4 \cdot (\sum_{i=1}^{N} \frac{\{v_i\} \cdot < g_i >}{j\omega - \lambda_i} + \frac{\{v_i\}^* \cdot < g_i^* >}{j\omega - \lambda_i} + \frac{1}{(j\omega)^2} \cdot LR + UR) \tag{21}$$

2.3 Hydraulic Energy Characterization

It is hypothesized that the noise energy in a simple hydraulic circuit can be characterized using FBN and SBN sound power metrics and then predicted at downstream locations using a power flow approach known as energy balancing. The ABN contribution to the total hydraulic energy flow is assumed negligible.

2.3.1 Fluidborne Sound Power

Fluid power available to do work in a hydraulic system is the product of the fluid mean pressure and mean flow. The power available to generate FBN in the system is the product of the dynamic elements of the flow and pressure signals. The total source FBN can be quantified using equation (22) which is the sum of the product of the source flow ripple, $Q_{s.i}$, and pump outlet pressure ripple, $P_{outlet\ i}$, evaluated at each pump order, i. Any downstream mount location FBN can be estimated at location n using equation (23) if the local pressure ripple, $P_{n\ i}$, is known. It is assumed that the flow ripple is uniform through the pump outlet hose to the first restriction since there is no change in cross-sectional area for significant reflections occur.

$$FBN_{Source} = \sum_{i=1}^{N} Q_{s.i} \cdot P_{outlet\ i} \tag{22}$$

$$FBN_{n} = \sum_{i=1}^{N} Q_{s.i} \cdot P_{n\ i} \tag{23}$$

The source flow ripple of a hydraulic piston pump can be measured using ISO 10767-1 also known as the two pressures – two systems method [27]. This method requires a test setup with measurement of dynamic pressure at two locations separated by a reference pipe with two inline direct acting load valves downstream separated by an extension pipe. The maximum frequency of interest for the test setup is determined using equation (24) based on the hydraulic fluid speed of sound, c, and the reference pipe length, L_R.

$$f_{max} = \frac{c}{2 \cdot L_R} \cdot 75\% \tag{24}$$

Two unique standing waves are generated in the pipe from two measurements using load valves at two different locations independently. The complex source flow ripple quantity can be determined using equation (25) by measuring the complex pressure ripple at both locations, P_1 and P_2, in two measurements runs where $'$ denotes the second measurement. The characteristic impedance, Z_c, wave propagation coefficient, β, and unsteady viscous friction coefficient, $\xi(\omega)$, can be determined with equations (26), (27) and (28) respectively defined by mean system pressure, p, speed of sound, c, pipe radius, r_o and dynamic viscosity, v. The speed of sound of the hydraulic fluid is estimated using the bulk modulus, B, and density of the hydraulic oil, ρ, shown in equation (29).

$$Q_{s.i} = j\frac{1}{Z_c}\frac{P_{1.i}P'_{2.i} - P'_{1.i}P_{2.i}}{(P_{1.i} - P'_{1.i})\sin(\beta L_R)} \tag{25}$$

$$Z_c = \frac{p\ c\ \xi(\omega)}{\pi\ r_o^2} \tag{26}$$

$$\beta = \frac{\xi(\omega)\ \omega}{c} \tag{27}$$

$$\xi(\omega) = 1 + \sqrt{\frac{v}{2r_o^2\omega}} - j\left(\sqrt{\frac{v}{2r_o^2\omega}} + \frac{v}{r_o^2\omega}\right) \tag{28}$$

$$c = \sqrt{\frac{B}{\rho}} \tag{29}$$

The distribution of FBN energy in the outlet hose can be observed with the fluid ODS at a given operating speed. The ODS shape is a superposition of the excited fluid and structural modes. The theoretical fluid mode frequencies of a straight pipe with open end – closed end boundary conditions can be predicted analytically as shown in equation (30) for each harmonic using the speed of sound of the fluid and the standing wave wavelength, λ. The analytical fluid mode shapes are sinusoids having integer increments of ¼ wavelength.

$$f_n = \frac{n \cdot c}{4 \cdot \lambda} \qquad n = 1,2,3 \ldots . n \tag{30}$$

2.3.2 Structureborne Power

An SBN power metric using measured force, F, and velocity, v, at each pump order i was used to evaluate the SBN generated at the hydraulic circuit mounts. Evaluating SBN power with both force and velocity is preferred over using either parameter alone since the combination is robust against the effects of structural resonances. It is assumed that the force and velocity will change proportionally near resonances and produce a valid SBN power metric for all evaluated frequencies. It is assumed that the sum of the SBN power measured at each pump order produces an estimate for the total SBN power transmitted through a single mount at each operating speed as shown in equation (31).

$$SBN_n = \sum_{i=1}^{N} F_i \cdot v_i \tag{31}$$

2.3.3 Energy Balancing

Energy balancing is a power flow approach for the assessment of the FBN and SBN power through the outlet line of a hydraulic circuit. Starting with the source FBN power metric and SBN power losses at the first mount established using equation (22) and (31) respectively, the local FBN at the location of the first and subsequent mounts can be predicted with equation (32) for each incremental mount location n.

$$FBN_{n+1} = FBN_n - SBN_n \qquad n = 0,1,2, \dots n \tag{32}$$

The ABN power losses will be significantly smaller than the FBN and SBN power and are therefore considered negligible for the balancing of energy. The energy balance results can be validated with the local FBN predictions at the mount using equation (23).

3 Test Bench Development

A generalized hydraulic circuit test bench was developed at Michigan Tech for assessment of FBN and SBN energy transfer. The primary design considerations are discussed followed by component selection and setup, operation, safety, and correlation to the machine.

3.1 Test Bench Design Considerations

A hydraulic circuit that has SBN issues was used as a reference circuit for the development of the hydraulic noise test bench. Correcting the problems of this circuit is not the primary purpose of the test bench. The test bench will be used to understand the physics involved in the FSI of a working hydraulic fluid and the hose at hose clip locations. This knowledge can then be applied to all heavy equipment hydraulic systems. A rotary valve circuit as discussed in 1.2.2.2.1 was explored, but a valve capable of meeting the reference circuit pressures was cost prohibitive. The prime mover is intentionally oversized to allow for future expansion of the current research to larger circuits with minimal component changes required. Components were selected to meet the following design objectives.

- Replicate the dynamics of the reference hydraulic circuit.
- Easily reconfigurable hose routing.
- Remote control of system pressure and motor speed.
- Safe and repeatable operation.

3.2 Test Bench Component Selection and Setup

The test bench components were selected to simulate the reference hydraulic circuit as well as follow general hydraulic circuit design guidelines for performance and safety. A comparison of the reference hydraulic circuit requirements and the capability of the test bench are shown in Table 1. The selection of the pump, motor, hose routing fixtures, hydraulic oil and reservoir, and end-of-line components are discussed in detail. The complete component list for the test bench is shown in appendix A.

Table 1: Hydraulic Circuit Requirements

	Motor Speed [RPM]	Flow [GPM]	Power [HP]	Torque [Ft-Lb]
Reference Hydraulic Circuit Requirements	800-2340	17.3	25.7	74.9 @ 1800 RPM
Test Bench Capability	0-2700	17.3	100	295 @ 1800 RPM

3.2.1 Hydraulic Pump

The pump used in the reference hydraulic circuit is a 28cc variable axial piston pump with a nominal pressure of 3626 psi and a maximum pressure of 4569 psi. The tapered shaft on this pump made it difficult to find a suitable low-cost pump shaft coupling. A different 28cc pump with a straight shaft from the same Bosch Rexroth product line was selected to mitigate this issue. The maximum cutoff pressure for the test bench pump is 2320 psi whereas the reference hydraulic circuit pump has a cutoff pressure of 3263 psi. The outlet and suction port diameters are identical for both circuits being ¾ inches and 1 ¼ inch respectively. The rated speed for the test bench pump is 2100 RPM. This means

that overspeeding the pump is required to meet the reference hydraulic circuit maximum speed range. It was determined that this is acceptable due to the short running durations needed for data collection. Using equation (1), the test bench pump maximum flow rate meets the requirements of the fan-brake circuit.

The test bench pump was mounted to a 1-inch thick steel fixture and bolted directly to the lab bedplate as shown in Figure 4. A driving point FRF at the corner of the pump mounting fixture was measured during a pre-test analysis to document resonances and is shown in Appendix B.4. The test bench pump was broken in using break-in procedures found in Appendix C.2.

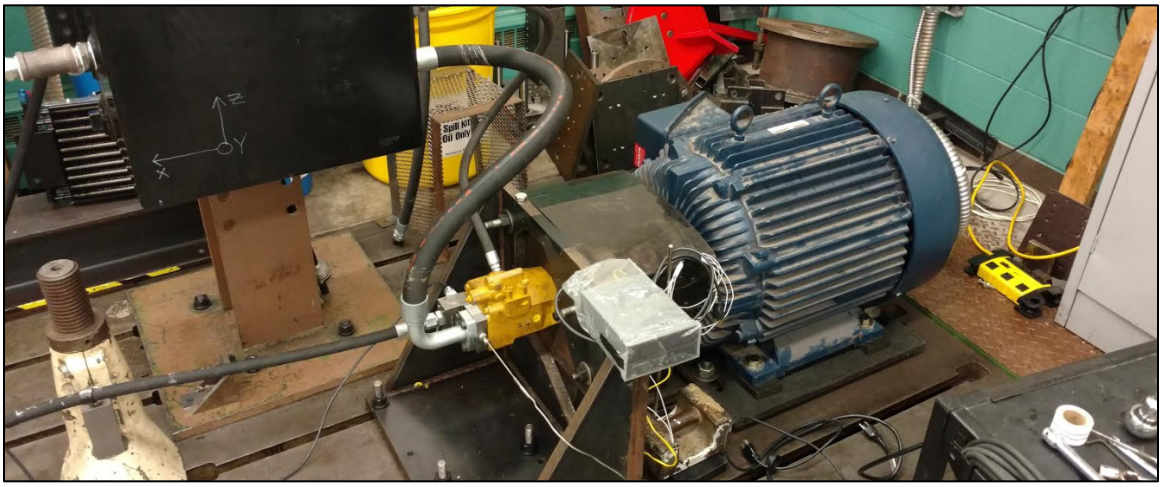

Figure 4: Hydraulic Test Bench Pump and Motor

3.2.2 Motor Selection and Setup

Based on equation (2) and (3) and the pump flow and rated speed parameters, there were two 3-phase electric motor choices, 25 HP or 100 HP, available at MTU that could be used for the test bench. The 25 HP motor had an 1800 RPM rated maximum speed which would have limited the pumping frequency range of interest. The 100 HP motor was

chosen since it exceeded the minimum requirements. The motor was mounted on rubber pads to protect the motor and minimize the vibration transmission path from the motor feet to the hose mounts. This was tested in a pre-test analysis by sweeping the motor speed from 0 RPM to 1800 RPM and measuring the acceleration response at the base of the hose mount and at the hose clipping point. It was determined that there was no significant vibration contribution to the hose mount from the motor through the floor at these operating conditions. The results are shown in Appendix B.3. The motor is shown in Figure 4 and is controlled by an ABS ACS550 drive unit. The selected drive unit allows for direct control the motor speed using a remote. The motor and pump were assembled carefully using feeler gauges to minimize misalignment. An elastomeric spider was placed in between the pump-side and motor-side couplers to minimize torsional vibration.

3.2.3 Circuit Hoses and Routing

Easily reconfigurable and in-plane with the outlet of the pump were the primary component selection criteria for hose mounting. This was achieved by modifying massive jack stands as shown in Figure 5. A 5-inch length of 2-inch steel square stock was used as a spacer that was connected through the jack stand to a T-nut in the bed plate with ¾ inch threaded rod. A hose can be mounted anywhere where there is a bedplate slot which allows for ease and efficiency in testing multiple circuit configurations. The hose clip was attached to the top of the spacer block with M8 bolts with the additional stack height of a dynamic force transducer. The final mount height is in-plane with the outlet of the pump. There are 4 different jack stands denoted A-D available for circuit routing. Driving point FRF's of jack stand A-D was performed to document fixture resonances that may be present in data

collected from future tests. The results of this test are found in Appendix B.1. The reproducibility of the jack stand setups was analyzed in Appendix B.2.

A 2.13-meter length of SAE 100R16-10 (5/8-inch ID) was chosen for the first circuit configuration used on the test bench circuit to match the reference hydraulic circuit. The same hose clips used on the machine were used to attach the hoses to the fixtures. M8 bolts instead of the M10 were required to attach the hose clips due to the limitations of the through-hole in the dynamic force transducers.

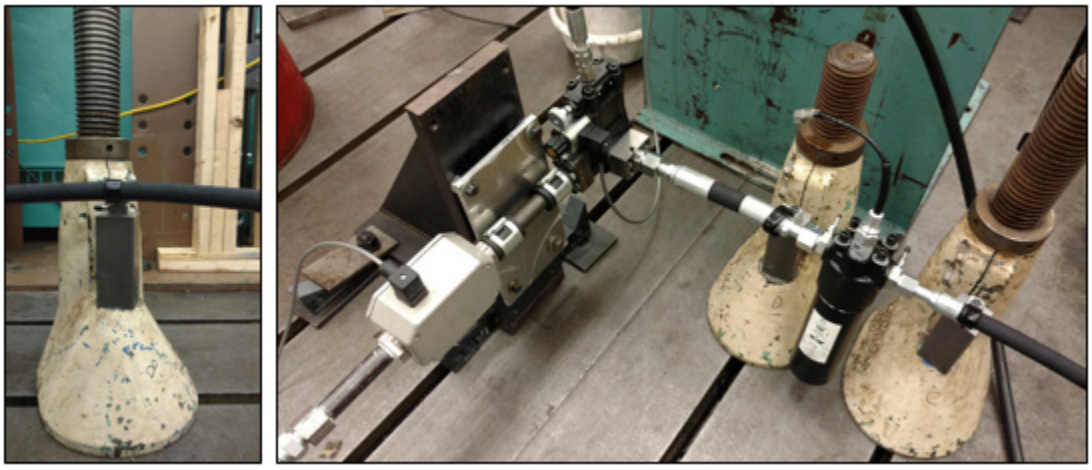

Figure 5: Hydraulic Hose Mount (Left) and End-of-Line System (Right)

3.2.4 Hydraulic Oil and Reservoir

The reference hydraulic circuit uses a 10W oil with a viscosity of 39.8 cSt at 40°C and between 6.0 and 7.0 cSt at 100°C. Chevron – Rando HDZ 32 was selected for use with the test bench circuit since it can be purchased locally through MTU facilities. This oil has a viscosity of 32 cSt at 40°C and 6.2 cSt at 100°C. The density of this oil is 0.8433 g/cc and the adiabatic bulk modulus is 285,000 psi.

A 25-gallon reservoir was selected based on the 3x capacity of the circuit rule-of-thumb. All data collection was started at 50°C oil temperature measured by a Type K thermocouple at the end of the suction line. It is important the oil in the circuit does not heat too rapidly or take too long to reach temperature. A temperature test was performed during pre-test check-out runs**.** It was found that it took 20 minutes to reach 50°C at 750 psi and 5 minutes at 1500 psi with 18-gallon tank capacity.

3.2.5 End-of-Line System

The end-of-line system shown in Figure 5 provides the hydraulic load for the test bench. The fluid goes through a high-pressure filter, loading valve and a variable-area type flow meter before returning to the reservoir in an SAE 100R3-16 hose. A short section of SAE 100R16-12 hose connects the filter to the loading valve. The loading valve is a 3-port proportional pressure relief valve where the through-port is blocked allowing for variable control of the system pressure and flow remotely with control of the solenoid. The loading valve can achieve maximum pressure and flow rates of 5076 psi and 23.7 GPM respectively. A length of schedule 40 pipe connects the outlet of the load valve to the flow meter to steady the fluid before flow measurement. The flow meter is used as a reference transducer to monitor the system's operating conditions. A loading valve drain hose back to the reservoir was required.

3.3 Test Bench Safety

The safety of the test bench was addressed by enclosing all rotating machinery and ensuring the pressure ratings of all hydraulic components used in the working line exceed

the rated cutoff pressure (2320 psi) of the selected pump. The pump is designed to destroke if the pressure demand exceeds the set cutoff pressure. Emergency stops for the motor and load valve were installed for use should the test bench operator require rapid shutdown or need immediate pressure relief. A spill kit capable of absorbing the complete tank capacity is available in the lab.

3.4 Test Bench Operation

The test bench operating conditions were monitored using three transducers and wired as shown in Figure 6. A laser tachometer was directed at the motor shaft with 1 pip/rev. The static pressure transducer was threaded into a spacer block at the outlet of the pump to monitor mean system pressure. The flow meter was used as a reference check for motor speed and target system performance. The complete wiring diagram to provide power to the load valve and operating condition transducers is found in Appendix A.3.

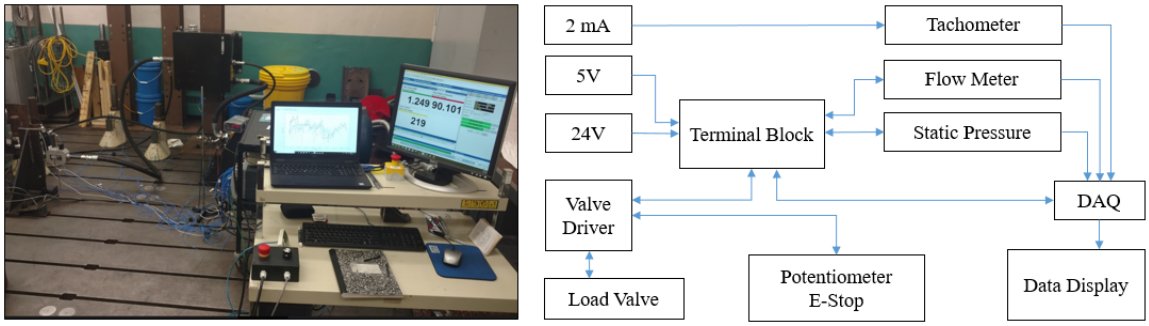

Figure 6: Test Bench Operation and Control

The test bench motor speed was controlled manually with a remote wired to the motor drive unit. The system mean pressure was controlled by a potentiometer on the load valve control remote as shown in Figure 6. A data collection run requires simultaneous use of both remotes to achieve desired system conditions. The data collected in this project was

constant pressure motor speed sweeps (CPSS) and steady-state (SS) runs which were easily obtained with this control configuration. All data sets were collected with a starting inlet oil temperature of 50°C. The startup guidelines can be found in Appendix C.1.

3.5 Hydraulic Noise Test Bench and Machine Correlation

The final assembly of the hydraulic noise test bench is shown schematically in Figure 7. The primary components are shown in Table 2. The complete component list can be found in Appendix A. The pressure ripple levels were measured at the outlet of the pump, inlet of the filter and outlet of the filter for a given SS run condition. A comparison of the test bench measurements and the reference hydraulic circuit field measurements at this condition is shown in Table 3. The correlation is acceptable and provides confidence that the test bench data collected throughout the project will be applicable to mobile heavy equipment field measurements.

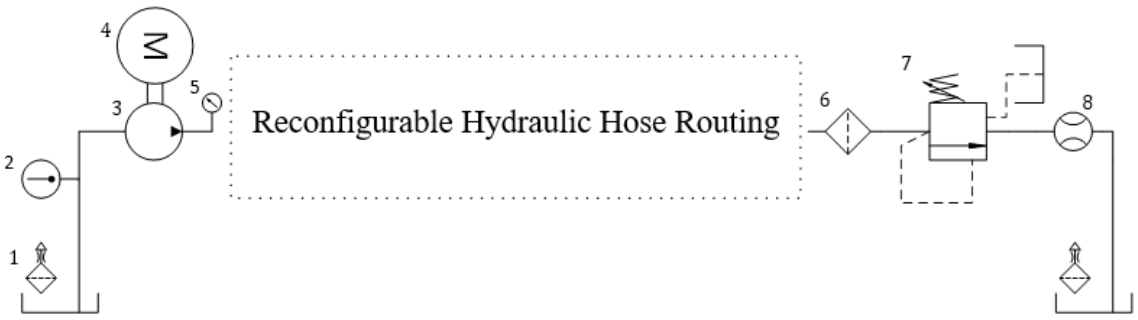

Figure 7: Reconfigurable Michigan Tech Hydraulic Test Bench Schematic

Table 2: Primary Test Bench Components and Instrumentation

1	Vented Hydraulic Reservoir	25 Gallon
2	Thermocouple	Omega Type K
3	Axial Piston Pump	Bosch Rexroth LA10VO28 series
4	Electric Motor	100 HP - Marathon Y575
5	Static Pressure Gauge	Omega PX309-5KGV
6	High Pressure Filter	3,000 psi
7	Pilot-Operated Proportional Pressure Control Valve	R5V06-513-16-P2-G0Q-A1
8	Variable Area Flow Meter	Omega FLMH-3425SS-MA

Table 3: Pressure Ripple Level Comparison between the Reference Hydraulic Circuit and MTU Test Bench

Total	Mobile Equipment Reference [kPa]	MTU Test Bench [kPa]
Pump Outlet	633.6	581.9
Filter Inlet	53.4	51.8
Filter Outlet	94.9	87.6

4 Source FBN Characterization

Characterization of the source FBN requires measurement of the outlet pressure ripple and pump source flow ripple. The pump source flow ripple was measured using ISO 10767-1 test procedures. The test bench configuration, data collection, and results are discussed in detail.

4.1 Test Bench Configuration

The hydraulic noise test bench was configured as shown schematically in Figure 8 with the primary components and instrumentation shown in Table 2. The complete test bench setup in the lab is shown in Figure 9. Three ¾ inch schedule 80 pipes were used to create the test section. This pipe diameter matches the size of the outlet port of the pump and has a working pressure rating of 3500 psi which exceeds the 2320 psi rated pressure of the test pump. A direct acting pressure relief valve set above the maximum desired test pressures was included in the test section as specified in the standard for added safety.

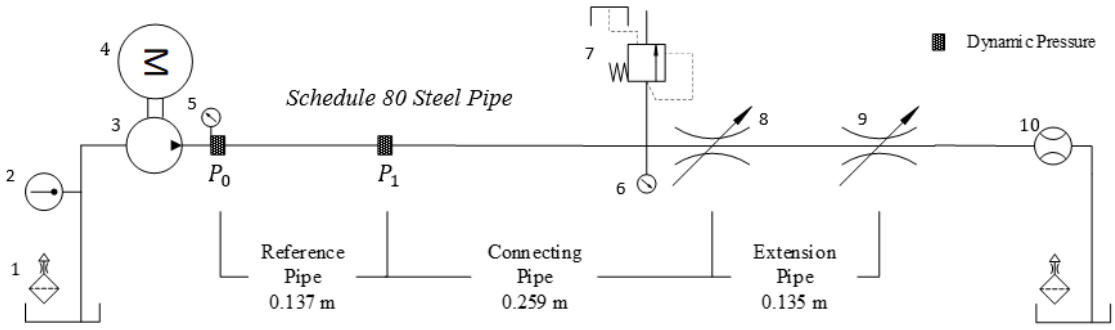

Figure 8: ISO 10767-1 Test Bench Schematic

Table 4: Primary Components and Instrumentation for Source Flow Ripple Testing

P_i	Dynamic Pressure	PCB 113B22
1	Vented Hydraulic Reservoir	25 Gallon
2	Thermocouple	Omega Type K
3	Axial Piston Pump	CAT 333-3788
4	Electric Motor	100 HP - Marathon Y575
5	Static Pressure Gauge	Bourdon Type
6	Static Pressure Gauge	Omega PX309-5KGV
7	Direct Operated Pressure Relief Valve	Sun Hydraulics RDFALWN
8	Load Valve 2	Parker N1200S
9	Load Valve 1	Parker N1200S
10	Flow Meter	Omega FLMH-3425SS-MA

Figure 9: ISO 10767-1 Test Bench Setup

Using equation (24) and a reference length of 0.137 meters, the maximum frequency of interest was determined to be 4,182 Hz. The ISO standard was used as a guide and not strictly followed due to budget limitations. Deviation in setup from the standard's configuration was not expected to alter the flow ripple results. There was no back pressure

relief valve or oil cooler used and the flow meter was of a variable-area type and not a positive-displacement type.

4.2 Data Collection and Procedures

The ISO 10767-1 test section is shown in Figure 10. Data was collected using dynamic pressure transducers (PCB 113B22) from two pressure transducer locations, P_1 and P_2. This was done for two system conditions with identical operating conditions in separate measurement runs. System 1 is defined by LV2 being fully open and LV1 set to a desired system operating condition. System 2 is defined by $LV1$ being fully open and $LV2$ set to the same system operating condition. Same operating conditions are defined by identical motor speed sweeps, flows, mean pressure and oil temperature. Motor speed, flow and static pressure data was recorded for both runs and inlet oil temperature was viewed on a digital display. All measurement runs began at an inlet oil temperature of 50°C. Pressure ripple data was collected at a sample rate of 10,240 Hz as recommended by the standard to observe the first 10 harmonics. Data was collected in 0.8s measurement periods for a CPSS. A hanning window was used to minimize leakage error. The direct acting load valves were controlled manually to maintain a constant pressure during motor speed run ups. This test procedure was performed for system 1 and system 2 at 1000 psi, 1500 psi and 2000 psi as well as a replicated load curve from the reference hydraulic circuit. The replicated load curve was performed by setting the pressure at 800 RPM motor speed and letting the increased flow with a constant restriction drive the mean pressure. The measured replicated conditions correlated well with measured machine data.

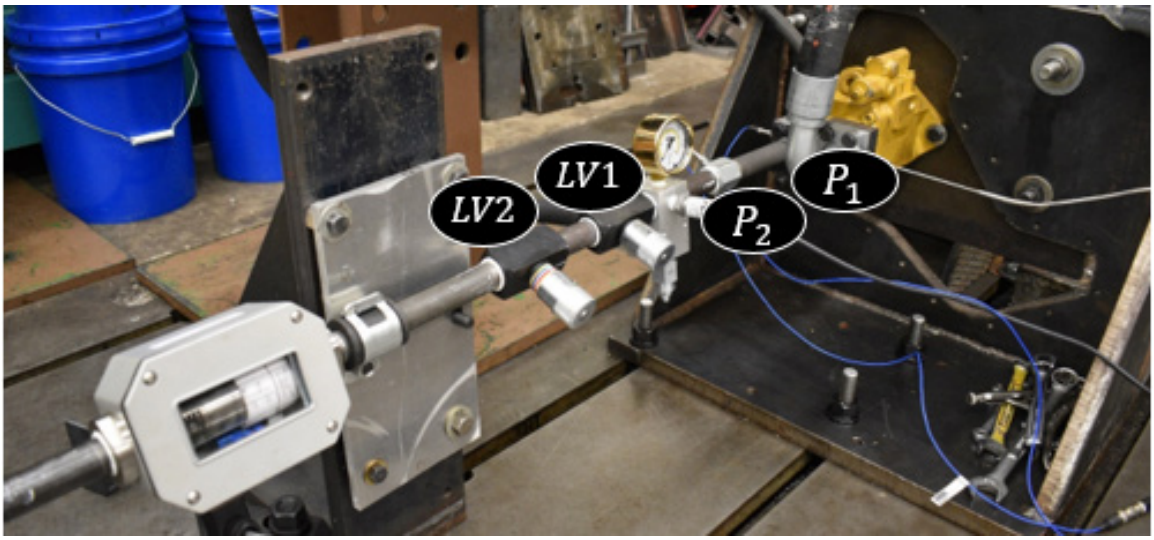

Figure 10: ISO 10767-1 Test Section

4.3 Source FBN Results

An example of a colormap and extracted pump order sections from the P_1 pressure measurement is shown in Figure 11. It is observed that most of the energy is in the 9th, 18th, 27th, 36th and 45th orders. 9th order is the fundamental pump order since there are 9 pistons in the test bench pump. Order sections were extracted from the colormaps using FFT based order tracking. A ½ order bandwidth was considered acceptable since there are no closely spaced or crossing orders. The order cuts show that nearly all of the energy contributing to the overall level is in the 9th order. There is also energy in 1st order caused by motor shaft imbalance. It is determined that capturing all of the energy in the system can be accomplished by analyzing the first 5 pump orders.

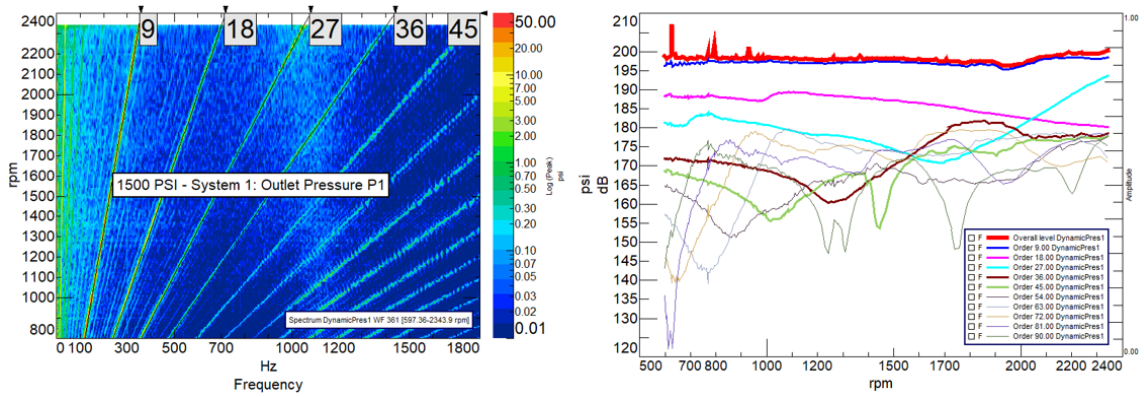

Figure 11: P_1 Colormap and Order Sections from System1 - 1500 psi CPSS

Using equations (25)-(29) the source flow ripple was determined for all CPSS. An example of the 1500 psi CPSS results for the first 5 pump orders is shown in Figure 12. Significant variation was observed in the raw flow ripple results output. The results were smoothed using a 7-point moving average filter. Large flow ripple spikes were also observed and linked to the subtraction of complex pressure ripple measurements. Flow ripple spike occurrence could not be correlated to observed differences in operating conditions. It is supposed that there are small system nonlinearities affecting the phase of the measured dynamic pressures and not the dynamic pressure magnitude. A detailed explanation into the observed anomalies can be found in Appendix D. The occurrence of spikes in the flow ripple results was mitigated by decreasing the frequency resolution to 0.5 Hz or 0.25 Hz. Since the total sweep time was typically 4 minutes and 40 seconds, a measurement period of 2 or 4 seconds is still acceptable for FFT based order tracking methods.

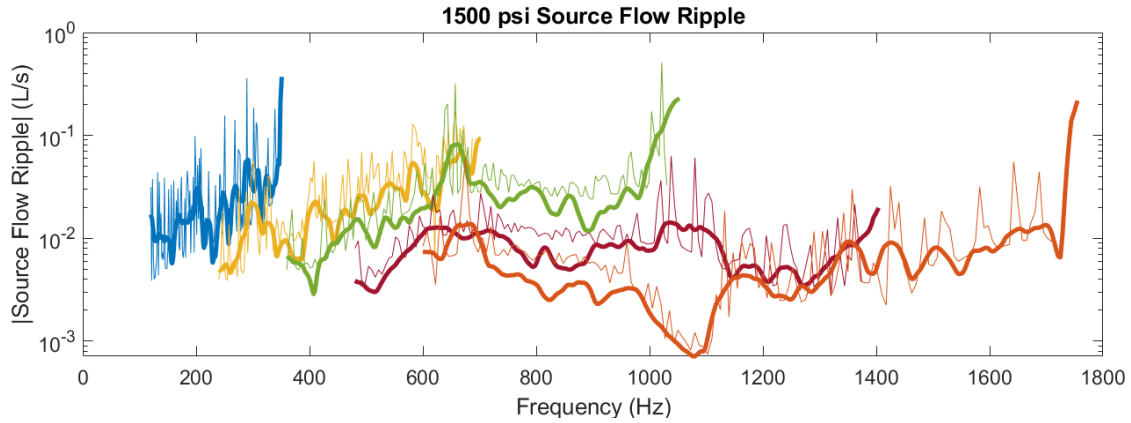

Figure 12: 1500 psi CPSS Source Flow Ripple Results

Pump orders were used to compare lab and reference hydraulic circuit results. The processed single-spectra source flow ripple from test bench data are shown in Figure 13.

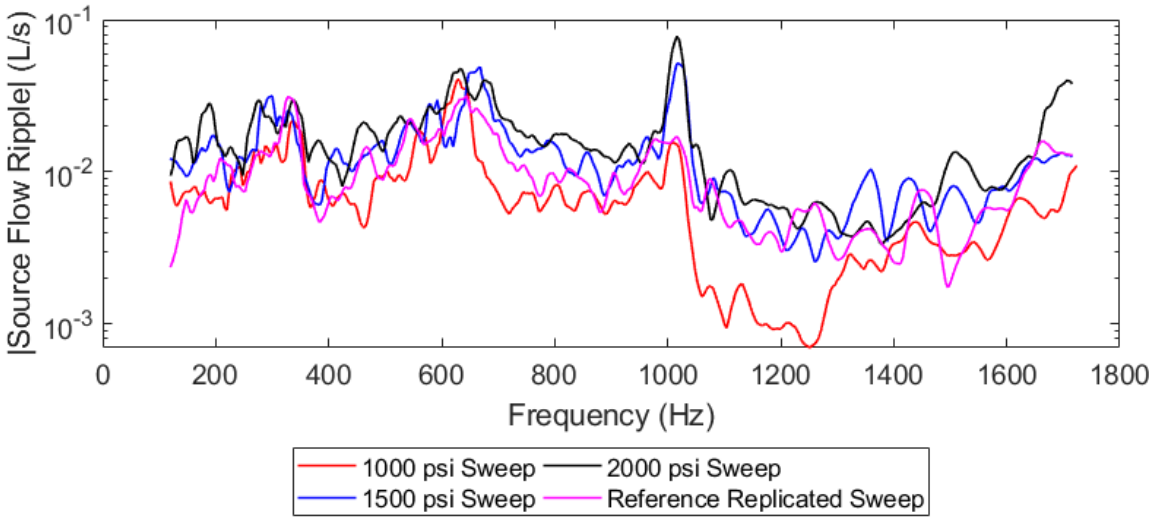

Figure 13: Single-Spectrum Source Flow Ripple Processing

It was found that the source flow ripple results correlate well with the reference hydraulic circuit data below 1000 Hz. The pumps used for comparison are not identical which could be cause for some of the deviation. It is supposed that the dissimilarities could be due to slight differences in operating conditions between the system 1 and system 2 measurements or errors in the speed of sound estimates.

5 Operational Deflection and Mode Shapes

Data sets for a straight 2.23-meter hose configuration were collected and processed to observe the structure and fluid ODS and mode shapes.

5.1 Test Bench Configuration

The test bench was configured as shown schematically in Figure 14 using the primary components and instrumentation shown in Table 2. The complete test bench setup in the lab is shown in Figure 15. Hoses denoted A, B, and C of length 486 mm, 667.5 mm and 892 mm respectively were connected in 4 setups. Pressure ripple was measured through the hose adapters to get 8 unique measurement locations. The hose lengths were specified so that measured pressure locations were not at integer multiples and it could be ensured that measurements were not made at the same point on the fluid wave in the hose. A single hose mount was placed at a point that could remain consistent with for all configurations.

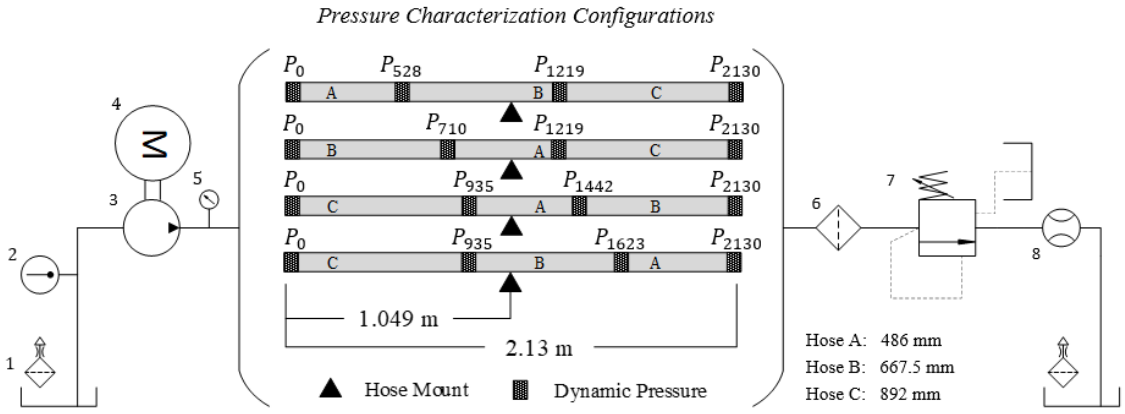

Figure 14: Fluid Pressure Characterization Schematic

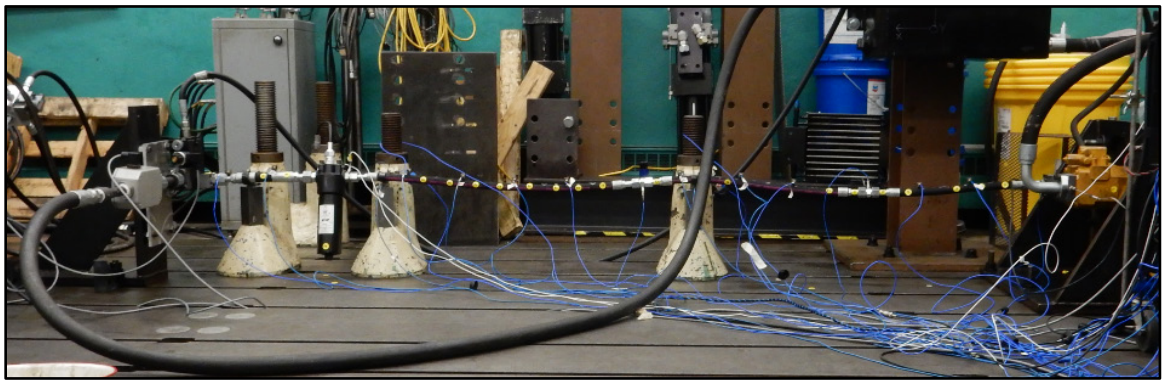

Figure 15: Pressure Characterization A-B-C Configuration

5.2 Data Collection Procedures

Dynamic pressure data sets were collected at the 8 pressure measurement locations shown in Figure 16 using 1500 psi CPSS conditions. A sample rate of 10,240 Hz with 1 second measurement periods was used. A Hanning window was applied to minimize leakage error. The 1500 psi CPSS was chosen as the best operating condition because the test bench was most stable and there was a low risk of sensor overloads due to transient events. The typical total speed sweep time was 4 minutes.

Measured concurrently with pressure ripple ODS, 11 single-axis accelerometers were roved across the top of the hose structure collecting 57 ODS deflection measurement points as shown in Figure 16. The accelerometers were spaced uniformly across the length of the structure in each run to minimize mass loading effects. A reference accelerometer was placed on the hose near the first hose mount and kept constant for all CPSS measurements. Deflection data was also captured circumferentially around the hose as shown in Figure 16 to visualize the expansion of the hose. This was done with

accelerometers at 1079 mm and with dynamic strain gauges at 528 mm. Both measurements recorded radial motion effectively, however, concerns with the durability of the dynamic strain gages led to more confidence in the accelerometer methods.

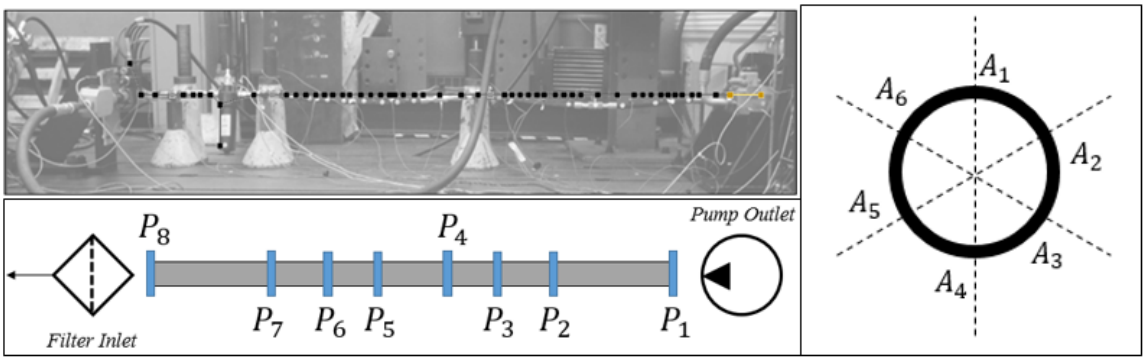

Figure 16: Vertical Deflection Measurements (Top-Left), 8 Pressure Ripple Measurements (Bottom-Left) and Circumferential Deflection Measurements (Right)

5.3 Operational Deflection and Mode Shape Results

The ODS of the fluid and the hose can be viewed in a combined and overlaid manner for any motor operating speed for a given excitation frequency. The FSI relationships between the fluid pressure and the hose can be observed for any order excitation. The 9th order excitation at 820 RPM is shown in Figure 17. The hose ODS along the hose length may be dominated by a structural mode at this frequency.

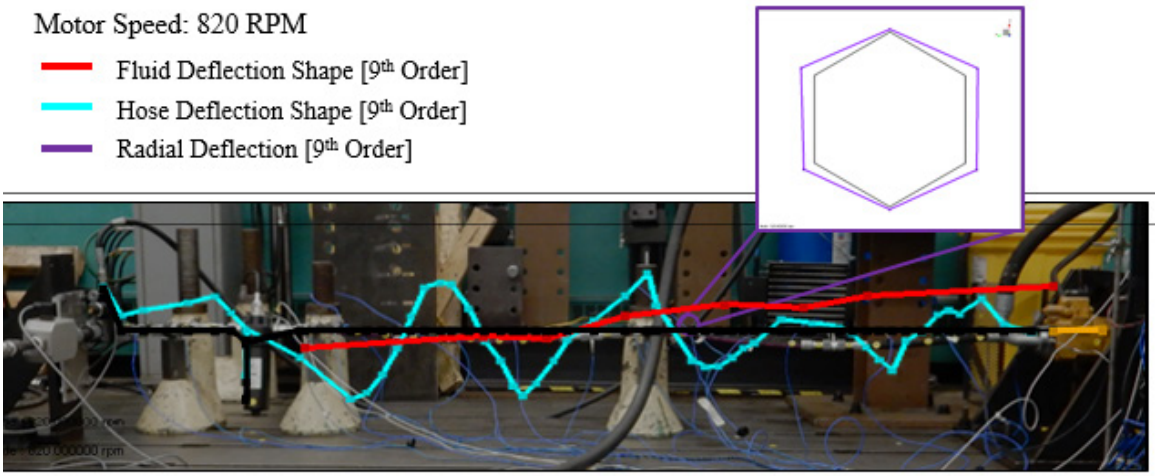

Figure 17: Combined Deflection Shape Analysis at 820 RPM

The theoretical fluid modes in a cylindrical pipe can be determined using equation (30) assuming open end - closed end boundary conditions. It is assumed that the test bench hose system would have fluid modes similar to this analytical solution with a closed end condition at the pump and open end condition at the filter inlet. The fluid modes are integer multiples of a fundamental frequency and have sinusoidal shapes that are multiples of ¼ wavelength. OBMA was attempted without success to extract theses fluid modes. Similar shapes and frequencies to the analytical results were observed in the deflection shapes of the first three pump orders. It is assumed that excitation with significant energy at a frequency near the fluid mode produces an ODS dominated by that mode shape. The observed shapes are flipped about a midline through the center of the hose which means boundary conditions may not be completely understood. The first 6 fluid modes were found in the fluid ODS shapes as shown in Table 5 and Figure 18. There is not enough spatial resolution in the dynamic pressure measurements to extract mode shapes from the ODS above the 6th harmonic.

Table 5: Fluid Modes from Operating Deflection Shapes

$f_1 = \frac{c}{4 \cdot \lambda}$ $c \sim 1528\ ^{m}/_{s}$ $\lambda = 2.13\ m$	Theoretical ¼ Wavelength Frequencies [Hz]	ODS ¼ Wavelength Frequencies [Hz]	9th Order 120 – 351 Hz [RPM]	18th Order 240 – 702 Hz [RPM]	27th Order 360 - 1053 Hz [RPM]
f_1	179	129	860	---	---
$2 \cdot f_1$	359	228	1520	---	---
$3 \cdot f_1$	538	338	2250	1110	---
$4 \cdot f_1$	717	423	---	1410	950
$5 \cdot f_1$	897	585	---	1950	1300
$6 \cdot f_1$	1076	687	---	2290	1530

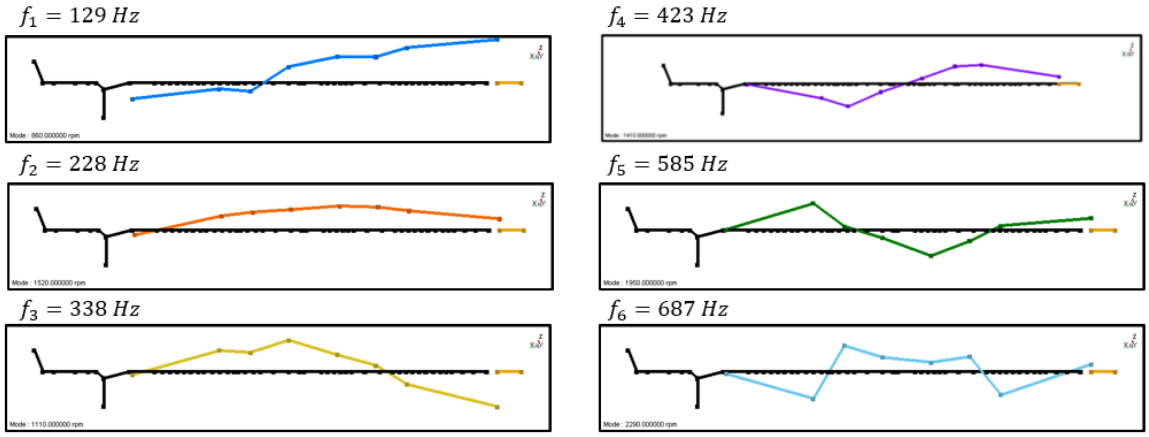

Figure 18: Fluid Mode Shapes from Operating Deflection Shapes

The 9th order energy is the dominant contributor to the overall ripple energy in the fluid. Using equation (20) for the CPSS performed from 800 – 2340 RPM, the 9th order frequency range is 120 – 351 Hz. This means that fluid modes above the third harmonic are not excited by 9th order energy. Additionally, the first and second fluid modes theoretically do not have nodes in their shapes. Nodal locations are ideal locations for hose clips since they are locations of minimum FBN energy. The third harmonic was selected for closer analysis since it is excited by 9th order energy and has both a node and peak wave amplitude in its shape.

The third fluid mode dominating the ODS at 2300 RPM is shown in Figure 19. The 9th order forcing frequency at 2300 RPM is 345 Hz which is near the predicted location of the third fluid mode. There is significantly less energy in the higher pump orders and there is no significant contribution from higher pump orders to the overall deflection shape.

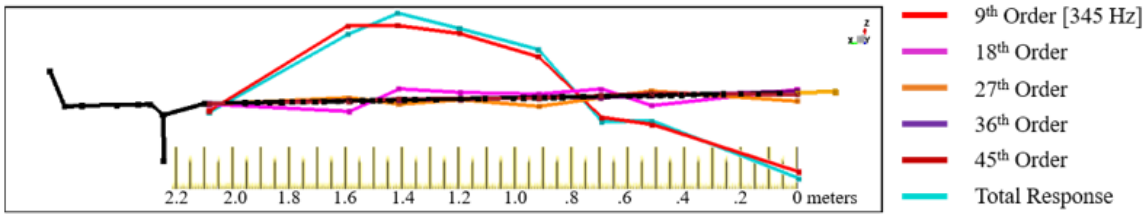

Figure 19: Order-Based Deflection Shapes at 2300 RPM

The absolute magnitude of the pressure ODS for a 1500 psi CPSS is shown Figure 20 in three operation speed segments. It is observed that as motor speed approaches 2300 RPM the third fluid mode is amplified. There is an FBN minimum near 0.7 meters from the pump outlet and a maximum near 1.4 meters from the pump outlet. These are noted regions of high and low FBN energy.

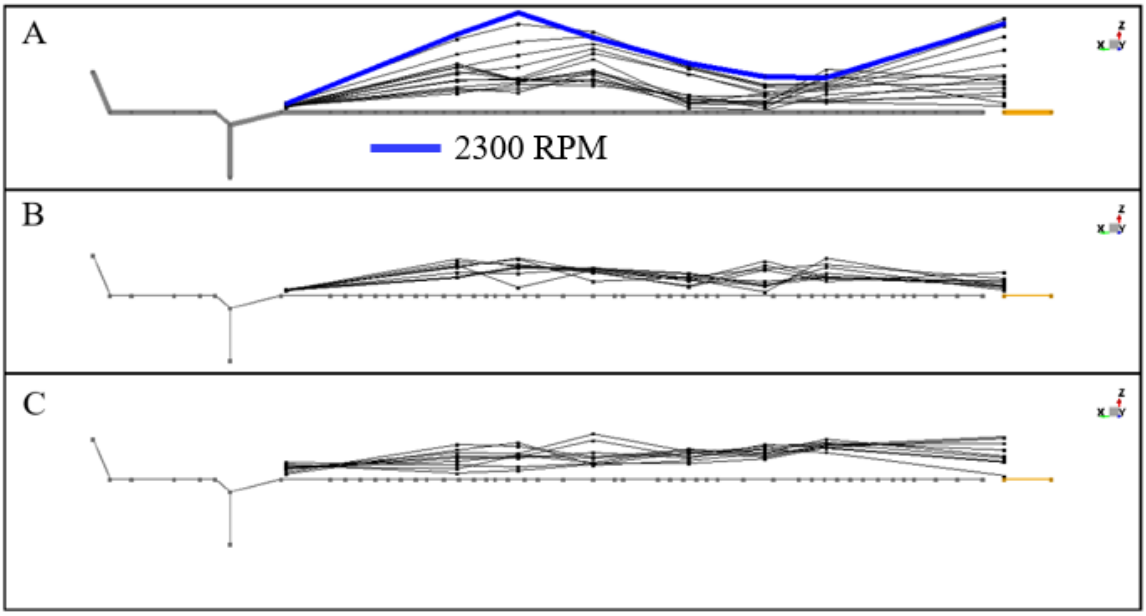

Figure 20: Absolute Magnitude of Operating Deflection Shapes at A) 1600 - 2340 RPM, B) 1200-1600 RPM, C) 800-1200 RPM

6 Structureborne Noise Characterization

An SBN metric was established using measured acceleration and dynamic force. Two hose configurations, a straight hose and a curved hose, were tested to determine the measured mount SBN level and compared it to the FBN level in the hose. It is predicted that regions within the hose with high FBN energy will have a higher SBN levels. This result will validate the prediction that hose clip placement is a viable solution to SBN reduction. The test bench configurations are described followed by data collection procedures and results.

6.1 Test Bench Configurations

A 2.13-meter hose that matches the combined total length of the hose segments used in the hydraulic pressure characterization tests was used for SBN characterization measurements. The test bench was configured for a straight and curved hose with the same hose mount locations. The test bench configuration is shown schematically in Figure 21 and Figure 23 respectively. The primary components and instrumentation used are found in Table 2. The location of the hose mounts, denoted A and B, match the pressure ripple measurements from the segmented hose at 710 mm and 1442 mm from the pump outlet. They are also near locations where there is an expected minimum and maximum FBN energy at 2300 RPM. The lab setup of the test bench for the curved and straight hose is shown in Figure 22 and Figure 24. The mounts were moved to locations A' and B' in a curved hose setup perturbation test to observe the effect of different mounting locations.

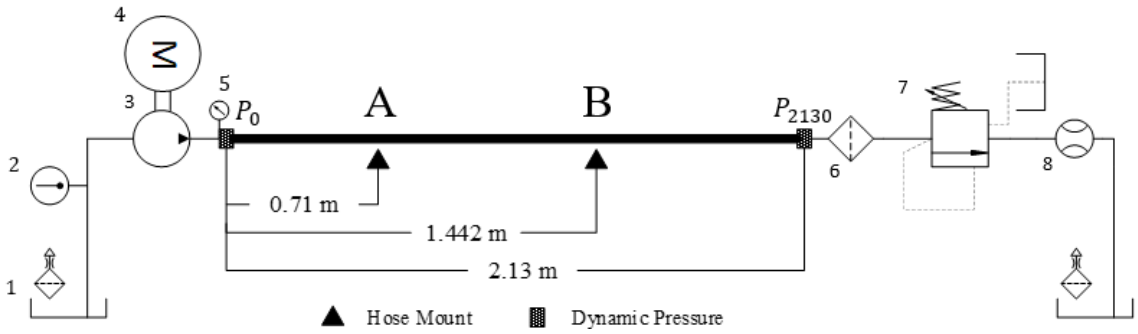

Figure 21: Straight Hose Configuration Schematic

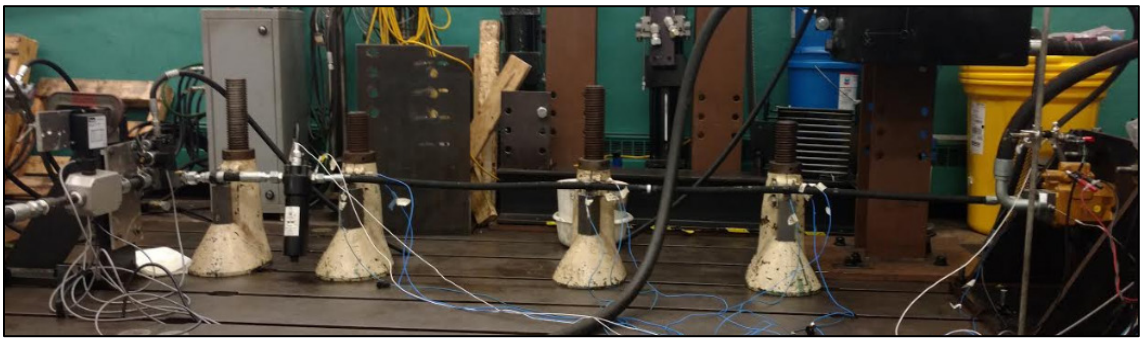

Figure 22: Straight Hose Configuration Setup

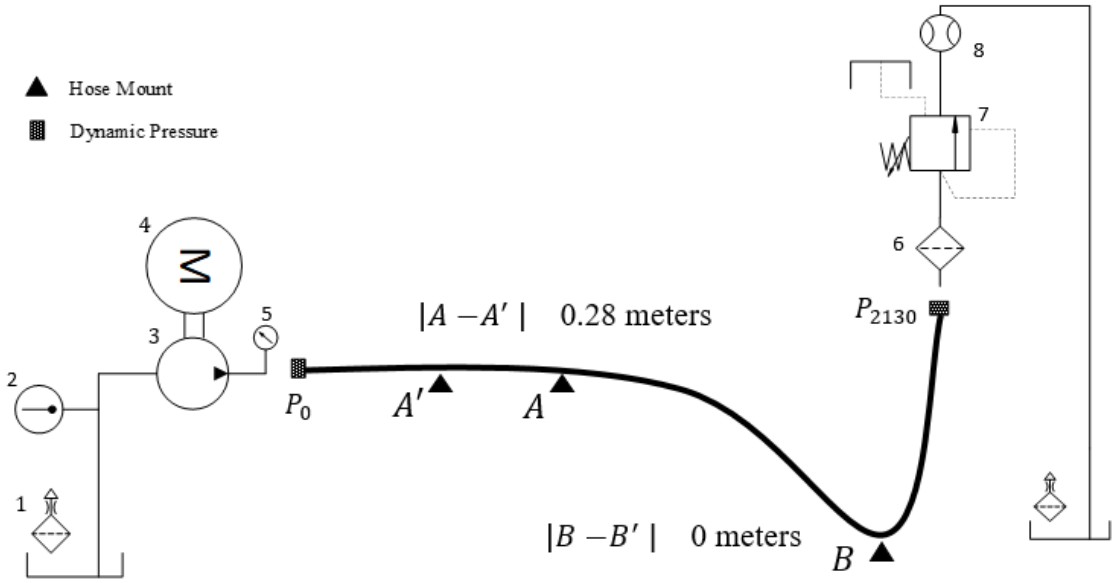

Figure 23: Curved Hose Configuration Schematic

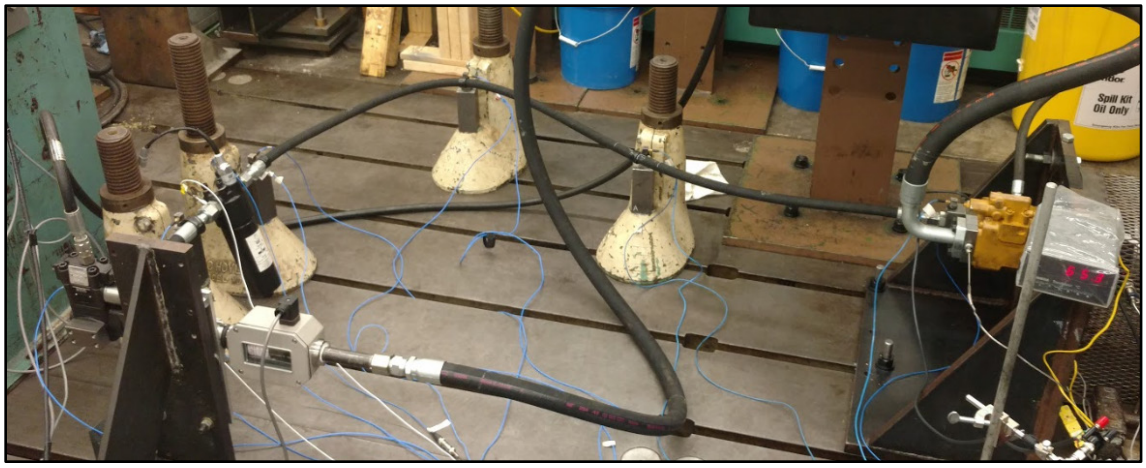

Figure 24: Curved Hose Configuration Setup A-B

6.2 Data Collection Procedures

A SBN metric was formulated using operational force and velocity measurements. This was done with the integrated tri-axial acceleration measured on the bolt head of the hose mount and the tri-axial dynamic force measurements using PCB 260A01 dynamic force transducers. Care was taken to assemble the hose mount with 28 N-m of torque using a digital torque wrench. This provides the 23 kN clamp load needed for an M8 bolt to achieve the calibrated sensor sensitivity. The hose end pressures were measured with PCB 113B22 dynamic pressure transducers. The hose mount and hose end transducer setups are shown in Figure 25.

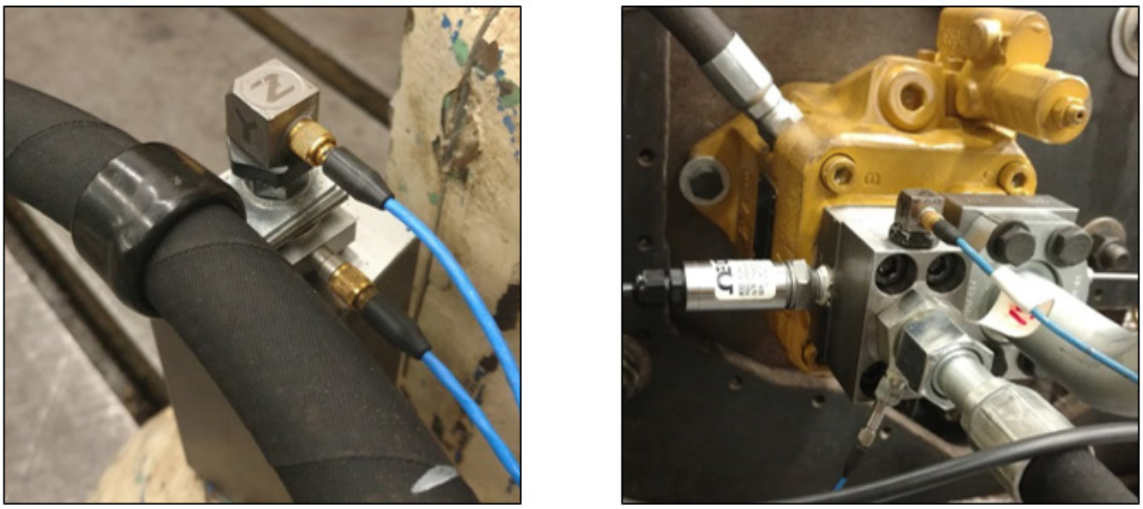

Figure 25: SBN metric data collection (Left) Pump Outlet Pressure Measurement (Right)

Data was collected in 1000 psi, 1500 psi, and 2000 psi CPSS runs from 800 – 2340 RPM. SS runs at 800 RPM-580 psi, 1500 RPM – 1500 psi and 2300 RPM – 2300 psi were also collected. The 1500 psi CPSS results were analyzed since associated ODS data was available from previous characterization testing. Data sets were collected with a sample rate of 3200 Hz and 1 second measurement periods. A Hanning window was used to minimize leakage error. Total time for a complete CPSS was typically 4 minutes.

A perturbation test was performed by moving hose mount A 0.28 meters closer to the pump outlet in the curved hose configuration. The perturbation amount was arbitrary, however, the mount was moved to a location where higher FBN energy in the hose was expected at 2300 RPM. Hose mount B was not moved. The hose mount locations for the perturbation test are shown in Figure 26.

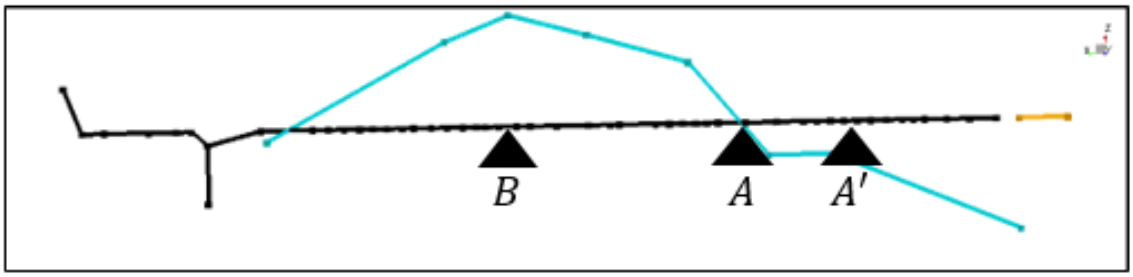

Figure 26: Perturbation Test

6.3 Structureborne Noise Characterization Results

The colormaps shown in Figure 27 show the cross-correlation between the measured dynamic force and pump outlet pressure and the measured acceleration and the pump outlet pressure. The colormaps show that apart from a few fixture resonances near 800 Hz and 1200 Hz documented in Appendix B, the significant energy in the measured force and acceleration spectrums occur predominantly in the pumping frequencies.

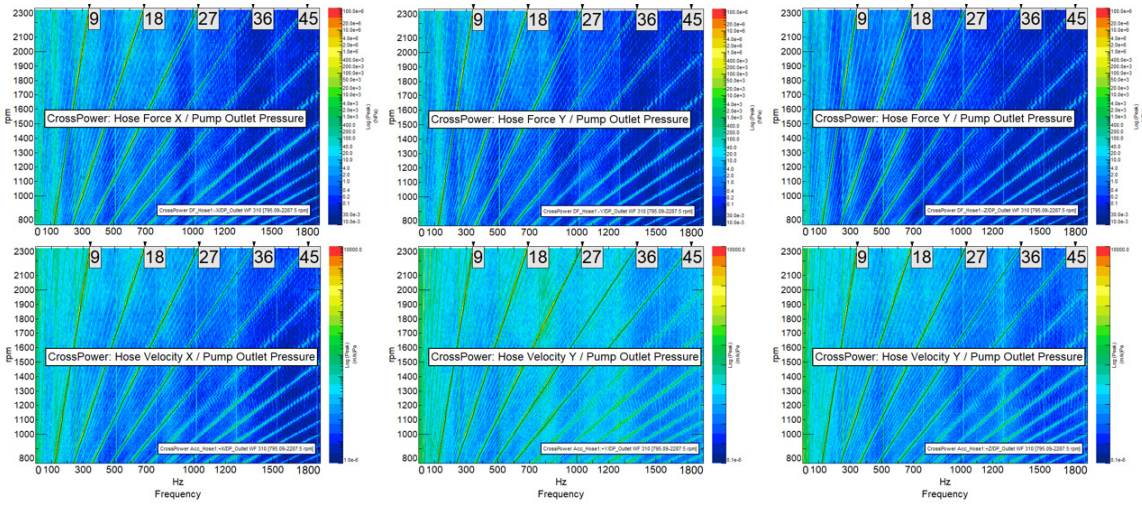

Figure 27: Crosspower of Dynamic Force Measurements and Pump Outlet Pressure Ripple (Top) Crosspower of Velocity Measurements and Pump Outlet Pressure Ripple (Bottom)

The results of the straight hose SBN characterization test using equation (31) is shown in Figure 28 in both a logarithmic and linear scale. It is observed from the SBN

curves that above 1600 RPM the measured SBN at mount B is significantly higher than the measured SBN at the mount A location. This observation follows the prediction of high FBN at mount B and low FBN at mount A at motor speeds where the third fluid mode is excited. It is assumed that the fluid modes are highly damped and the peak effects occur over a wide frequency range. A video analysis processing routine was developed to show the SBN metric overlaid on the hydraulic circuit image at all motor speeds. A snapshot of the video analysis at 2300 RPM is shown in Figure 29**.** The 2300 RPM ODS measurement was overlaid on the video frame to show the FBN and SBN relationship.

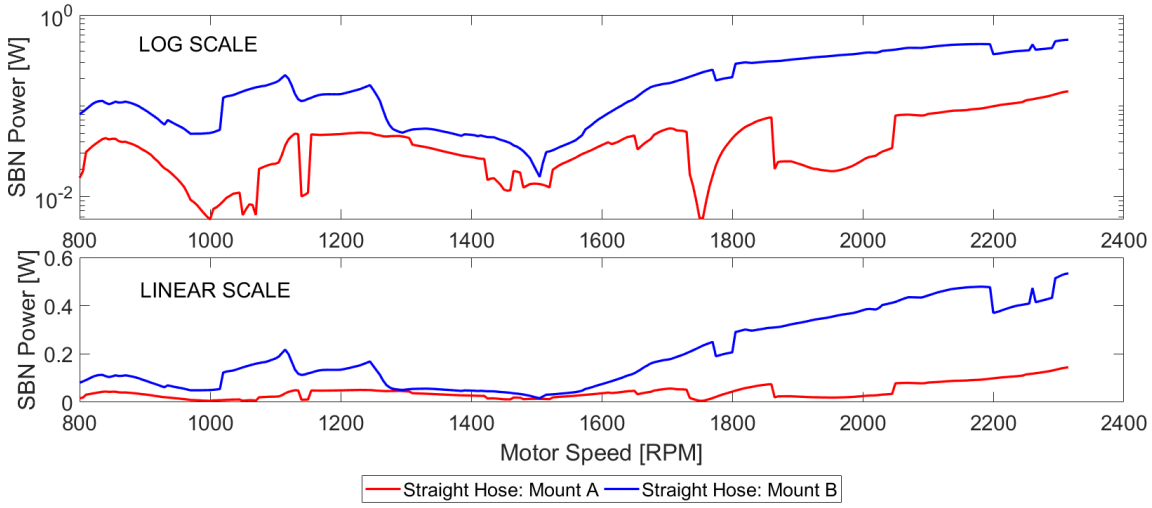

Figure 28: Comparison of Straight Hose Mount A and Mount B SBN

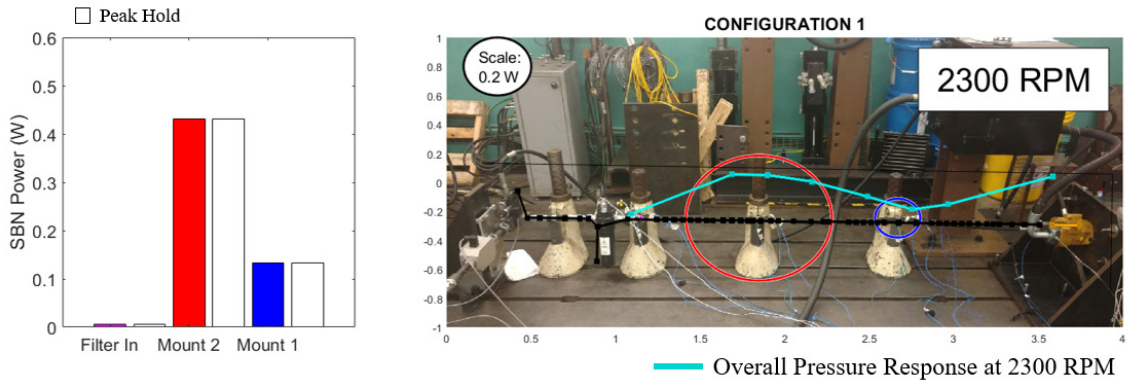

Figure 29: Snapshot at 2300 RPM of Straight Hose Video SBN Analysis

The SBN metric was evaluated and compared for multiple runs for the same circuit configuration. A comparison of two measurement runs is shown in Figure 30. The repeatability of the measurements is acceptable.

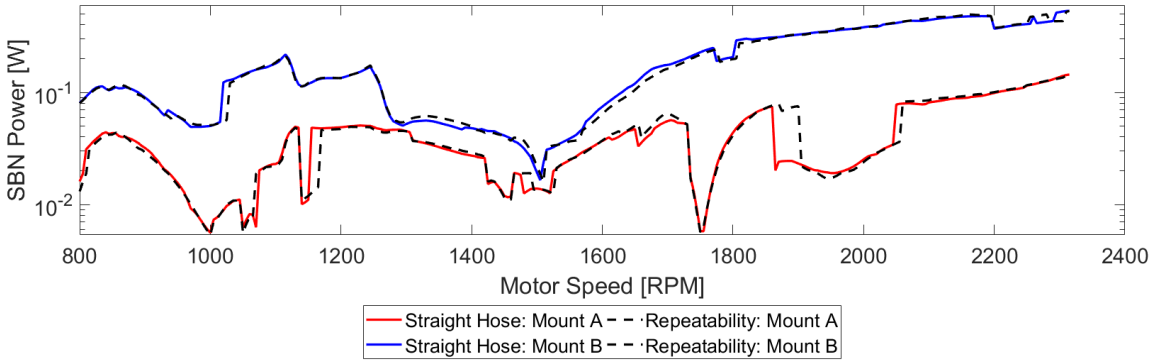

Figure 30: Repeatability of SBN Measurements

The results of the curved hose SBN characterization test using equation (31) is shown in Figure 31 and shows similar results compared to the straight hose test. Above 1800 RPM, the measured SBN at the mount B location is significantly higher than the measured SBN at the mount A location.

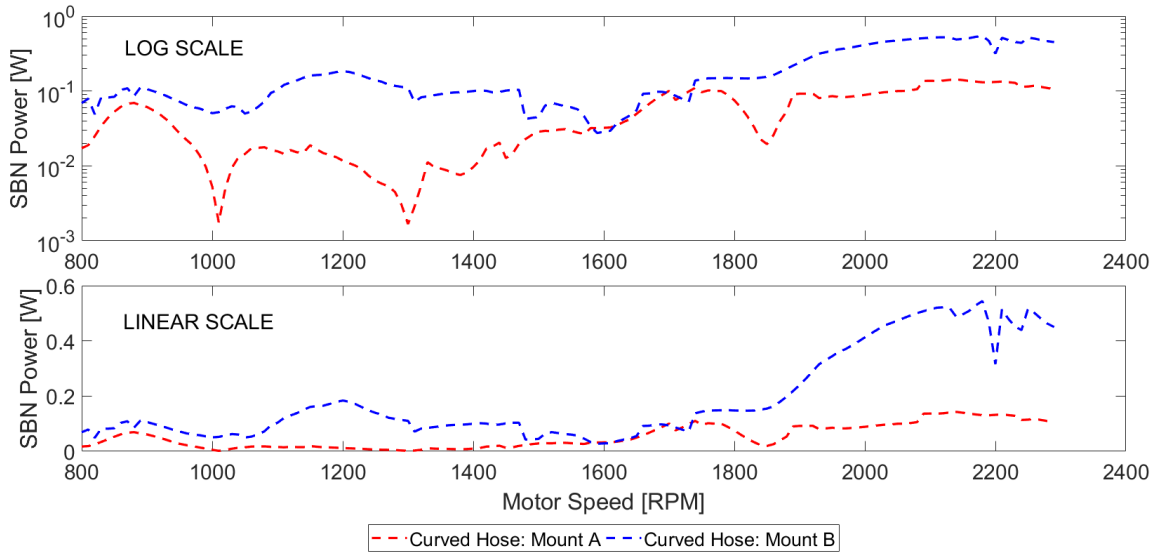

Figure 31: Comparison of Curved Hose Mount A and Mount B SBN

The results of the curved and straight hose characterization tests are shown in the same plot in Figure 32. A significant difference between the two tests was not observed for the data sets processed. It was expected that there would some SBN contribution at mount B for the curved configuration due to a junction coupling effect that would not be present in the straight hose data. The similar SBN curves for mount A and mount B are a single example of the reproducibility of the SBN measurement for a given mount configuration.

A controlled DOE to quantify the reproducibility and SBN curve contribution is recommended.

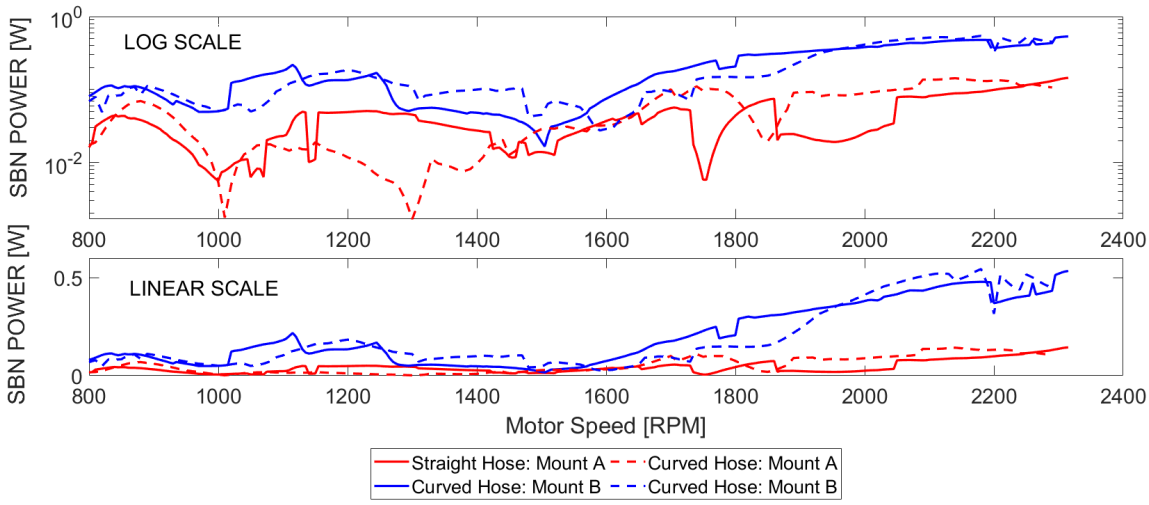

Figure 32: Comparison of Straight Hose and Curved Hose SBN Results

A perturbation test was designed where mount A was moved closer to the pump to a location denoted A'. There was more FBN energy predicted at A' using the fluid pressure ODS. Mount B and Mount B' remained in the same location for both measurements. It was predicted that the measured SBN would be higher for mount A' at motor speeds where the third fluid mode is excited and that the Mount B and B' locations would be similar. The results of the perturbation test are shown in Figure 33 and match the pre-test predictions. More testing is necessary to determine whether the SBN minimum near 1850 RPM is real or an artifact of processing. The results of the perturbation test show that different hose mount configurations for the same hydraulic circuit produce different measured SBN

results. This shows that optimizing the placement of hose clips to a minimized SBN metric could be a viable solution to SBN problems for mobile heavy equipment hydraulic circuits.

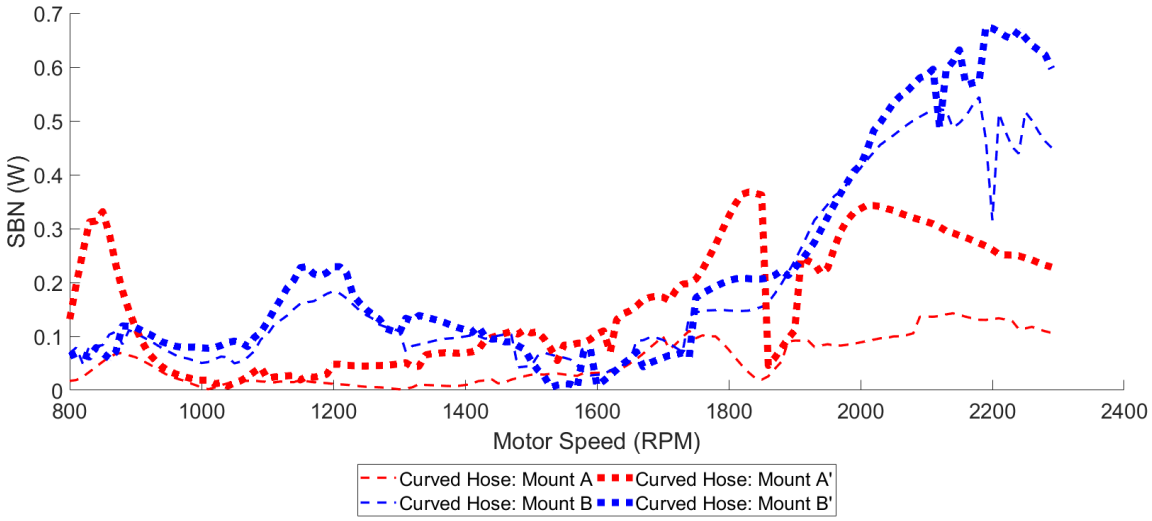

Figure 33: Curved Hose Perturbation Test Results

7 Energy Balancing

Energy balance processing as described in section 2.3.3 requires source FBN power, mount FBN power and mount SBN power for all motor speeds being evaluated. The straight hose configuration data used in the SBN characterization tests were used to evaluate the method and no new data was collected. The source FBN power was determined with source flow ripple and measured outlet pressure ripple using equation (22). The SBN power was determined with measured mount force and velocity using equation (31). The mount FBN power according to equation (23) requires local flow ripple and local pressure ripple at each mount location. The flow ripple anywhere in the hose can be assumed equivalent to source flow ripple before the first fluid restriction. Determining the pressure ripple anywhere in the hose presents a significant measurement challenge. It is not possible to simultaneously measure pressure ripple and the SBN generated at a clipping point because intermediate hose pressure ripple measurements are collected through a drilled and tapped hole in a hydraulic hose adapter. This is shown in as shown in Figure 34.

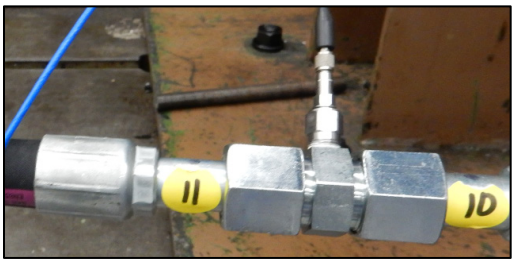

Figure 34: Intermediate Hose Pressure Ripple Measurements

Two methods for generating an FRF were explored to predict hose mount pressure ripple levels based on pump outlet pressure ripple level. The first method generates FRF's

for only the measured locations from the hydraulic pressure ODS tests. The second uses OBMA to extract modal parameters and expand the mode shapes to unmeasured locations. This expanded data is used to generate predictive FRF's. Using the FRF's from measured locations at mount A (710 mm) and Mount B (1442 mm) in the straight hose SBN characterization tests, the accuracy of the energy balance method described by equation (32) was evaluated. The energy balance results were compared with mount FBN predictions using equation (23).

7.1 FRF based on Pressure Ripple Measurements

FRF's based on pressure ripple measurements uses the measured pressure data from the pressure ODS characterization tests described in chapter 5. The mounting locations available are limited by the spatial resolution of the ODS characterization tests. The FRF for each measurement location was determined using equation (12) and is shown diagrammatically in Figure 35. The FRF for the mount A location in chapter 6 is shown in Figure 36. The accuracy using each FRF to predict the measured pressure ripple at each potential hose mount location was tested using SS data recorded at 1500 RPM and 1500 psi. The percent error between each FRF prediction and the pressure ripple measured for 9^{th} and 18^{th} pump order is shown in Table 6. The accuracy of the pressure ripple predictions

appears acceptable although there are instances of significant deviation that would produce significant error in mount FBN predictions.

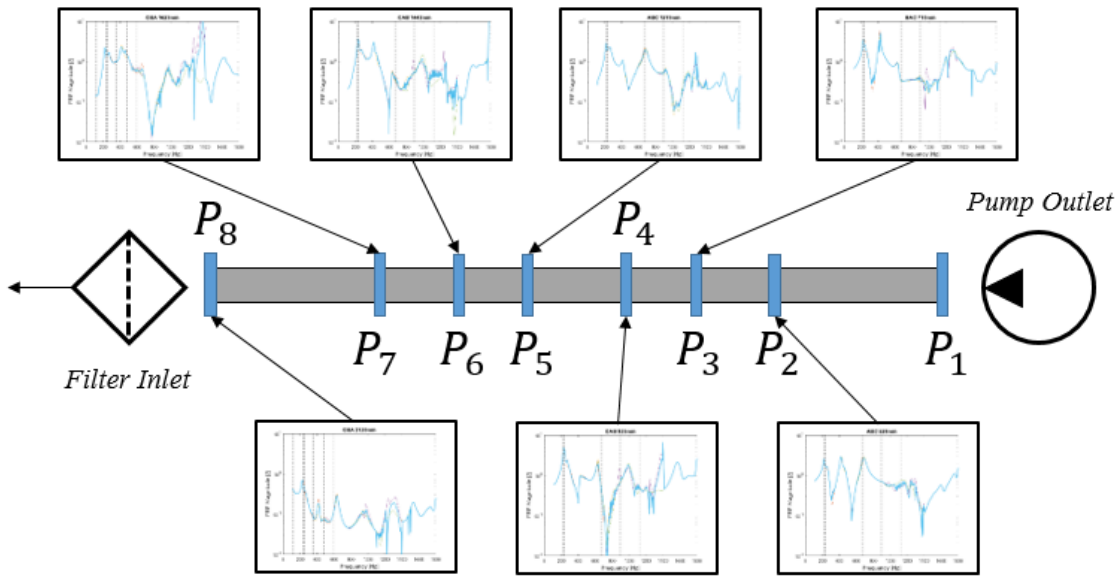

Figure 35: FRF's from Measured Pressure Ripple Data Referencing Pump Outlet Pressure

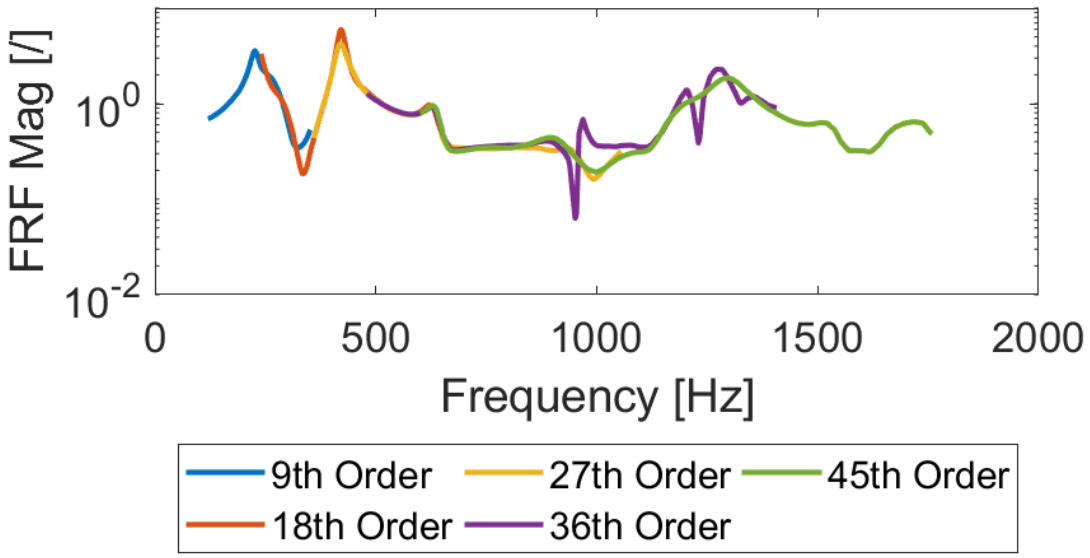

Figure 36: FRF from first 5 Pump Orders at Mount A (710 mm from Pump Outlet)

Table 6: Percent Error Predicting Downstream Pressure Using Measured Pressure FRF's and SS 1500 RPM - 1500 psi Data

	A-B-C		B-A-C		C-A-B		C-B-A	
	9th	18th	9th	18th	9th	18th	9th	18th
528 mm	5%	14%	----	----	----	----	----	----
710 mm	----	----	10%	1%	----	----	----	----
935 mm	----	----	----	----	4%	11%	12%	8%
1219 mm	2%	13%	0%	15%	----	----	----	----
1442 mm	----	----	----	----	6%	15%	----	----
1623 mm	----	----	----	----	----	----	24%	7%
2130 mm	6%	452%	2%	17%	1%	21%	15%	48%

7.2 FRF based on Modal Parameters

FRF based on modal parameters uses the measured pressure data from the pressure ODS characterization tests in chapter 5 and the OBMA techniques in section 2.2.3. Using the extracted order sections and LMS Test.Lab OBMA processing add-in, the frequencies and shapes from each selected stable pole can be determined from each order evaluated. The process for generating an FRF at an expanded location in the outlet hose was determined in the following steps.

1. Organize the measured order sections for each measured location from each pump order of interest using the ODS characterization test data.
2. Use LMS Test.Lab OBMA and the organized order sections to get the modal parameters (frequency, shape, damping, upper and lower residual, complex reference factor) for each pump order of interest.
3. Interpolate the desired expanded location into mode shape vector ensuring the resulting shape is smooth.

4. Use SEREP techniques to generate a transformation matrix and expand the upper and lower residuals to include the new pressure location using equation (18) and equation (19) respectively.
5. The order section can be synthesized using the expanded modal parameters with equation (21) and then used to produce FRF's using the measured outlet pressure ripple order sections and equation (12).

The accuracy of the method was tested by eliminating one DOF from the OBMA processing set and synthesizing order sections using modal parameters extracted from the remaining DOF (Synthesized 6DOF). This synthesized order section was compared against the measured order section. The best case result for the expanded synthesized order is the synthesized order from all DOF (Synthesized 7DOF). This is the accuracy limit based on the finite number of poles selected in the stabilization diagram. The accuracy can be quantified using the least-square error from the measured order evaluated shown in equation (14). The synthesized order section comparison for the mount A and mount B locations from the SBN characterization test is shown in Figure 37 and Figure 39 respectively. The synthesized and measured order sections for all measured DOF's can be found in Appendix E. A comparison of the least-square error between synthesized 6DOF and synthesized 7DOF for all measurement locations is shown in Table 7. The synthesized order section based on modal parameters appears to not work well for 2130 mm when extrapolation of the mode shape is required.

The FRF's generated using synthesized 6DOF order sections are compared with the FRF's using measured order sections for mount A and mount B locations for 9^{th} and 18^{th}

order in Figure 38 and Figure 40 respectively. The synthesized and measured FRF's for 9th and 18th orders for all measured DOF's can be found in Appendix E. The FRF shapes can be quantitatively compared using CSAC and the FRF amplitudes can be compared using FRFSF. The comparison results are shown in Table 8. Increasing the spatial resolution of the ODS tests could improve the synthesized order section and produce FRF's with a better correlation.

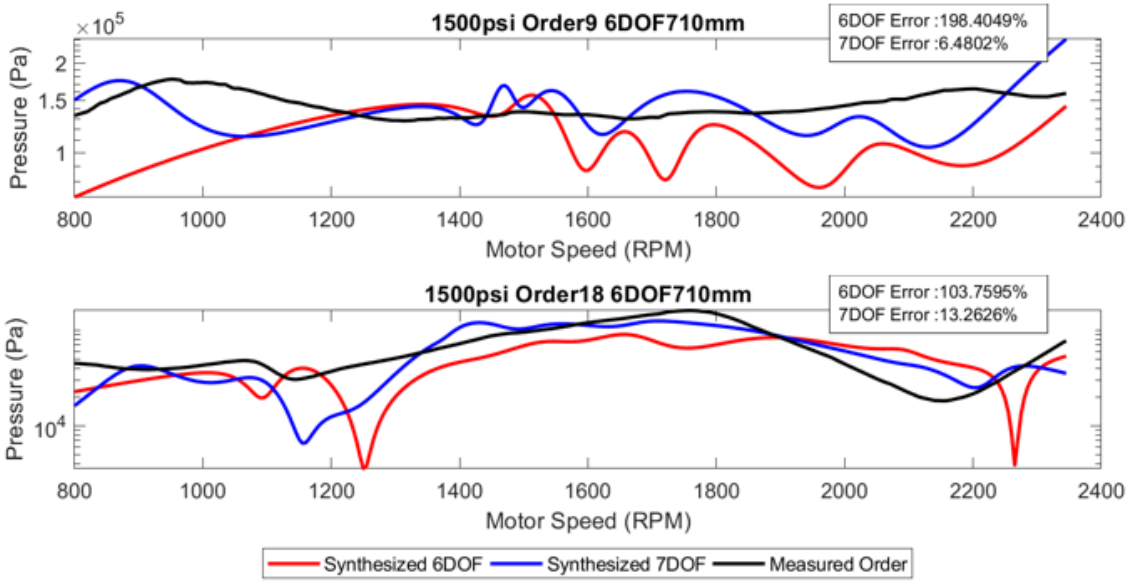

Figure 37: Synthesized and Measured Comparison of 9th and 18th Order Sections at Mount A location (710 mm from Pump Outlet) for 9th Order (Top) and 18th Order (Bottom)

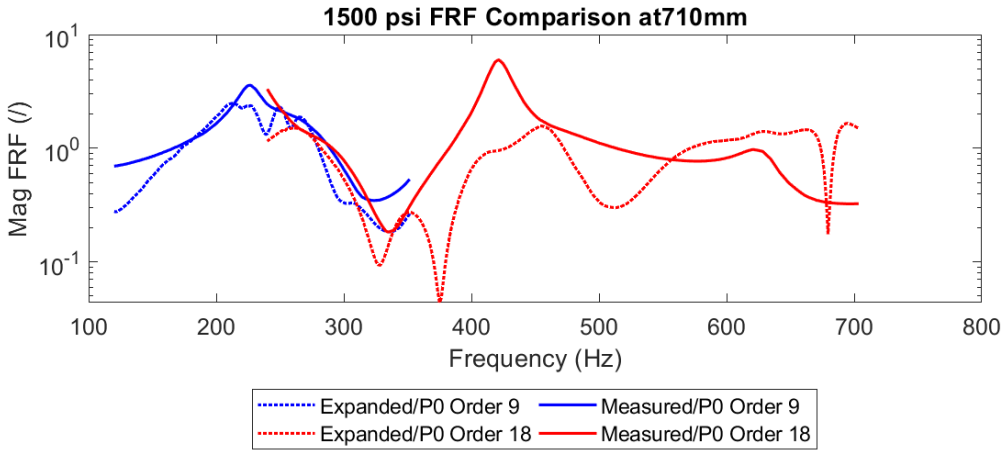

Figure 38: Comparison of Measured FRF and FRF Expanded using Modal Parameters at Mount A Location (710 mm from Pump Outlet)

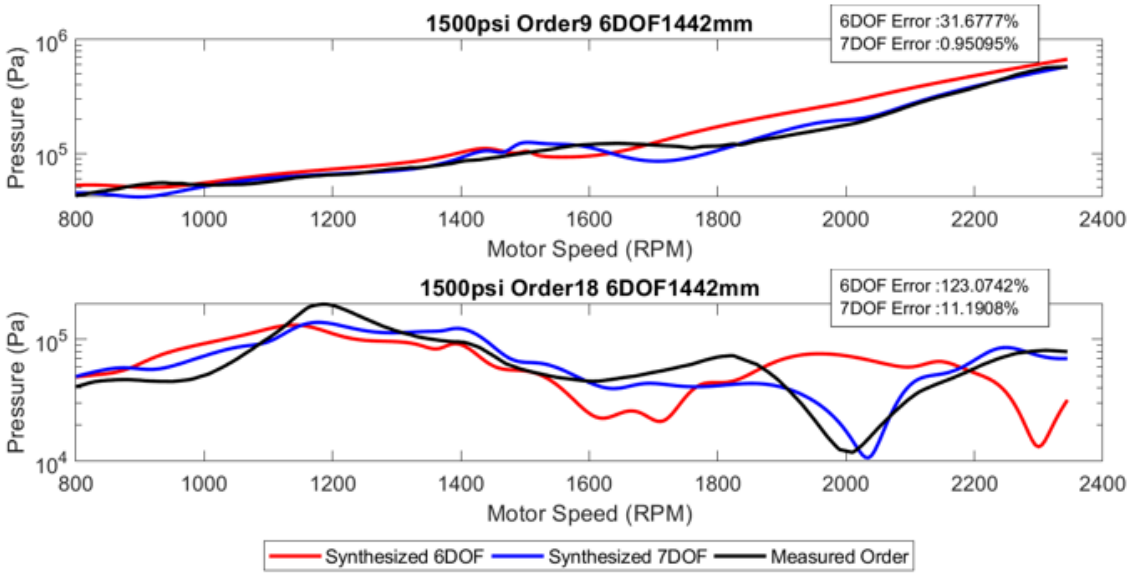

Figure 39: Synthesized and Measured Comparison of 9th and 18th Order Sections at Mount B location (710 mm from Pump Outlet) for 9th Order (Top) and 18th Order (Bottom)

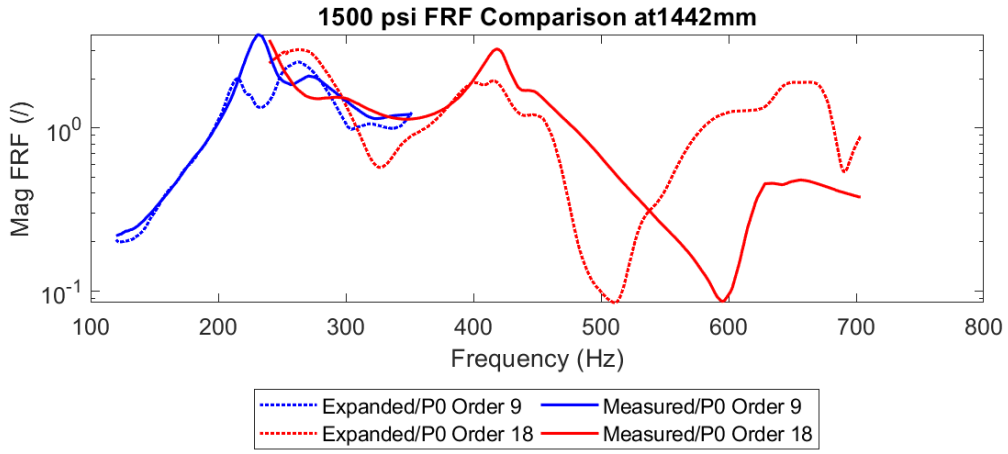

Figure 40: Comparison of Measured FRF and FRF Expanded using Modal Parameters at Mount B Location (1442 mm from Pump Outlet)

Table 7: Least Square Error of Synthesized Orders from Modal Parameters using 7DOF and All DOF

	528 mm	710 mm	935 mm	1219 mm	1442 mm	1623 mm	2130 mm
9th Order							
7 DOF	184%	198%	104%	42%	32%	120%	99654%
All DOF	6%	7%	2%	1%	1%	1%	7%
18th Order							
7 DOF	194%	104%	88%	161%	123%	102%	225852%
All DOF	15%	13%	11%	13%	11%	9%	15%

Table 8: Comparison of Measured FRF to FRF from Extracted Modal Parameters using CMAC and FRFSF

	528 mm	710 mm	935 mm	1219 mm	1442 mm	1623 mm	2130 mm
9th Order							
CSAC	11%	5%	3%	0%	5%	5%	13%
FRFSF	1.5	0.8	0.8	0.8	0.9	0.9	19.9
18th Order							
CSAC	13%	5%	11%	5%	6%	0%	2%
FRFSF	1.4	0.7	1.1	1.2	1.2	1.2	59.4

7.3 Energy Balance Results

The energy balance was quantified for straight hose configuration test data using equation (32) and the FRF's from measured order sections. The noise metric power flow for the 2000 RPM condition is shown diagrammatically in Figure 41. The energy balancing for the entire motor speed sweep is shown in Figure 42 for mount A and in Figure 43 for mount B.

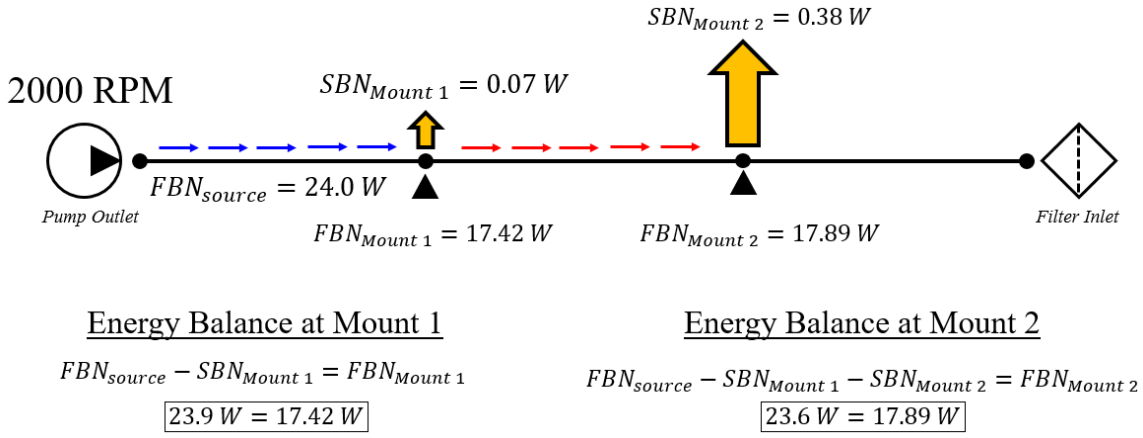

Figure 41: Energy Balance Results at 2000 RPM for both Mounts in the Straight Hose Configuration

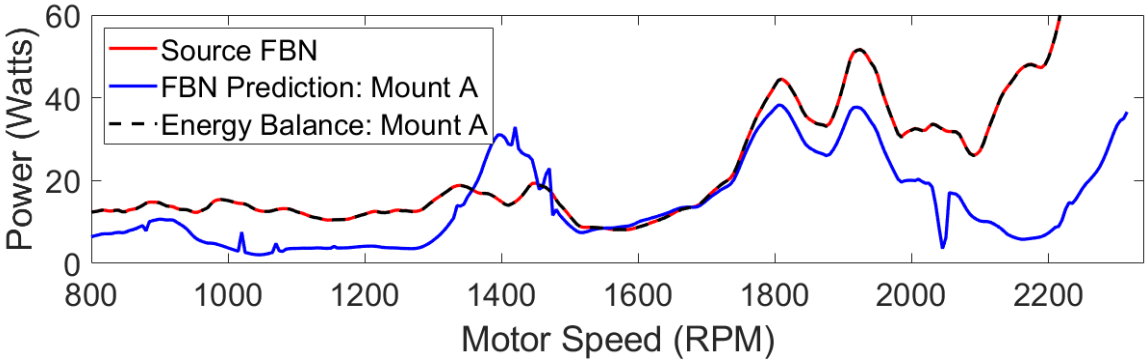

Figure 42: Energy Balancing at Mount A

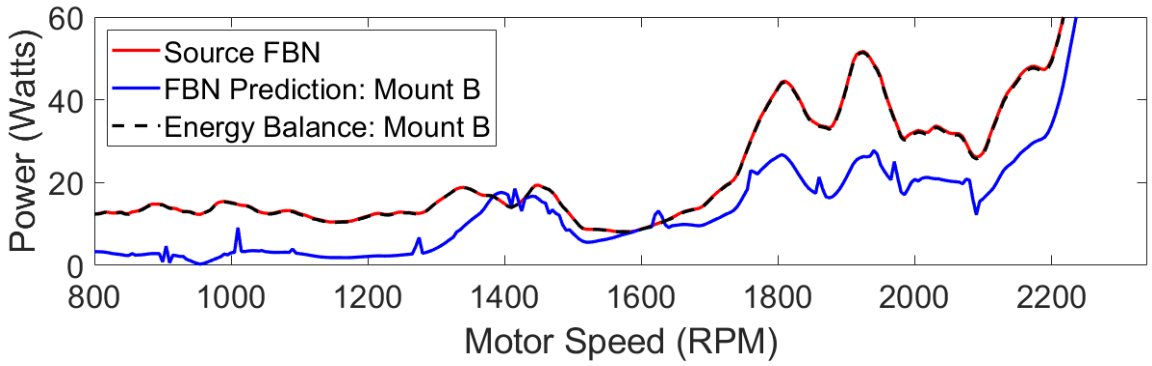

Figure 43: Energy Balancing at Mount B

The expected balance of power through the outlet hose does not match with FBN predictions at each mount location. There may be unmeasured loss mechanisms or pressure ripple prediction methods are not accurate enough to validate the current formulation of the energy balance equation. Averaging measured FRF's from multiple speed sweep data sets could improve measured FRF approach. Increasing the spatial resolution of the fluid characterization process could improve the pressure ripple FRF's based on modal parameters.

8 Discussion

This project has produced a test bench that replicates machine circuit FBN without the influence of other noise sources present in situ. The test bench design isolates the SBN analysis to primarily FBN and hose deflection contributions. Test procedures were developed to characterize the FBN and SBN for a simple hydraulic circuit using measured pressures in the hose and hose deflections both vertically and radially. It was found that the FBN at the hose clipping point is directly proportional to the SBN measured at the hose clip for a specific excitation condition. This was supported by a lower measurement of SBN at a hose clip placed at a perceived node in a fluid standing wave compared to a measurement at a location with higher FBN. This shows promise that the optimized placement of hose clips can be a viable solution to SBN reduction in heavy equipment circuits.

The experimental test bench developed is unique from existing test rigs that use hydraulic circuits on compliant structures for FSI model validation [39]. The likelihood of errors due to base excitation of fixture resonances was significantly reduced by attaching the hoses as close as possible to the bedplate using the massive jack stands. Additionally, use of a real axial piston pump conserved the pumping dynamics and pump casing contributions.

The observed direct FBN to SBN relationship occurred over a wider frequency range than expected and the shape of the pressure ODS in the hose was dominated by fluid modes excited primarily by first pump order energy. The broader range is believed to be a result of high modal damping that producing a wide peak in the FRF at the fluid resonance.

The same broad frequency range result was observed in an experimental hose clip optimization study at the University of Bath [25]. SBN reductions were analyzed for each order in this study and not the sum of the orders. Differences between best and worst placement were only observed in the first pump order. The circuit that was used in the University of Bath experiments had a 90° bend and the optimal clip locations were assumed to be primarily based on the junction coupling effects at this elbow and not the fluid modes. Junction coupling does not appear to be a significant FSI contributor to SBN based on the lack of differences observed between the straight and curved configurations. It is expected that junction coupling SBN contribution is significant and that this could be proven and quantified with a controlled DOE using multiple hose lengths and mount configurations. Poisson coupling is the assumed dominant FSI mechanism for the straight hose configuration.

An EMA performed on the hydraulic pipelines of an aircraft system quantified the curvature effect on natural frequencies of long aircraft hydraulic hoses. It was also concluded that long line lengths will reduce the hydraulic line resonances to within pump operating frequencies [32]. This result was observed and it is proposed as a general design guideline that long hose lengths that will excite higher order fluid modes with first pump order energy should be avoided. This aircraft hydraulic study also concluded that most SBN energy is lost through the first hose mount. This was not observed and it is thought that this result was primarily due to pump casing SBN being transmitted through rigidly attached pipelines. The pump casing SBN in this project is assumed to have been damped by the flexible hoses and the SBN measured is due to FBN and hydraulic line resonances.

The observed errors in the balancing of transmitted FBN power may be associated with either unmeasured noise loss mechanisms or the pressure ripple prediction methods are inaccurate. It is assumed that the latter is more probable than the former. Averaging multiple formulated FRF's for a given measurement location using the measured approach or a finer spatial resolution for the OBMA approach could improve the pressure ripple predictions.

Additional hose clip configurations should be tested to validate the concluded FBN to SBN results. The small number of configurations tested limits the confidence in generalizing the conclusions of this project to all possible circuit designs. The results show promise that the test methods are able to quantify and rank various hose clip locations effectively. There was a tested configuration that did not match the concluded FBN to SBN relationship for a straight hose, but it is believed that this was due to an incorrect mount assembly. A closer analysis into measurement reproducibility by repeated mount assemblies for each configuration is recommended.

A noted flaw in the study design is that the ODS shapes of the hose structure were not performed for the circuit used in the curved and straight hose SBN tests. It is expected that any reconfiguration of the hose mounts will alter the structural modal parameters of the hydraulic line. In future tests, the hose deflection should be characterized in the configuration used for mount SBN analysis. In this way, the contribution of hose deflection can be correctly evaluated as a contributor to the SBN measurement. It is also recommended that the hose deflection is measured using triaxial accelerometers for a more representative understanding.

Reproducing the observed FBN and SBN relationship at clipping points, improving energy balance results and assessing inaccessible clip locations is the recommended future direction for this project. The conclusions of the presented work can be validated using the same test procedures and a longer hose that will excite the fourth fluid mode with first pump order frequencies. It is expected that this will produce significantly different ODS shapes over the pump operating range for hose clip SBN evaluation. The optimal hose clip locations can be further evaluated by reintroducing the ABN mechanism to the scope. The SBN to ABN transfer could be measured with a microphone and a characterized plate beneath the hose clip. The locations can be ranked using radiated sound power or sound intensity. It is assumed that by improving the methods for predicted pressure ripple based on pump outlet pressure, the energy balance results will be improved. Averaging generated FRF's or a finer spatial resolution for the modal superposition approach is recommended. A controlled DOE with the metrics and methods established in this project could be used iteratively to quantify the effect of attachment parameters. Estimating each term of the equation of motion of a hose using these predicted effects and hydraulic noise metrics could provide an SBN prediction at an inaccessible mount location.

The test methods and conclusions that have been drawn from this research will be applied to planned continued hydraulic noise research at MTU. The procedures and metrics established will be expanded to more complex circuits by the systematic reintroduction of hydraulic components and variables until the complete reference hydraulic circuit is reproduced. The knowledge gained through this project will be used to update hydraulic

system design guidelines and best practices. The data sets will be used to correlate models for virtual development.

9 Conclusions

The purpose of this project was to confirm that optimized placement of hose clips on a hydraulic hose is a viable solution to SBN reduction. This was accomplished by developing a set of test procedures and energy metrics for characterizing the hydraulic fluid and hydraulic line resonances and predicting local FBN to SBN transfer efficiencies. An attempt was made at balancing the FBN and SBN through the circuit using a power flow approach.

Characterization of the hydraulic noise mechanisms using a typical EMA approach could not be used since it was not possible to isolate and measure the excitation input. Additionally, the measurements needed to be collected in a specific operational condition due to stiffness properties of the system being different for different fluid mean pressure levels. An attempt to characterize using OBMA, an OMA method designed specifically for rotating equipment, was not able to distinguish the theoretical fluid modes from interacting structural modes. A finer spatial resolution may improve OBMA results in future tests. An ODS approach to identifying the frequency of the fluid modes was an acceptable alternative.

The ODS approach relies on an assumption that the fluid mode shape dominates the ODS at pumping frequencies near the fluid natural frequencies. There were no curve fitting techniques used in this approach. An estimate for frequency and shape of the fluid modes were assumed by visual inspection of the ODS and knowledge of the theoretical shapes based on hose length, wave speed and assumptions of the hose end boundary conditions. It was observed that the fluid modes excited by the energy in the first pump

order dominate the shape of the fluid ODS over the pump operating range. It was assumed that the structural mode contribution to the dynamic pressure ODS was negligible.

The described ODS characterization procedure was able to identify the third fluid mode excited at 2300 RPM. The third fluid mode at this speed had a peak and node near 1/3 and 2/3 of the total hose length from the pump outlet respectively. These locations were selected as optimal hose clip locations assuming an FBN minimum and FBN maximum. Two hydraulic circuits, a straight 2.13-meter hose and a curved 2.13-meter hose, were configured with mounts at these locations. The SBN was measured over a sweep of the pump operating range with a constant 1500 psi system pressure. Both circuit tests revealed a direct relationship between the FBN in the hose and the measured SBN at the hose clip when the third fluid mode was excited. Moving the hose clip away from the node toward a location of higher FBN produced higher SBN. This observation showed the test methods developed are capable of ranking SBN at hose clips and that hose clip placement can be a viable solution to SBN reduction. This was supported by a perturbation test. Validation of this result using identical methods with a variety of hydraulic circuits is recommended.

The expected results of the power flow balancing approach were not achieved. It was theorized that the FBN power at any location in the outlet hose could be predicted by subtracting the SBN power at the hose mounts from the initial pump source FBN power. Two methods for determining the pressure ripple in the hose were developed since measuring mount location pressure ripple and mount SBN simultaneously was not possible.

It is expected that planned further investigations will increase the confidence level of the concluded FBN to SBN relationship that is currently limited by the small number of configurations tested. Additional experiments to quantify the SBN to ABN efficiency and junction coupling SBN contributions is recommended. This research has successfully provided a test bench, test framework and promising results for continued test-based hydraulic noise research at MTU.

10 Reference List

[1] *Occupational Noise Exposure, 29 CFR § 1910.95, 2008.*

[2] E. Spencer and P. Kovalchik, "Heavy construction equipment noise study using dosimetry and time-motion studies," *Noise Control Engineering Journal,* vol. 55, no. 4, pp. 408-416, 2007.

[3] S. J. Skaistis, "Hydraulic fluidborne noise mechanics," in *SAE Committee A-6 Aerospace Fluid Power and Control Technologies Symposium, October 8, 1995 - October 8, 1995*, Palm Springs, CA, United states, 1975: SAE International.

[4] K. Edge, "DESIGNING QUIETER HYDRAULIC SYSTEMSSOME RECENT DEVELOPMENTS AND CONTRIBUTIONS," *Proceedings of the JFPS International Symposium on Fluid Power,* vol. 1999, no. 4, pp. 3-27, 1999.

[5] (2018). *Prasp - hydraulic fluid-borne noise modelling software* [Web Page]. Available: http://www.bath.ac.uk/mech-eng/research/ptmc/prasp/index.html

[6] (2018). *DSH plus by FLUIDON* [Web Page]. Available: https://altairhyperworks.com/partner/dshplus

[7] R. D. Strunk, "Silencer for hydraulic piston pump pressure pulsations," in *International Off-Highway and Powerplant Congress and Exposition, September 9, 1991 - September 12, 1991*, Milwaukee, WI, United states, 1991: SAE International.

[8] M. Qatu, D. Llewellyn, and R. Edwards, "Correlation of Hydraulic Circuit Dynamic Simulation and Vehicle," 2000-03-06, 2000.

[9] H. Wang, O. Patil, Q. Yuan, and A. H. Jagoda, "NVH Development of Digital Hydraulics System for Off-Highway Vehicle Applications," 2015-09-29, 2015.

[10] G. Silva, "Wear Generation in Hydraulic Pumps," 1990-09-01, 1990.

[11] S. Skaistis, *Noise control of hydraulic machinery*. New York; Basel: M. Dekker, 1988.

[12] M. Maess and L. Gaul, "Simulation of Vibro–Acoustics in Flexible Piping Systems," *GAMM-Mitteilungen,* vol. 28, no. 1, pp. 37-55, 2005/06/01 2014.

[13] H.-Y. Lai, *Experimental Comparison of Test Methods for Structure-borne Sound Power Measurement*. 2007.

[14] Y. Braikia, M. Melon, C. Langrenne, É. Bavu, and A. Garcia, "Evaluation of a separation method for source identification in small spaces," *The Journal of the Acoustical Society of America,* vol. 134, no. 1, pp. 323-331, 2013/07/01 2013.

[15] T. Opperwall and A. Vacca, "A combined FEM/BEM model and experimental investigation into the effects of fluid-borne noise sources on the air-borne noise generated by hydraulic pumps and motors," *Proceedings of the Institution of Mechanical Engineers, Part C: Journal of Mechanical Engineering Science,* vol. 228, no. 3, pp. 457-471, 2014.

[16] T. Yamazaki and E. Kojima, "Prediction of sound power radiated from oil hydraulic pump using FEM and BEM," *Acoustical Science and Technology,* vol. 24, no. 2, pp. 103-105, 2003.

[17] A. S. Tijsseling and A. Anderson, "A. Isebree Moens and D.J. Korteweg: On the speed of propagation of waves in elastic tubes," in *11th International Conferences on Pressure Surges, October 24, 2012 - October 26, 2012*, Lisbon, Portugal, 2012, pp. 227-245: BHR Group Limited.

[18] P. Moussou, Lafon, PH., Potapov,S.,Paulhiac,L., Tijsseling,A.S., "Industrial Cases of FSI due to Internal Flows," in *Proceedings of the 9th International Conference on Pressure Surges*, Chester, UK, 2004.

[19] D. C. Wiggert, F. J. Hatfield, and S. Stuckenbruck, "ANALYSIS OF LIQUID AND STRUCTURAL TRANSIENTS IN PIPING BY THE METHOD OF CHARACTERISTICS," *Journal of Fluids Engineering, Transactions of the ASME,* vol. 109, no. 2, pp. 161-165, 1987.

[20] D. K. Longmore and A. Schlesinger, "Relative Importance of the Various Vibration Transmitting Mechanisms in Hoses in Typical Hydraulic Systems," *Proceedings of the Institution of Mechanical Engineers, Part I: Journal of Systems and Control Engineering,* vol. 205, no. 2, pp. 105-111, 1991/05/01 1991.

[21] D. C. Wiggert and A. S. Tijsseling, "Fluid transients and fluid-structure interaction in flexible liquid-filled piping," *Applied Mechanics Reviews,* vol. 54, no. 5, pp. 455-481, 2001.

[22] D. Ferràs Segura, "Fluid-structure interaction during hydraulic transients in pressurized pipesexperimental and numerical analyses," EPFL.

[23] S. Li, B. W. Karney, and G. Liu, "FSI research in pipeline systems – A review of the literature," *Journal of Fluids and Structures,* vol. 57, pp. 277-297, 2015/08/01/ 2015.

[24] S. Riedelmeier, S. Becker, and E. Schlucker, "Identification of the strength of junction coupling effects in water hammer," *Journal of Fluids and Structures,* vol. 68, pp. 224-244, 2017.

[25] A. H. M. Kwong and K. A. Edge, "Structure-Borne Noise Prediction in Liquid-Conveying Pipe Systems," *Proceedings of the Institution of Mechanical Engineers, Part I: Journal of Systems and Control Engineering,* vol. 210, no. 3, pp. 189-200, 1996/08/01 1996.

[26] K. A. Edge, O. P. Boston, S. Xiao, M. J. Longvill, and C. R. Burrows, "Pressure pulsations in reciprocating pump piping systems. Part 2: experimental investigations and model validation," *Proceedings of the Institution of Mechanical Engineers. Part I, Journal of systems and control engineering,* vol. 211, no. 13 I 3, pp. 239-250, 1997.

[27] *Hydraulic fluid power - Determination of pressure ripple levels generated in systems and components - Part 1: Method for determining source flow ripple and source impedance of pumps.*, 2015.

[28] K. A. Edge and D. N. Johnston, "'Secondary source' method for the measurement of pump pressure ripple characteristics part 1. Description of method," *Proceedings of the Institution of Mechanical Engineers. Part A. Power and process engineering,* vol. 204, no. 1, pp. 33-40, 1990.

[29] C. Bramley and N. Johnston, "Comparison of Methods for Measuring Pump Flow Ripple and Impedance," no. 58332, p. V001T01A008, 2017.

[30] A. G. T. J. Heinsbroek, "Fluid-structure interaction in non-rigid pipeline systems," *Nuclear Engineering and Design,* vol. 172, no. 1-2, pp. 123-135, 1997.

[31] D. Ferras, P. A. Manso, A. J. Schleiss, and D. I. C. Covas, "Fluid-structure interaction in straight pipelines with different anchoring conditions," *Journal of Sound and Vibration,* Article vol. 394, pp. 348-365, 2017.

[32] P.-X. Gao, J.-Y. Zhai, Y.-Y. Yan, Q.-K. Han, F.-Z. Qu, and X.-H. Chen, "A model reduction approach for the vibration analysis of hydraulic pipeline system in aircraft," *Aerospace Science and Technology,* vol. 49, pp. 144-153, 2016.

[33] T. Opperwall and A. Vacca, "A Transfer Path Approach for Experimentally Determining the Noise Impact of Hydraulic Components," 2015-09-29, 2015.

[34] J. E. Drew, D. K. Longmore, and D. N. Johnston, "Measurement of the longitudinal transmission characteristics of fluid-filled hoses," *Proceedings of the Institution of Mechanical Engineers. Part I, Journal of systems and control engineering,* vol. 211 I 3, no. 13, pp. 219-228, 1997.

[35] T. A. Fiorentin, N. S. Ferguson, J. M. Renno, and A. Lenzi, "Structural response of an aircraft fuselage to hydraulic system - A wave and mobility approach," *Noise Control Engineering Journal,* vol. 61, no. 1, pp. 87-99, // 2013.

[36] E. T. Lee, "Optimization of Local Stiffness for Reducing Off-Highway Machinery Interior Noise," 2017-06-05, 2017.

[37] G. H. Koo and Y. S. Park, "VIBRATION REDUCTION BY USING PERIODIC SUPPORTS IN A PIPING SYSTEM," *Journal of Sound and Vibration,* vol. 210, no. 1, pp. 53-68, 1998/02/12/ 1998.

[38] K. Yang, Q. S. Li, and L. Zhang, "Longitudinal vibration analysis of multi-span liquid-filled pipelines with rigid constraints," *Journal of Sound and Vibration,* Article vol. 273, no. 1-2, pp. 125-147, 2004.

[39] A. Waitschat, L. Nordmann, F. Thielecke, and V. Pommier-Budinger, "Enhanced toolbox for the combined analysis of fluid-And structure-borne noise of hydraulic systems," in *BATH/ASME 2016 Symposium on Fluid Power and Motion Control, FPMC 2016, September 7, 2016 - September 9, 2016*, Bath, United kingdom, 2016, p. Fluid Power Systems and Technology Division: American Society of Mechanical Engineers.

[40] B. Peeters, H. Van Der Auweraer, P. Guillaume, and J. Leuridan, "The PolyMAX frequency-domain method: A new standard for modal parameter estimation?," *Shock and Vibration,* vol. 11, no. 3-4, pp. 395-409, 2004.

[41] G. K. J. Golinval. *Experimental Modal Analysis*. Available: http://www.ltas-vis.ulg.ac.be/cmsms/

[42] T. Marinone and A. Moya, "Comparison of FRF correlation techniques," in *33rd IMAC, a Conference and Exposition on Structural Dynamics, 2015, February 2, 2015 - February 5, 2015*, Orlando, FL, United states, 2015, vol. 3, pp. 299-310: Springer New York LLC.

[43] P. Avitabile, "Model reduction and model expansion and their applications Part 1 - Theory," in *23rd Conference and Exposition on Structural Dynamics 2005, IMAC-XXIII, January 31, 2005 - February 3, 2005*, Orlando, FL, United states, 2005, p. Society for Experimental Mechanics (SEM): Springer New York LLC.

[44] Siemens, "LMS TestLab Operational Modal Analysis," in "Help Documentation," 2017.

[45] K. Janssens, Z. Kollar, B. Peeters, S. Pauwels, and H. Van der Auweraer, *Order-based resonance identification using operational PolyMAX*. 2006.

[46] J. Blough, *A survey of DSP methods for rotating machinery analysis, what is needed, what is available [1]*. 2003, pp. 707-720.

[47] Siemens, "LMS TestLab Order-based Modal Analysis," in "Help Documentation," 2017.

A Hydraulic Test Bench Component List

A.1 2.13-meter Hose Test Configuration

Table 9: 2.13-Meter Hose Configuration Component List

Component	Part Number	Description	Manufacturer
Power Unit			
Motor Drive Unit	ACS550	Drive Unit	ABB
Electric Motor	405THFS8036	100 HP 3-Phase	Marathon Motors
Motor Side Coupling	M70022824	2 7/8 – 3/4 keyed shaft	Magnaloy
Elastomeric Spider	M770H5	--	Magnaloy
Pump Side Coupling	M700A1316	13T splined shaft	Magnaloy
Hydraulic Circuit			
Hydraulic Reservoir	--	25 Gallon Reservoir	Buyers
Reducer	--	1 1/4 - 2 NPTF Reducer	--
Suction Hose	--	SAE 100R6-20	
Gauge Port Block	Main 2303-20-20	-20 C61 gauge port block	Main Mfg.
Pump	LA10VO28DR/52L-VSC-11N00-S1608	28cc Axial Piston Pump	Bosch Rexroth
Case Drain Hose		716 -8 to -8 STOR	
Gauge Port Block	Main 2303-12-12-M10	-12 C61 gauge port block	Main Mfg.
Adapter	Main 1173-12-12-M10	-12 C61 to -12 STOR	Main Mfg.
Adapter	--	-12 STOR to -10 ORFS	
Hose	--	2.13-meter SAE -10	
Adapter	--	-10 ORFS to -12 STOR	
Filter		High Pressure Filter	3000 psi
Adapter	--	-12 STOR to -12 ORFS	
Hose	--	1 foot SAE 100R6-12	
Adapter Block	1173-12-12	12 STOR to -12 C61	Main Mfg.
Load Valve	R5V06-533-16-P2-G0Q-A1	3-port electric proportional pressure relief valve	Parker
Hose	SAE -8 Hose	Drain Line	--
Adapter Block	1101-12-00	Block A Port	Main Mfg
Adapter Block	1149-12-12M10	Outlet Adapter	Main Mfg.
Sch. 40 Pipe	--	7.5 in	--
Flow Meter	FLMH-3420SS-MA	3/4"NPTF 20GPM	Omega
Sch. 40 Pipe	--	4 in	--
Adapter	--	¾ NPT to SAE -16	--
Return Hose	--	SAE 100R6-16	
Tee Adapter	--	1” X ¾” X ¾”	--
Instrumentation			
Tachometer	--	Laser Type	--
Thermocouple	--	Type K	Omega
Digital Temp. Display	--	Trendicator	Omega
Static Pressure	PX309-5KGV	5000 PSIG MV/V	Omega
Dynamic Pressure	113B22	ICP Piezo Transducer	PCB

Flow Meter	FLMH-3420SS-MA	3/4"NPTF 20GPM	Omega
Accelerometer		100 mv/g	PCB
Dynamic Force	260A01	2.5 mV/lb (X,Y) 10 mV/lb (Z)	PCB

A.2 Source Flow Ripple Test Configuration

Table 10: Source Flow Ripple Configuration Component List

Component	Part Number	Description	Manufacturer
Power Unit			
Motor Drive Unit	ACS550	Drive Unit	ABB
Electric Motor	405THFS8036	100 HP 3-Phase	Marathon Motors
Motor Side Coupling	M70022824	2 7/8 – 3/4 keyed shaft	Magnaloy
Elastomeric Spider	M770H5	--	Magnaloy
Pump Side Coupling	M700A1316	13T splined shaft	Magnaloy
Hydraulic Circuit			
Hydraulic Reservoir	--	25 Gallon Reservoir	Buyers
Reducer	--	1 1/4 - 2 NPTF Reducer	--
Suction Hose	--	SAE 100R6-20	
Gauge Port Block	Main 2303-20-20	-20 C61 gauge port block	Main Mfg.
Pump		28cc Axial Piston Pump	Bosch Rexroth
Case Drain Hose		716 -8 to -8 STOR	
Gauge Port Block	Main 2303-12-12-M10	-12 C61 gauge port block	Main Mfg.
NPTF Block	Main 1149-12-12M10	3/4 NPTF block	Main Mfg.
Sch. 80 Pipe	--	6 inch	--
Pipe Coupling	GG	3/4 GG NPTF	Parker
Sch. 80 Pipe	--	3 inch	--
Cartridge Manifold	CLD	Through port with gauge port	Sun Hydraulics
Direct-Operated Relief Valve	RDFALWN	Direct-Operated Relief Valve	Sun Hydraulics
Pressure Relief Hose	--	SAE 100R6-12	
Pipe Nipple	--	3/4 to 3/4 NPTF	--
Load Valve 1	N1200S	Direct Needle Type	Parker
Sch. 80 Pipe	--	3 inch	--
Load Valve 2	N1200S	Direct Needle Type	Parker
Sch. 40 Pipe	--	8 inch	--
Flow Meter	FLMH-3420SS-MA	3/4"NPTF 20GPM	Omega
Sch. 40 Pipe	--	6 inch	--
Adapter	--	¾ NPT to SAE -16	--
Return Hose	--	SAE 100R6-16	
Tee Adapter	--	1” X ¾” X ¾”	--
Instrumentation			
Tachometer	--	Laser Type	--
Thermocouple	--	Type K	Omega
Digital Temp. Display	--	Trendicator	Omega

Static Pressure	PX309-5KGV	5000 PSIG MV/V	Omega
Dynamic Pressure	113B22	ICP Piezo Transducer	PCB
Flow Meter	FLMH-3420SS-MA	3/4"NPTF 20GPM	Omega
Pressure Gauge	--	Bourdon Type	

A.3 Test Bench Controller

Table 11: Test Bench Control Component List

Component	Part Number	Description	Manufacturer
Power Supply			
2mA Supply	--	2mA Supply	--
+5V Supply	--	+5V Supply	--
+24V Supply	--	+24V Supply	--
Wiring Components			
Wire	--	Wire	Wire
Valve Driver Board	027-22071-0	Valve Driver Board	Parker
Potentiometer	RV4N103C-ND	POT 10K OHM 2W CARBON LINEAR	--
E-Stop	679-3757-ND	SWITCH PUSH SPST-NC 6A 240V	--
Terminal Connectors	WM5017-ND	CONN JUMPER TERM EDGEON 8POS	--
Terminal Block	WM5782-ND	CONN BARRIER STRP 12CIRC 0.375"	--
Plastic Box	377-1218-ND	BOX ABS BLACK 6.11"L X 4.61"W	--
Knob	450-1735-ND	KNOB FLUTED W/SKIRT 0.250" PLAST	--
Plastic Box	HM214-ND	BOX ABS BLACK 8.66"L X 4.33"W	--
BNC Output	WM5514-ND	CONN BNC RCPT R/A 50 OHM PCB	--
Cable Glands	377-2210-ND	LNG GRY CABLE GLAND .16-.31"	--

B Pre-Test Analysis

A pre-test fixture analysis was performed to understand and document the resonances that could appear in future tests. The 4 mounting posts, the motor-bedplate attachment, and the pump mounting fixture were analyzed at the annotated locations shown in Figure 44 with the associated coordinate systems. The maximum frequency of interest is 3200 Hz. Driving point measurements at the hose clip location in X, Y and Z directions performed using an impact hammer are shown in B.1. The reproducibility of mounting post-A is shown in B.2 after three assemblies of the post. Motor speed sweeps were performed with no motor shaft attachment and the acceleration response was measured on the rear-left motor foot and mounting post A located 5 feet away as shown in B.3. This test evaluates the motor feet to hose clip path through the bedplate. A driving point measurement on the top-left corner of the pump mounting fixture is shown in B.4

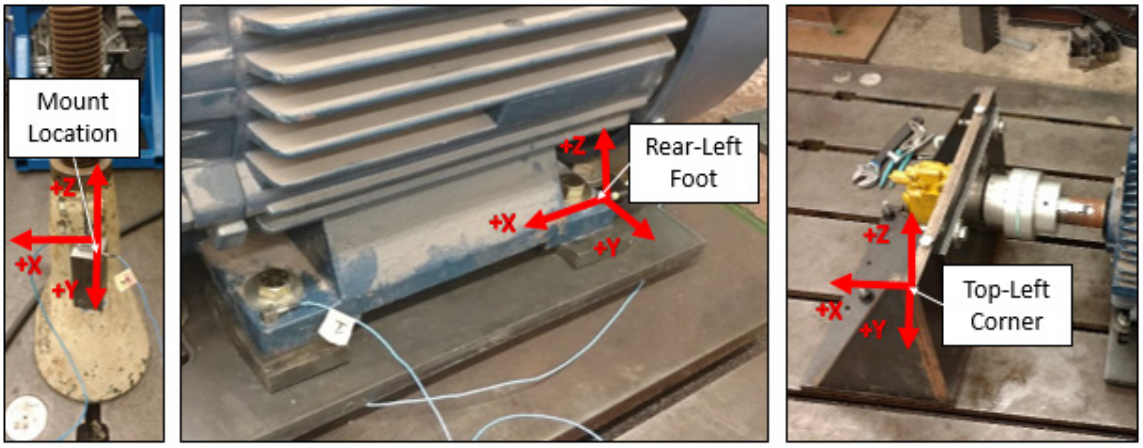

Figure 44: Pre-Test Analysis Locations

B.1 Mount Fixture Driving Points

A driving point measurement was recorded at the clip location on each mounting post in the X, Y and Z directions. The X-direction curves and significant resonances are

shown in Figure 45 and Table 12. The Y-direction curves and significant resonances are shown in Figure 46 and Table 13. The Z direction curves have resonances with less response potential below 3200 Hz and are shown in Figure 47. The coherence of each FRF is shown on the secondary Y-Axis of each figure. The significant mounting post resonant frequencies are higher than the pumping frequencies of interest in this project and should not affect the results.

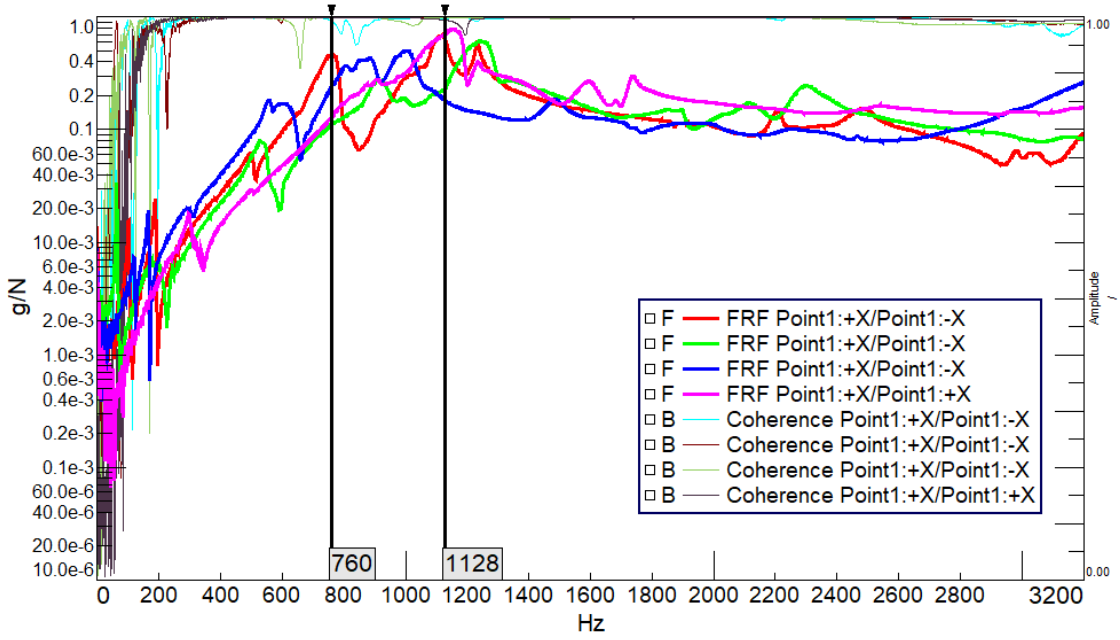

Figure 45: +X Direction Driving Point Measurements for All Jack Stands A-D

Table 12: Frequencies of Interest in +X Drive Point FRF

Jack Stand A		Jack Stand B		Jack Stand C		Jack Stand D	
Freq (Hz)	Ampl. (g/N)	Freq (Hz)	Ampl. (g/N)	Freq (Hz)	Ampl. (g/N)	Freq (Hz)	Ampl. (g/N)
763	0.47	530	0.08	557	0.18	909	0.28
1120	0.69	910	0.28	883	0.43	1158	0.78
1233	0.58	1245	0.61	1006	0.5	1236	0.4

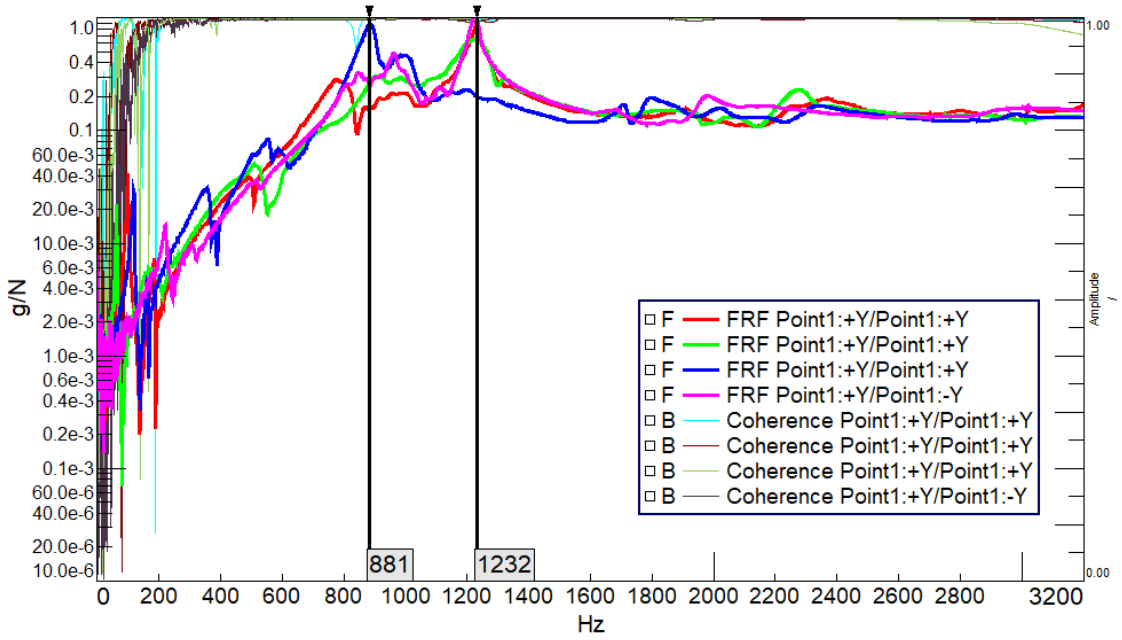

Figure 46: +Y Direction Driving Point Measurements for All Jack Stands A-D

Table 13: Frequencies of Interest in +Y Drive Point FRF

Jack Stand A		Jack Stand B		Jack Stand C		Jack Stand D	
Freq (Hz)	Ampl. (g/N)	Freq (Hz)	Ampl. (g/N)	Freq (Hz)	Ampl. (g/N)	Freq (Hz)	Ampl. (g/N)
776	0.28	506	0.05	553	0.08	848	0.33
983	0.22	910	0.31	887	0.89	962	0.49
1232	0.89	1223	0.65	996	0.47	1226	1.03

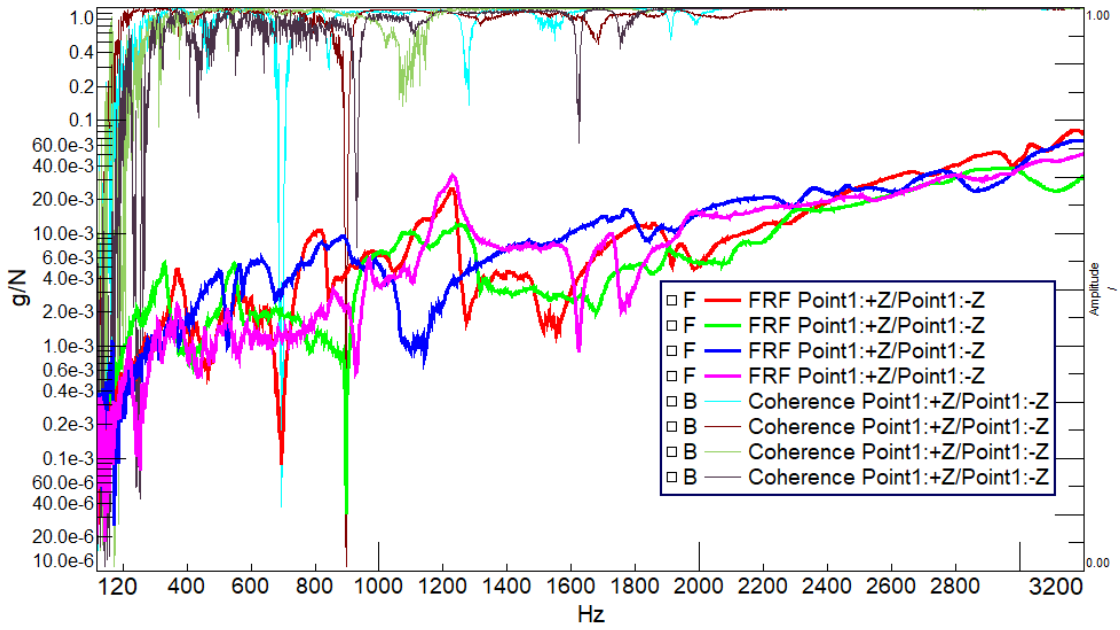

Figure 47: +Z Direction Driving Point Measurements for All Jack Stands A-D

B.2 Fixture Assembly Reproducibility

The reproducibility of each mounting post was evaluated by assembling mounting post-A with the same procedures and performing a driving point measurement at the clip location. The spacer block was attached to the bedplate with as much torque as possible using a 2-foot adjustable wrench. This clamp load was not a controlled variable. The

accelerometer was placed on top of the spacer block for each measurement. The reproducibility of each mounting post assembly is acceptable as shown in Figure 48.

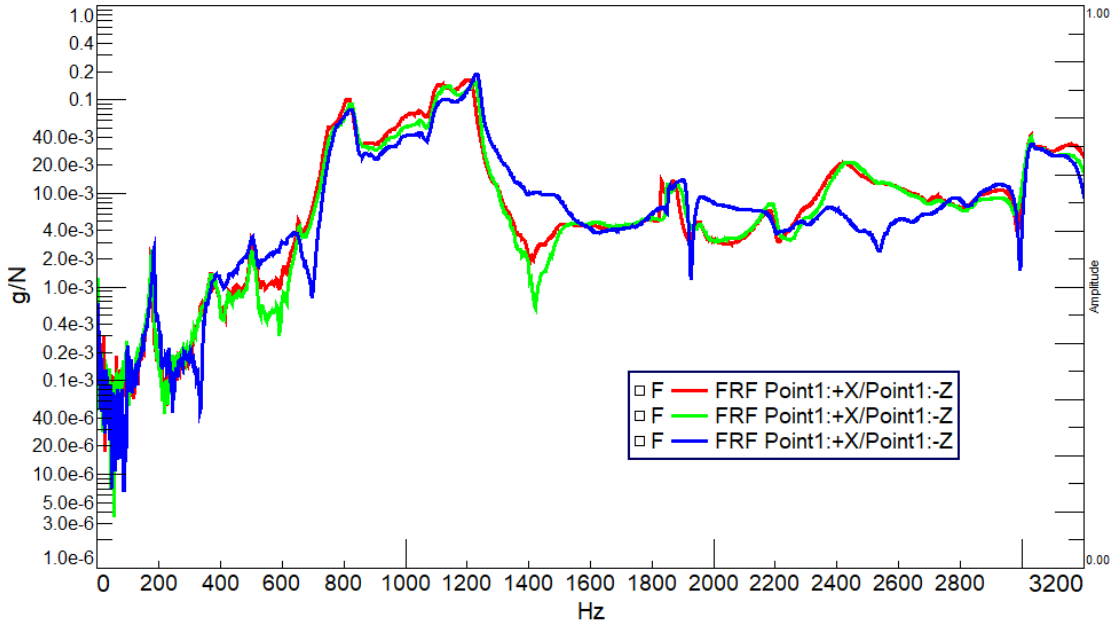

Figure 48: Jack Stand A Reproducibility

B.3 Unloaded Motor Speed Sweeps

The path from the motor feet to the hose clip location through the bedplate was evaluated by performing motor speed sweeps with no motor shaft attachment and measuring the responses at the rear-left motor foot and a mount location placed 5 feet away. A colormap of the response at the rear-left motor foot to a speed sweep from 0-1800 RPM is shown in Figure 49. The colormap of the X-direction response of hose mount post-A at a location 5-feet from the motor is shown in Figure 50. The mounting post-A resonances found in the driving point tests were excited by the motor through the bedplate. It is documented that measurements at a mounting post could have some contribution through the bedplate at the resonant frequencies of the mounting posts. The significant mounting

post resonant frequencies are higher than the pumping frequencies of interest in this project and therefore should not affect the results.

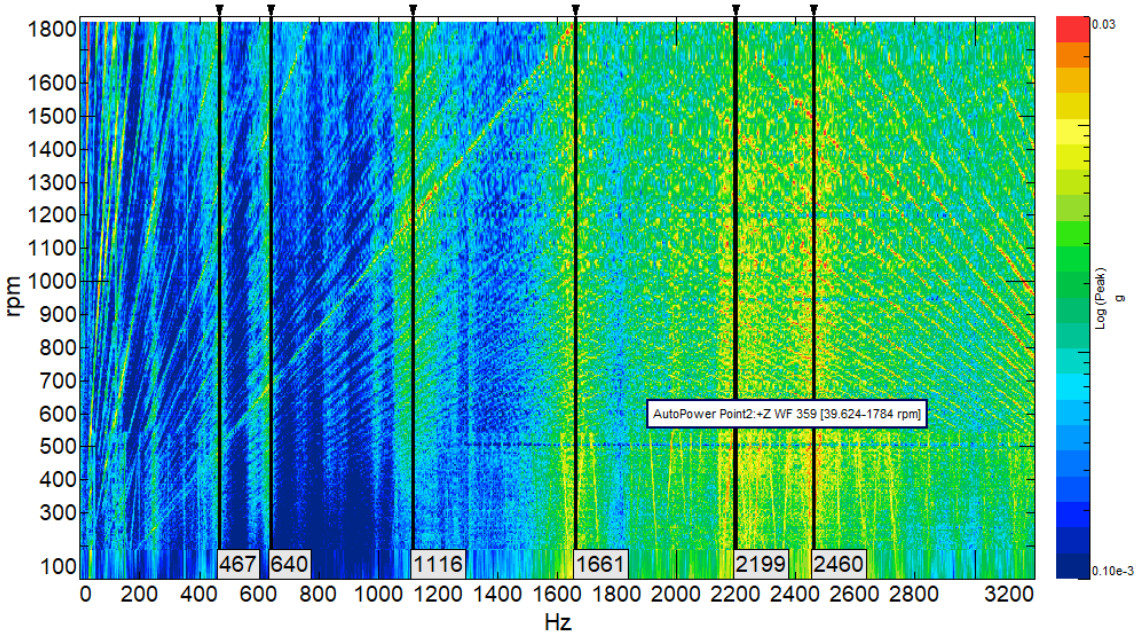

Figure 49: Response of Rear-Left Motor Foot to 0-1800 RPM Motor Speed Sweep (No Pump Shaft Coupling)

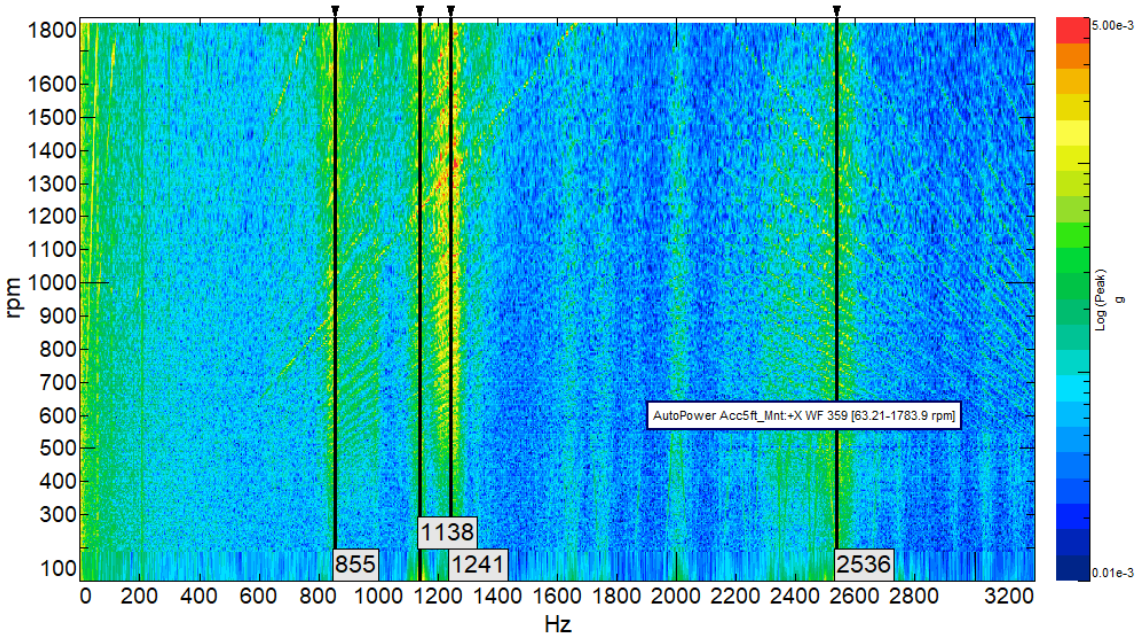

Figure 50: +X Response of Mount Location of Jack Stand A 5ft from Motor to 0-1800 RPM Motor Speed Sweep

B.4 Pump Mount Fixture Corner Driving Point

A driving point measurement was performed on the top-left corner of the pump mounting fixture and is shown in Figure 51 for all measured directions. The significant pump mount fixture resonant frequencies are higher than the pumping frequencies of interest in this project and should not affect the results.

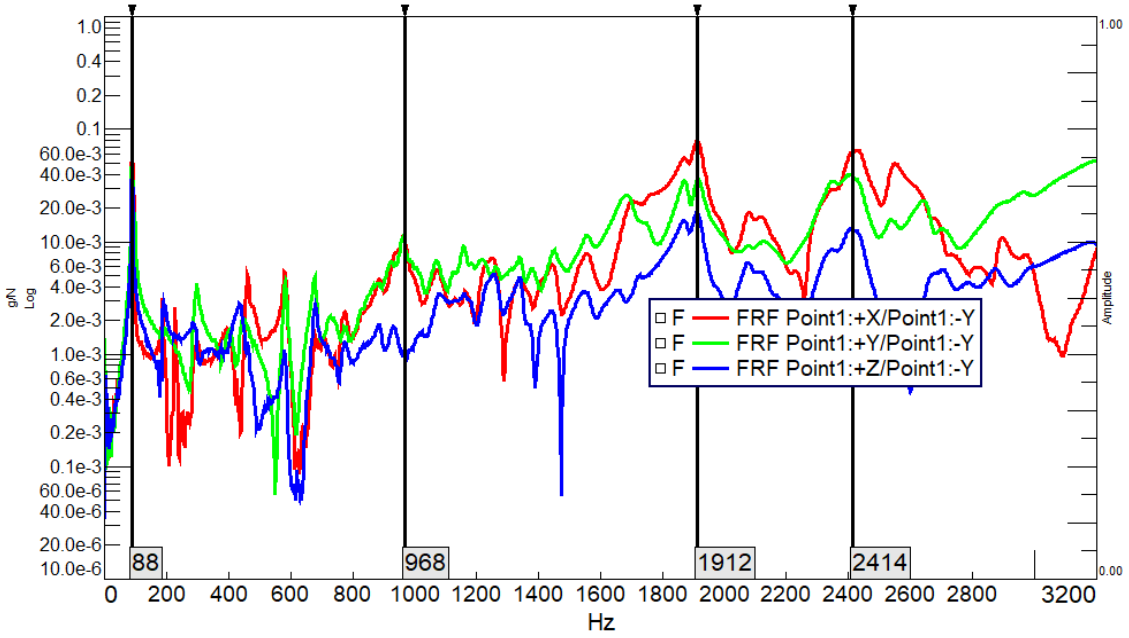

Figure 51: Driving Point Measurement at Corner of Pump Mount Fixture with Y-Dir Impact with Hammer

C Test Bench Setup and Startup Guidelines

C.1 Startup Guidelines

1. Perform safety walkaround and check for hydraulic oil leaks
2. Turn on motor power, +24 V power supply, +5V power supply, 2 mA current supply, LMS front end, temperature display
3. Open LMS Test.Lab Signature Testing Advanced. Direct to Measure tab and create analog display with online data for static pressure transducer, flow meter and motor speed signal. (It may be necessary to low-pass filter DC signals as they may be contaminated by power line frequencies from other components in the room).
4. Arm the system in measurement tab
5. Run test bench at 800 RPM unloaded for 5 minutes using drive unit remote. Ensure loading valve is fully open.
6. Carefully apply hydraulic load using the potentiometer on the test bench control. Run at 1000 RPM and 1000 psi or similar condition until inlet oil temperature reaches 50°C (~15 minutes)
7. Perform tests as desired

C.2 New Pump Break-In Procedure

Procedures for breaking in the test bench pump were followed as shown in Figure 52.

Step	Time	Discharge Pressure		Speed
	(min)	(Kpa)	(PSI)	(rpm)
1	10	3450	500	1000
2	20	5170	750	1000
3	20	10340	1500	1425
4	10	15000	2175	1200
5	10	15000	2175	1500
6	30	0	0	Sweep
7	10	3450	750	1000
8	10	10340	1500	1000
9	10	15000	2175	1200

Figure 52: Pump Break-In Procedures

C.3 Test Bench Control Wiring Diagram

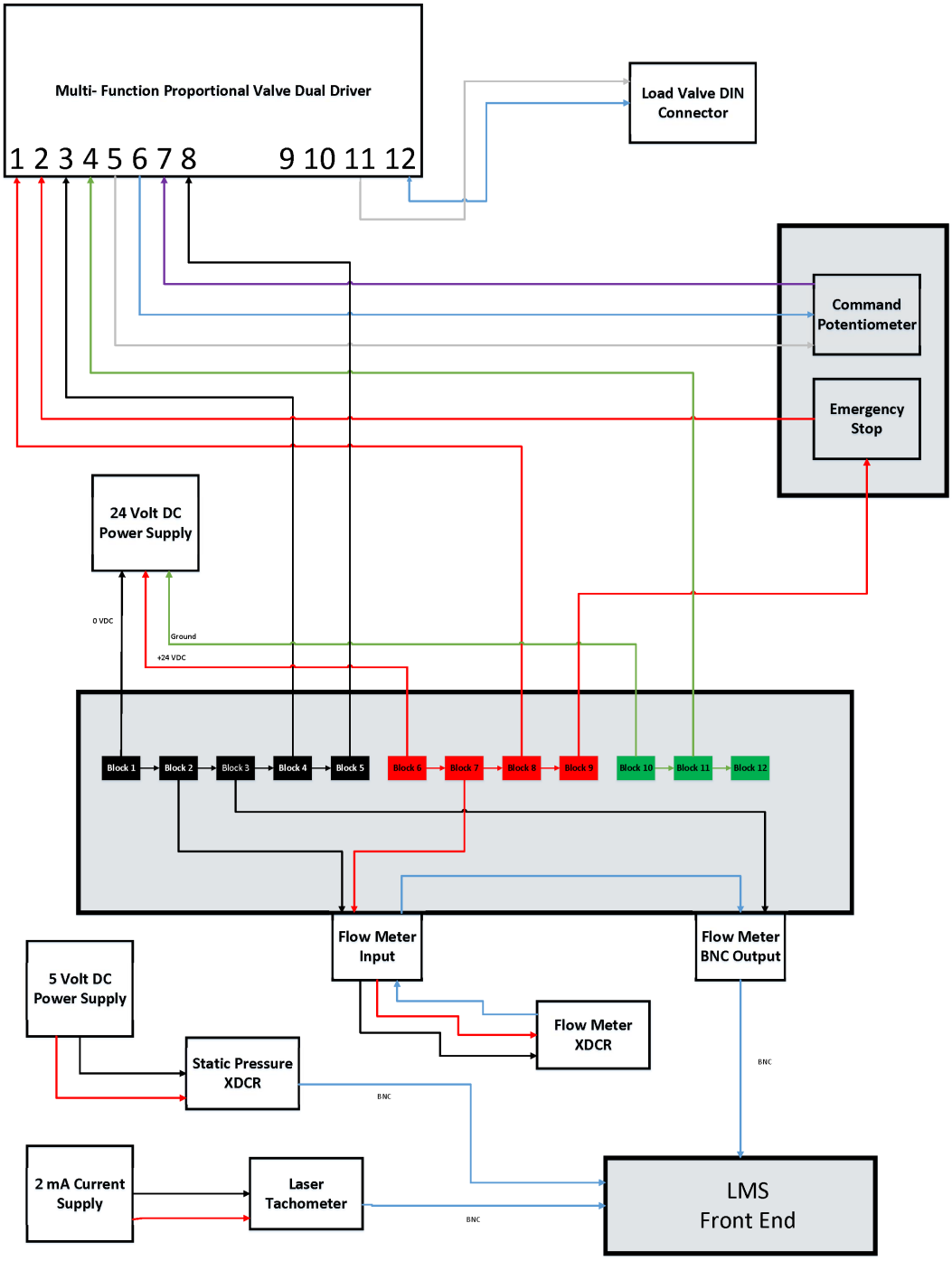

Figure 53: Test Bench Control Wiring Diagram

D Source Flow Ripple Spike Resolution

The source flow ripple for the test bench pump was determined using the pressure measurements and processing procedures described in section 2.3.1. The suggested measurement parameters according to ISO 10767-1 were a sample rate of 10,240 Hz and a measurement period of 0.8 seconds. This results in a frequency resolution of 1.25 Hz. The magnitude of the source flow ripple for a 1500 psi CPSS is shown in Figure 54. Spikes in the flow ripple results to unrealistic flow ripple quantities occurred at various frequencies that could not be correlated to events in operating condition data. The frequency of the flow ripple spikes was not consistent for all processed CPSS runs. A presumed cause and mitigation plan is described.

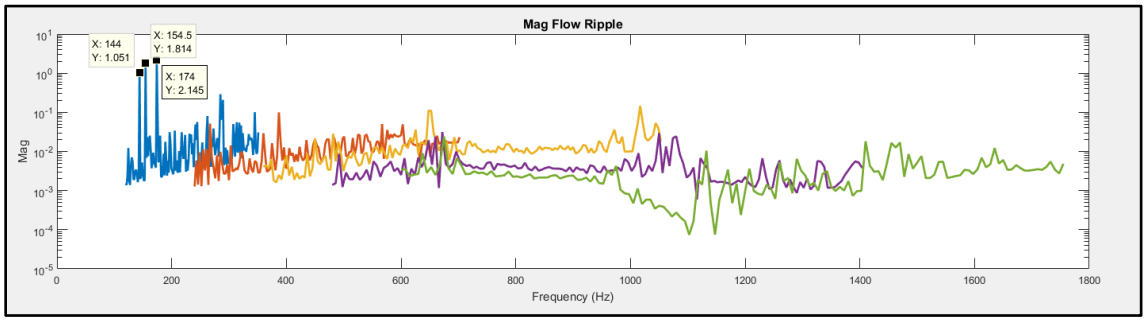

Figure 54: Source Flow Ripple Results for 1500 psi CPSS with 2.5 Hz Frequency Resolution

Figure 55 shows the pressure ripple measurements for system 1 and system 2. It is shown that subtraction of pressure measurements within the same measurement run produce peaks at frequencies that correspond to the spikes in source flow ripple results.

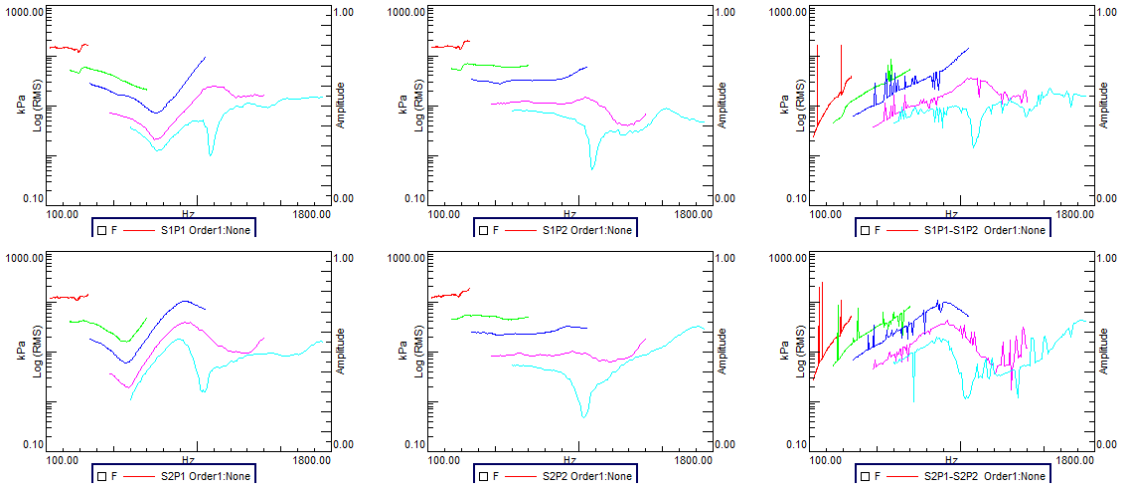

Figure 55: 1500 psi CPSS data with 1.25 Hz frequency resolution. System 1 - P_1 (Top-Left), System 1 - P_2 (Top-Mid), System 1 ($P_1 - P_2$) (Top-Right), System 2 - P_1 (Bottom-Left), System 2 - P_2 (Bottom -Mid), System 2 ($P_1 - P_2$) (Bottom -Right)

Stationary data at 800 RPM and 580 psi was processed to look at the repeatability of the source flow ripple result at a single operating condition. A source flow ripple value was evaluated at every 0.8 second block of a 30 second measurement run as shown in Figure 56 for the first 5 pump orders. Spikes occurred in various blocks that could not be correlated to operating condition events.

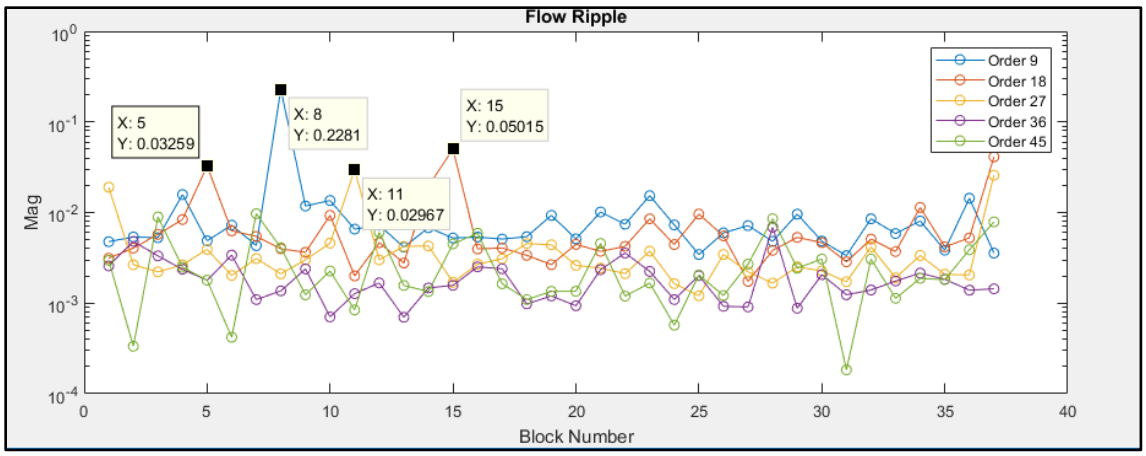

Figure 56: Flow Ripple Repeatability from 800 RPM - 580 PSI SS Data

The first pump order was examined in detail in Figure 57. A significant source flow ripple spike occurred only at the 8th measurement block. The difference in magnitude of the 8th block system 1 pressure measurements is shown in the top subplot and appears to be similar to other measurement blocks that do not produce source flow ripple peaks. The difference in phase of the 8th block is shown in the bottom subplot and is significantly different. It is expected that small nonlinear events are occurring in the system that do not affect the pressure magnitude but alter the phase of the measured complex pressure waveform.

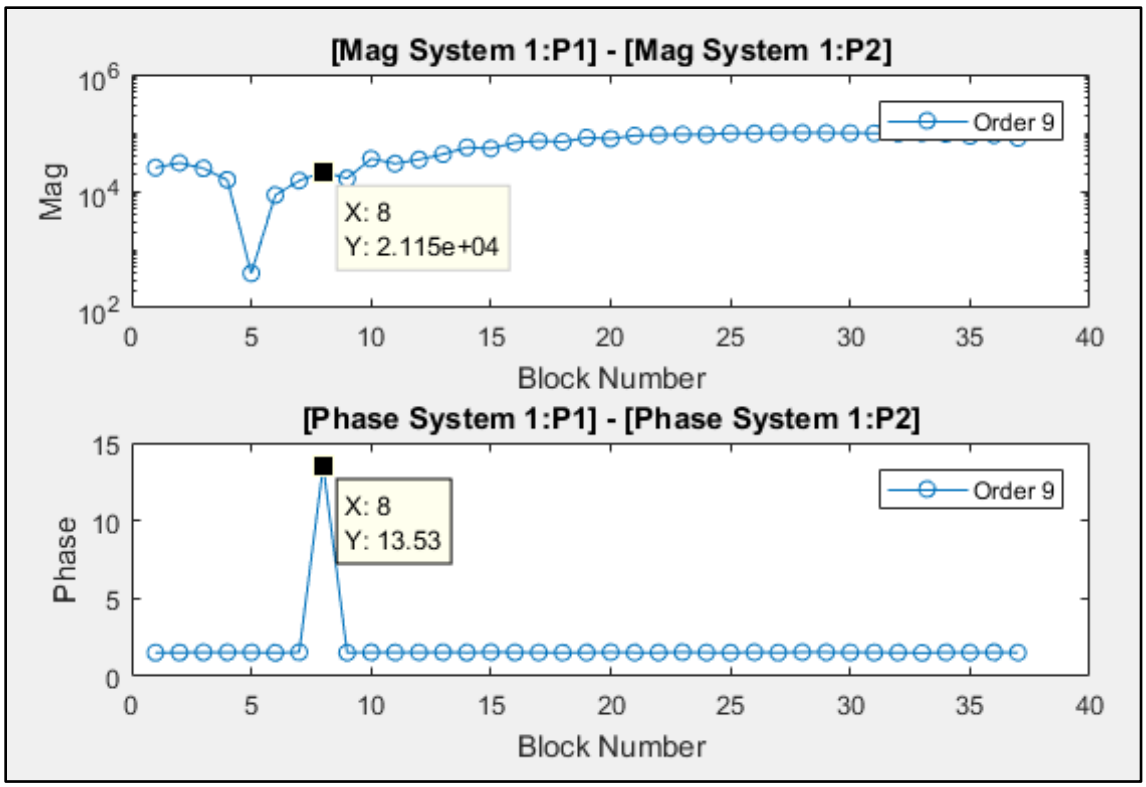

Figure 57: Measured 9th Order Pressure Ripple Differences for System 1

The measurement period was increased arbitrarily to 2 or 4 seconds to produce a frequency resolution of 0.5 or 0.25 Hz. The longer measurement time minimized the phase effect in the processing of the source flow ripple data. The same data from Figure 55 is shown in Figure 58 with a 2-second measurement period and the source flow ripple spike issue was significantly minimized. It is expected that since the CPSS runs were 4 minutes and 40 seconds long, the 5-6 RPM motor speed change over 2 seconds will still produce accurately tracked orders using an FFT-based method.

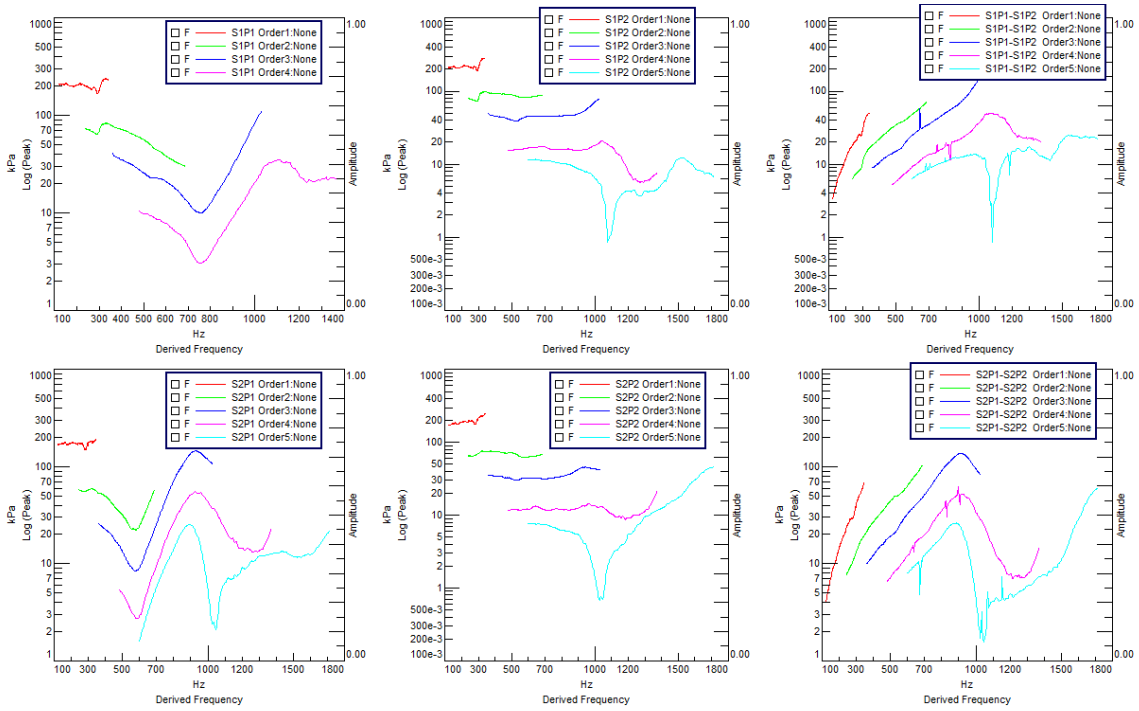

Figure 58: 1500 psi CPSS data with 0.5 Hz frequency resolution. System 1 - P_1 (Top-Left), System 1 - P_2 (Top-Mid), System 1 ($P_1 - P_2$) (Top-Right), System 2 - P_1 (Bottom-Left), System 2 - P_2 (Bottom -Mid), System 2 ($P_1 - P_2$) (Bottom -Right)

E Synthesized Orders and FRF comparison for all measurement locations

Order sections and FRF's based on modal parameters for pressure measurements at 528 mm, 710 mm, 935 mm, 1219 mm, 1442 mm, 1623 mm and 2130 mm are shown in sections E.1, E.2, E.3, E.4, E.5, E.6 and E.7 respectively.

E.1 Order and FRF synthesis for location 528 mm from pump outlet

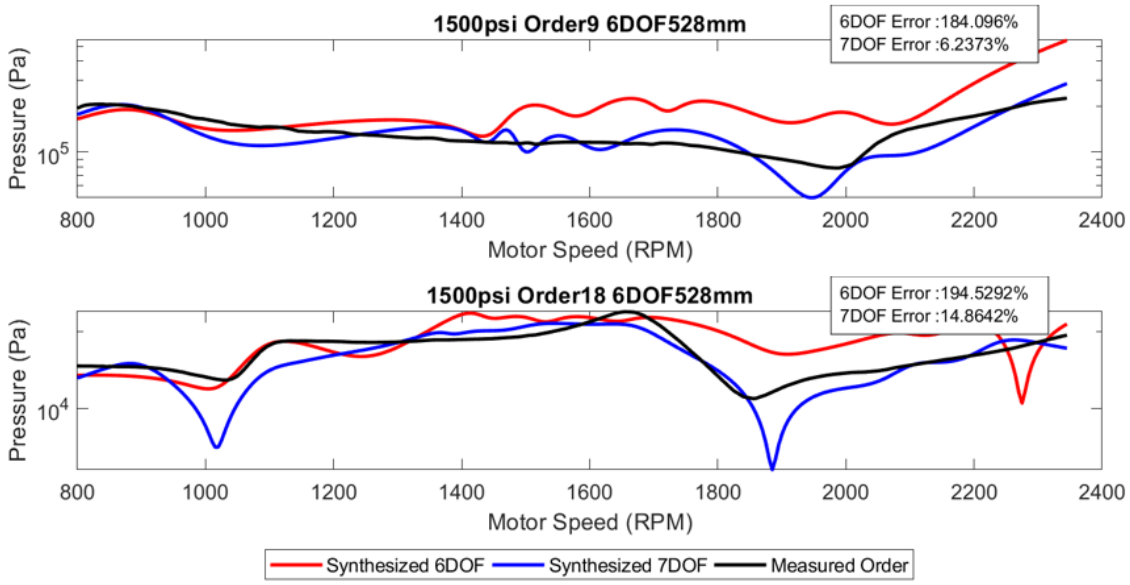

Figure 59: Synthesized and Measured Comparison of 9th and 18th Order Sections at location 528 mm from Pump Outlet for 9th Order (Top) and 18th Order (Bottom)

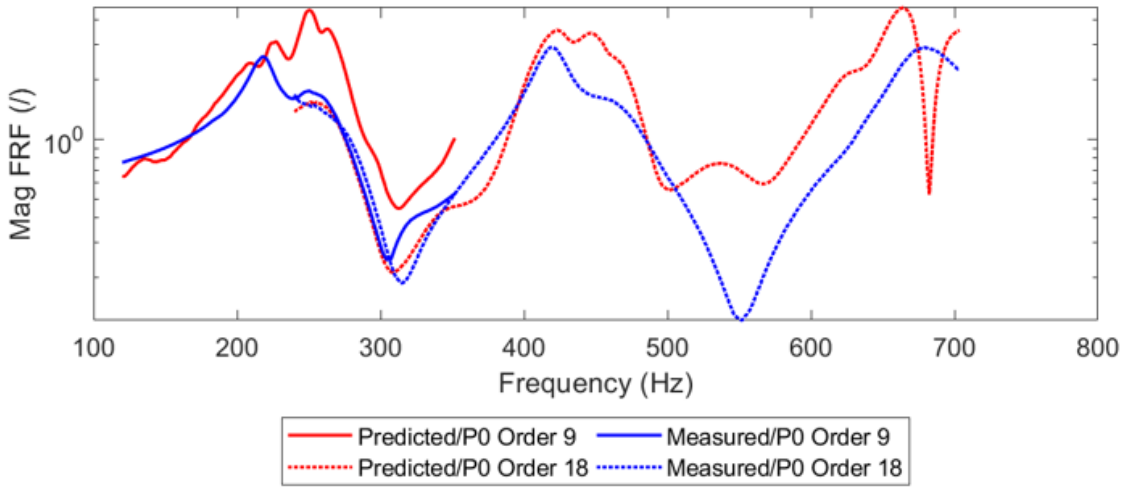

Figure 60: Comparison of Measured FRF and FRF Expanded using Modal Parameters at Location 528 mm from Pump Outlet

E.2 Order and FRF synthesis for location 710 mm from pump outlet

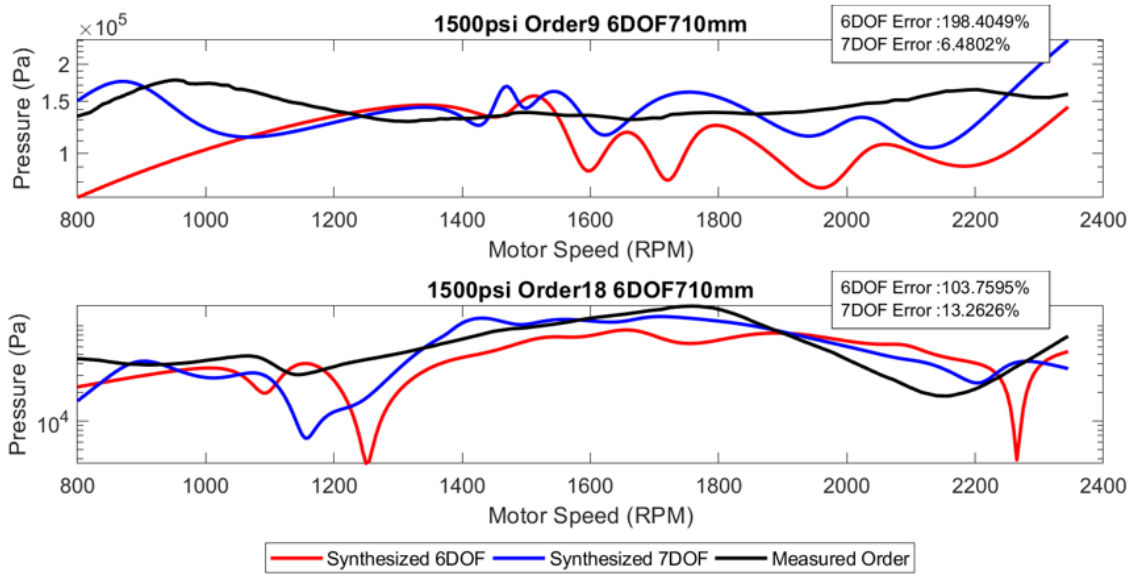

Figure 61:Synthesized and Measured Comparison of 9th and 18th Order Sections at location 710 mm from Pump Outlet for 9th Order (Top) and 18th Order (Bottom)

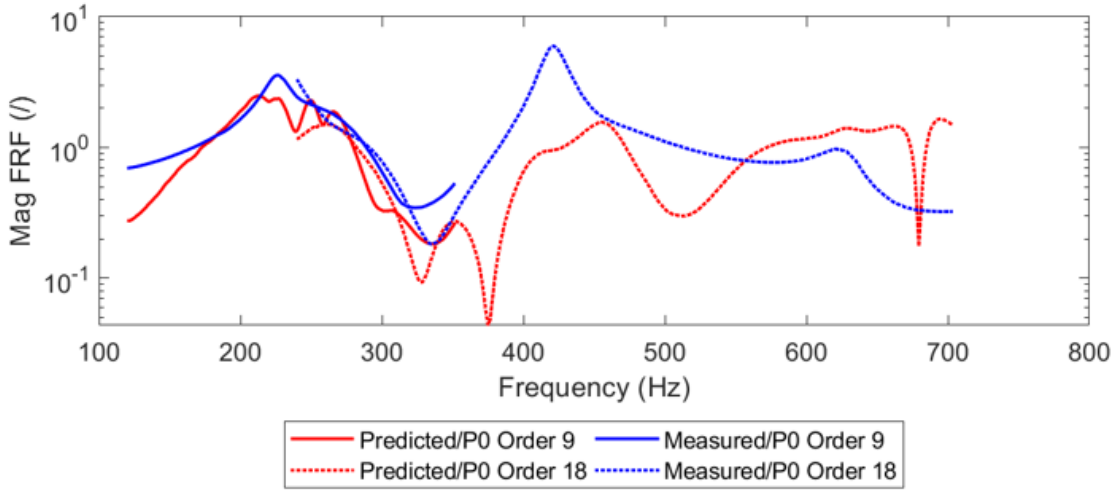

Figure 62: Comparison of Measured FRF and FRF Expanded using Modal Parameters at Location 710 mm from Pump Outlet

E.3 Order and FRF synthesis for location 935 mm from pump outlet

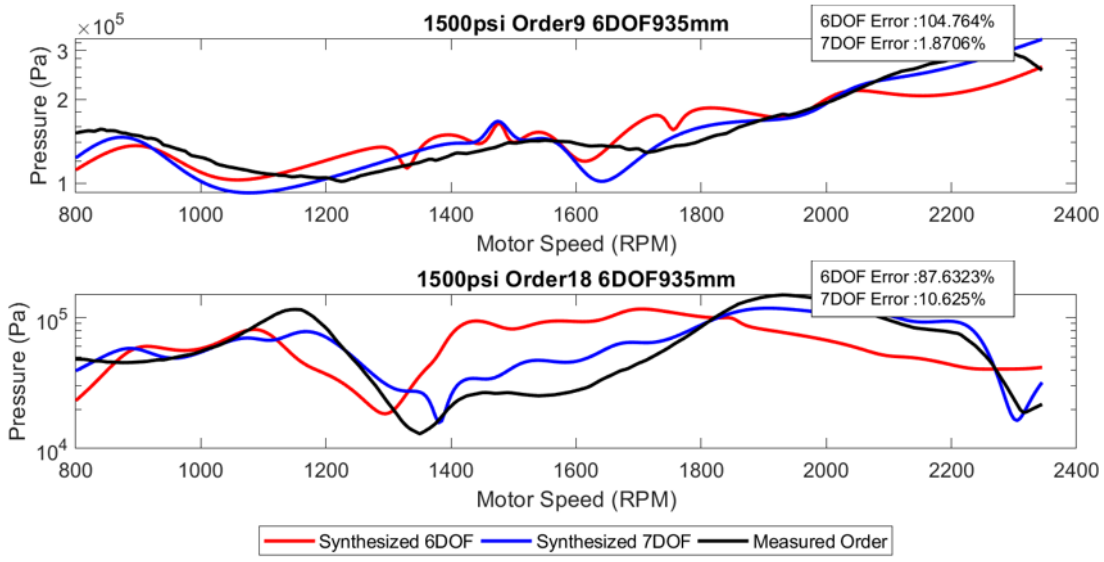

Figure 63: Synthesized and Measured Comparison of 9th and 18th Order Sections at location 935 mm from Pump Outlet for 9th Order (Top) and 18th Order (Bottom)

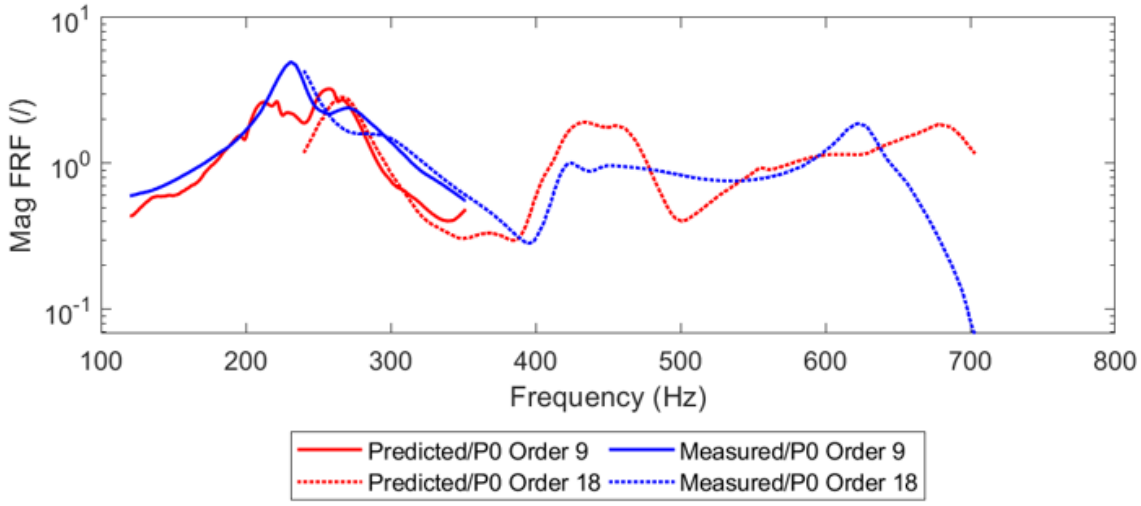

Figure 64: Comparison of Measured FRF and FRF Expanded using Modal Parameters at Location 935 mm from Pump Outlet

E.4 Order and FRF synthesis for location 1219 mm from pump outlet

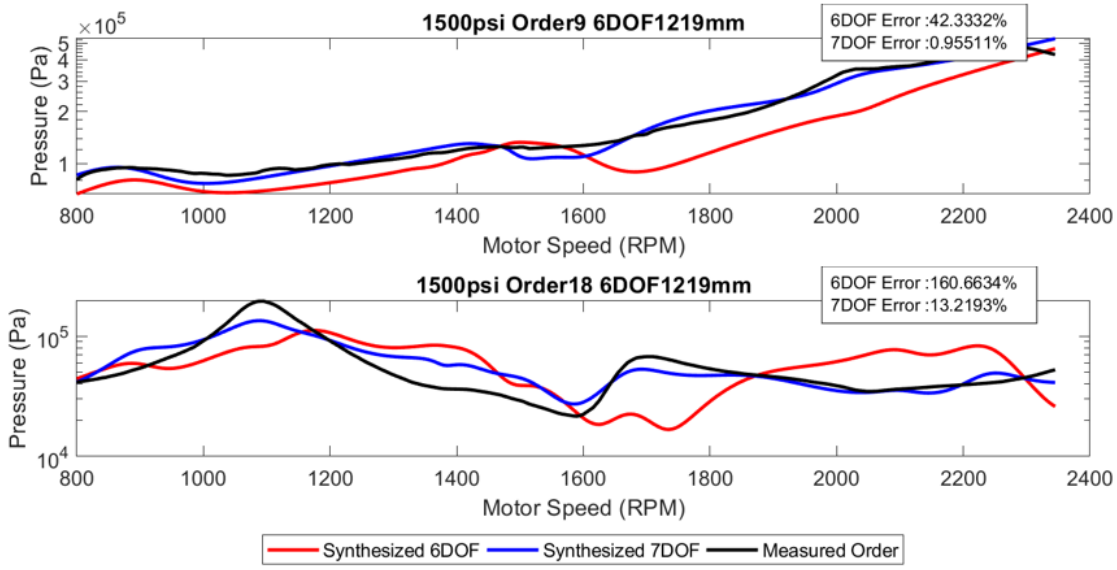

Figure 65: Synthesized and Measured Comparison of 9th and 18th Order Sections at location 1219 mm from Pump Outlet for 9th Order (Top) and 18th Order (Bottom)

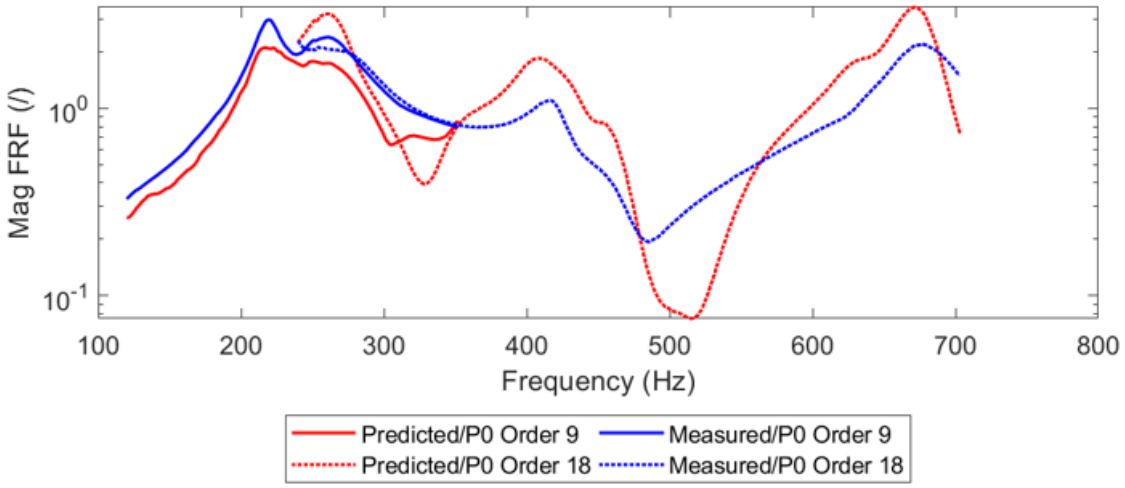

Figure 66: Comparison of Measured FRF and FRF Expanded using Modal Parameters at Location 1219 mm from Pump Outlet

E.5 Order and FRF synthesis for location 1442 mm from pump outlet

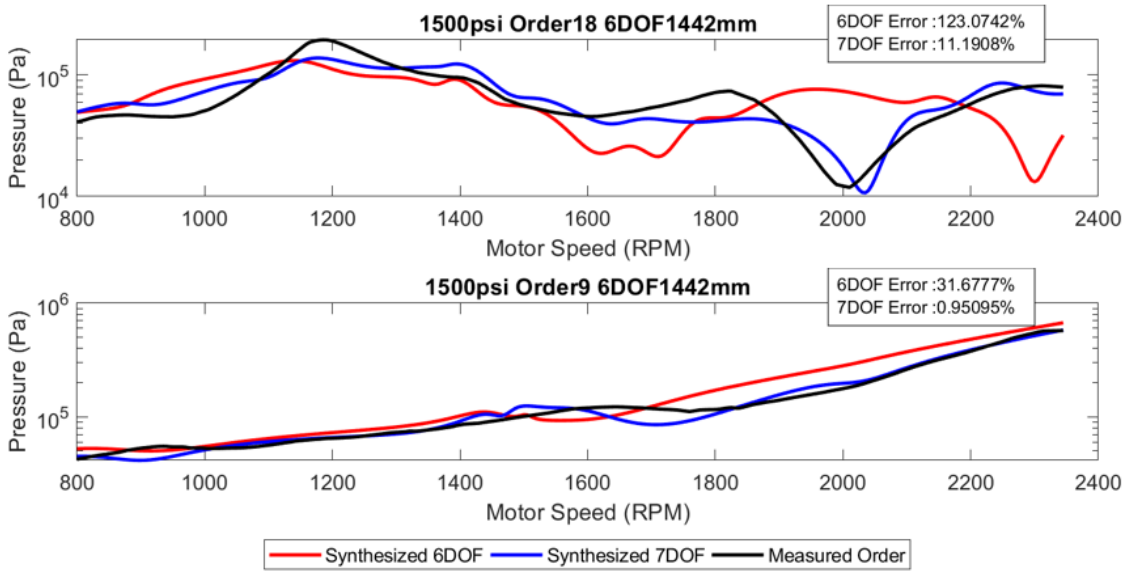

Figure 67: Synthesized and Measured Comparison of 9th and 18th Order Sections at location 1442 mm from Pump Outlet for 9th Order (Top) and 18th Order (Bottom)

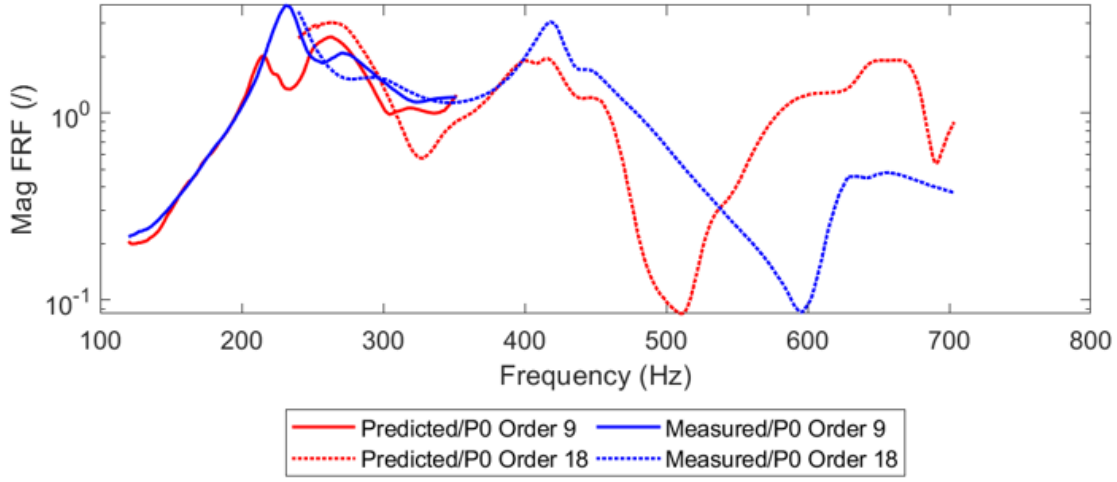

Figure 68: Comparison of Measured FRF and FRF Expanded using Modal Parameters at Location 1442 mm from Pump Outlet

E.6 Order and FRF synthesis for location 1623 mm from pump outlet

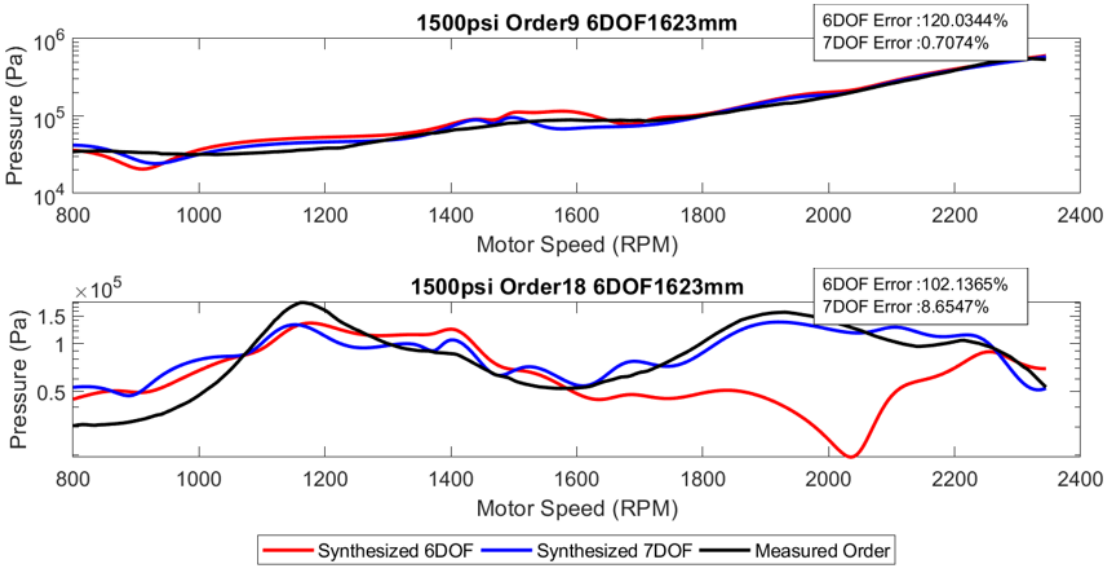

Figure 69: Synthesized and Measured Comparison of 9th and 18th Order Sections at location 1623 mm from Pump Outlet for 9th Order (Top) and 18th Order (Bottom)

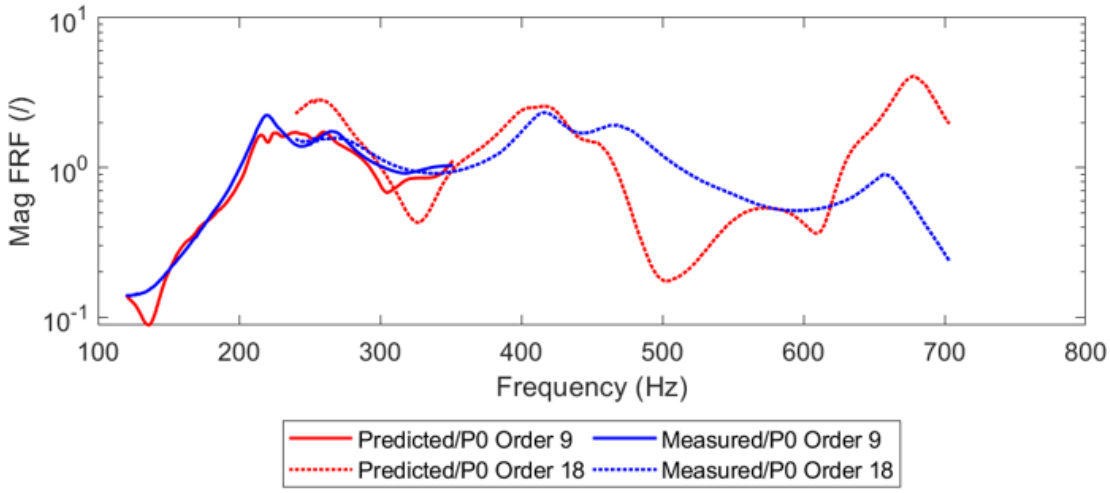

Figure 70: Comparison of Measured FRF and FRF Expanded using Modal Parameters at Location 1623 mm from Pump Outlet

E.7 Order and FRF synthesis for location 2130 mm from pump outlet

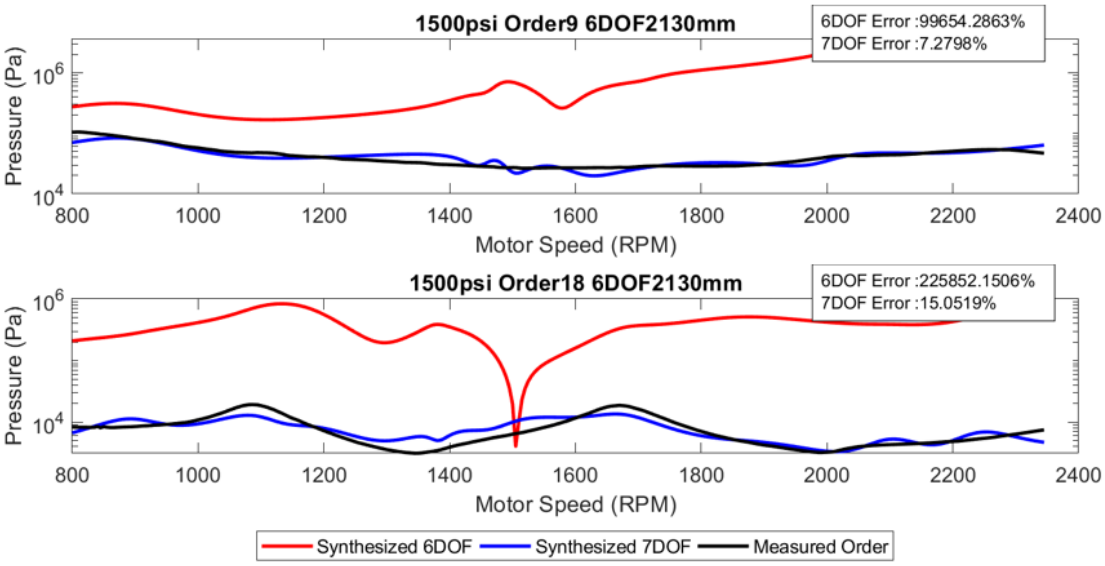

Figure 71: Synthesized and Measured Comparison of 9th and 18th Order Sections at location 2130 mm from Pump Outlet for 9th Order (Top) and 18th Order (Bottom)

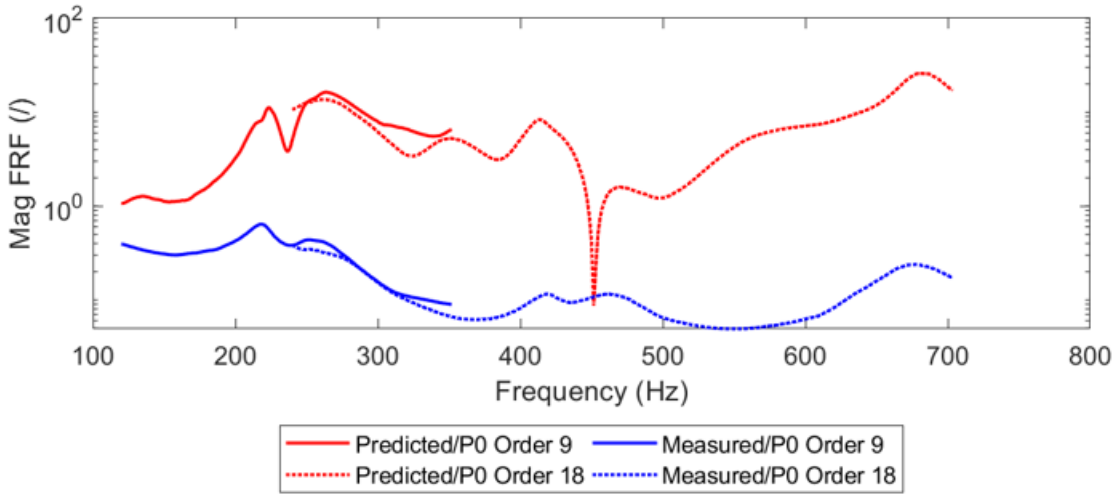

Figure 72: Comparison of Measured FRF and FRF Expanded using Modal Parameters at Location 2130 mm from Pump Outlet

F MATLAB Processing

MATLAB codes are provided for Source Flow Ripple processing and validation for 1500 psi CPSS, SBN Characterization and SBN Video creation, FRF based on pump outlet pressure using modal expansion and energy balancing method.

F.1 Source Flow Ripple Processing

The first 5 pump order sections must be exported from LMS Test.Lab to MATLAB in a single .MAT file for each pressure transducer measurement: System 1 – P0 (S1P0), System 1 – P1 (S1P1), System 2 – P0 (S2P0) and System 2 – P1 (S2P1). The motor speed range of the speed sweep, the order section RPM increment, and frequency resolution should be updated. The processing shown uses a 7-point moving average filter and uses a 4 Hz frequency resolution for the combined spectrum.

F.1.1 Source Flow Ripple Processing for 1500 psi CPSS

```
%This is the source flow ripple processing script for
the first 5 pump
%orders (9, 18, 27, 36, 45) for the 1500 psi speed
sweep

clc
clear
close all

%Load Pressure Ripple Data from P0 and P1 transducers
for both system
%measurements
S1P0 = load('S1P0_1500psi.mat');
S1P0 = S1P0.OrderSection.y_values.values  ;
S1P1 = load('S1P1_1500psi.mat');
S1P1 = S1P1.OrderSection.y_values.values  ;
S2P0 = load('S2P0_1500psi.mat');
```

```
S2P0 = S2P0.OrderSection.y_values.values  ;
S2P1 = load('S2P1_1500psi.mat');
S2P1 = S2P1.OrderSection.y_values.values  ;

%Initialize RPM range and freq. resolution that was
used
rpm = 800:10:2290;
df = 0.25;

%Solve for Source Flow Ripple (Qs) and Smooth Results
for ii = 1:5

    fmin = rpm(1)/60*9;
    fmax = rpm(end)/60*45;

bulk  = 1965006000; %285000 psi in Pa
rho = 843; %0.8433 g/cc in kg/m3;
c = sqrt(bulk/rho); %Speed of sound in m/s

v = 3.2*10^-5;
ro = 0.009525; %.375 inches in m

w = (9*ii)*(rpm'/60)*2*pi;
zeta = 1+sqrt(v./(2*ro^2.*w))-
1j*(sqrt(v./(2*ro^2.*w))+(v./(ro^2.*w)));

B = ((zeta.*w)/c);
Zc = ((rho*c*zeta)/(pi*ro^2));
Lr = 0.1905; %7.5 inches in m

f = rpm/60*9*ii;
numerator = 1000*(S1P0.*S2P1-S2P0.*S1P1)*1j;
denominator = (S1P0-S2P0).*sin(B*Lr).*Zc;

Qs = (numerator./denominator);

Order.(strcat('order',num2str(ii)))(:,1) = f;
Order.(strcat('order',num2str(ii)))(:,2) =
sqrt(Qs(:,ii).^2/df)*sqrt(2.108);

%Smooth Order Sections
[redacted]
```

% Sort Flow Ripple Results by Frequency Bin

```
% %% Import Machine Data from Excel File
[num,txt,raw] = xlsread('Machine_Flow_Ripple.xlsx');
Machine_freq = cell2mat(raw(:,1));
Machine_Qs =
sqrt(str2double(txt(:,1)).^2/2.108)*sqrt(2.108);

%% PLOTTING
for ii = 1:5
figure(1)
semilogy(abs(interp_freq),abs(Combined_Spectrum),'b','L
ineWidth',1.2)
hold on
semilogy(Machine_freq,abs(Machine_Qs),'k','LineWidth',2
)
```

```
legend('1500 psi Sweep','Machine
Sweep*','Location','SouthWest')
ylabel('|Source Flow Ripple| (L/s)')
xlabel('Frequency (Hz)')
set(gca,'FontSize',14)

Qs_1500psi(:,1)  = interp_freq;
Qs_1500psi(:,2)  = Combined_Spectrum;

save('Qs_1500psi.mat','Qs_1500psi')
end

%%

Qs_OrderSect_1500psi(:,1) = rpm;
Qs_OrderSect_1500psi(:,2:6) = [Order.order1(:,2)
Order.order2(:,2) Order.order3(:,2) Order.order4(:,2)
Order.order5(:,2)];

col = [0 .45 .74; .93 .69 .13; .47 .67 .19 ; .64 .08
.18 ; .85 .33 .10];

for ii = 1:5
   figure(2)

semilogy(abs(Qs_OrderSect_1500psi(:,1)/60*9*ii),abs(Qs_
OrderSect_1500psi(:,ii+1)))
   hold on

semilogy((800:10:2340)/60*9*ii,abs(Section(:,ii)),'Colo
r',col(ii,:),'LineWidth',3)

   figure(3)
   semilogy((800:10:2340)/60*9*ii,abs(Section(:,ii)),'-
-','Color',col(ii,:),'LineWidth',1.5)
   hold on

end

figure(2)
ylabel('|Source Flow Ripple| (L/s)')
xlabel('Frequency (Hz)')
```

```
set(gca,'FontSize',14)
title('1500 psi Source Flow Ripple')
lgd = legend('9th Order','Smoothed 9th Order','9th
Order','Smoothed 9th Order',...
    '9th Order','Smoothed 9th Order','9th
Order','Smoothed 9th Order',...
    '9th Order','Smoothed 9th
Order','Location','southoutside');
lgd.NumColumns = 5;

figure(3)
hold on
semilogy(abs(interp_freq),abs(Combined_Spectrum),'b','L
ineWidth',2)
semilogy(Machine_freq,abs(Machine_Qs),'k','LineWidth',2
)
ylabel('|Source Flow Ripple| (L/s)')
xlabel('Frequency (Hz)')
set(gca,'FontSize',14)
title('1500 psi Source Flow Ripple')
lgd = legend('9th Order','18th Order','27th
Order','36th Order','45th Order','1500 psi Combined
Spectrum','Machine Test','Location','southoutside');
lgd.NumColumns = 5;
save('Qs_1500psi.mat','Qs_OrderSect_1500psi')
```

F.2 SBN Characterization and SBN Video

This SBN processing script exports dynamic force data and integrated acceleration data from LMS Test.Lab in separate files for each of the first 5 orders. The order data is then sorted using a function called Sort_SBN_Data. The dynamic pressure measured at the outlet as well as the FRF's generated from either equation (12) or the OBMA modal expansion process are inputs that must be in the working directory.

F.2.1 Measured SBN Processing and SBN Video Processing

```
clc
clear
close all
```

```
%Load Hose Data
%Run 3 & 4 Dynamic Force
data.Run4.DF.Order9 = load('Run4_DF_Order9.mat');
data.Run4.DF.Order18 = load('Run4_DF_Order18.mat');
data.Run4.DF.Order27 = load('Run4_DF_Order27.mat');
data.Run4.DF.Order36 = load('Run4_DF_Order36.mat');
data.Run4.DF.Order45 = load('Run4_DF_Order45.mat');

%Run 3 & 4 Dynamic Force
data.Run4.Vel.Order9 = load('Run4_Vel_Order9.mat');
data.Run4.Vel.Order18 = load('Run4_Vel_Order18.mat');
data.Run4.Vel.Order27 = load('Run4_Vel_Order27.mat');
data.Run4.Vel.Order36 = load('Run4_Vel_Order36.mat');
data.Run4.Vel.Order45 = load('Run4_Vel_Order45.mat');

%Run 3 & 4 Pressure
data.Run4.P0= load('Run4_P0.mat');

%% Calculate SBN
[SBN] = Sort_SBN_Data (data);

%% SBN Loss Repeatability Movie
%Sum of SBN Losses over 5 Orders
rpm = 800:5:2315; %Input Motor Speed Range
ref_rad = 0.2; % Reference SBN Circle Radius

%SUM of each order and initialize peak hold
Mount1.Run4 = abs(sum(SBN.Run4.Mnt710,2));
Mount2.Run4 = abs(sum(SBN.Run4.Mnt1442,2));
Mount3.Run4 = abs(sum(SBN.Run4.Mnt2130,2));
Mount1.Run4_Max = 0;
Mount2.Run4_Max = 0;
Mount3.Run4_Max = 0;

%%
%SBN Movie saves a figure for the SBN result at each
RPM and overlays on an
%image of the hydraulic circuit and saves as a frame.
All frames are saved
%as an avi video
```

```
for ii = 1:length(rpm)
    f2 = figure(2);
    f2.Position = [1,1,1673,435];
    %RPM Display

    %Set SBN value and peak hold
    if Mount1.Run4(ii)> Mount1.Run4_Max
        Mount1.Run4_Max = Mount1.Run4(ii);
    end

    if Mount2.Run4(ii)> Mount2.Run4_Max
        Mount2.Run4_Max = Mount2.Run4(ii);
    end

    if Mount3.Run4(ii)> Mount3.Run4_Max
        Mount3.Run4_Max = Mount3.Run4(ii);
    end

    % Generate Bar Chart and Peak Hold in leftmost
subplot
    ax1 = subplot(1,3,1);
    y = [Mount3.Run4(ii) Mount3.Run4_Max
Mount2.Run4(ii) Mount2.Run4_Max Mount1.Run4(ii)
Mount1.Run4_Max];
    b = bar(y);
    b.FaceColor = 'flat';
    b.CData(1,:) = [ 1 0 1];
    b.CData(2,:) = [ 1 1 1];
    b.CData(3,:) = [ 1 0 0];
    b.CData(4,:) = [ 1 1 1];
    b.CData(5,:) = [ 0 0 1];
    b.CData(6,:) = [ 1 1 1];
    ax1.FontSize = 16;
    ylim([0 0.6])
    ylabel('SBN Power (W)')
    set(ax1,'XTick',[1 3 5],'XTickLabel',...
        {'Filter In','Mount 2','Mount 1'});


    subplot(1,3,[2:3])
    %Set Picture Background
    axis([0 4 -1 1])
```

```
    I = imread('Mnt710Mnt1442.png');
    hold on
    h = image(xlim,-ylim,I);
    title('CONFIGURATION 1','FontSize',16)

    %Create SBN Circles
    radii.Mnt1 = (ref_rad*Mount1.Run4(ii))/.2;
    radii.Mnt2 = (ref_rad*Mount2.Run4(ii))/.2;
    radii.Mnt3 = (ref_rad*Mount3.Run4(ii))/.2;
    viscircles([2.668 -0.2471],radii.Mnt1,'Color',[0 0
1]);
    viscircles([1.847 -0.2471],radii.Mnt2,'Color',[1 0
0])
    viscircles([1.15 -0.2471],radii.Mnt3,'Color',[1 0
1])

    %FORMATTING and ANNOTATIONS
    r = rectangle;
    r.LineWidth = 2;
    r.Curvature = [1,1];
    r.FaceColor = 'w';
    r.Position = [0.1 0.6 0.4 0.4];

    dim = [0.4299,0.6709,0.2179,0.235];
    scalestr1 = {'Scale:';'0.2 W'};
    scale1 =
annotation('textbox',dim,'String',scalestr1);
    scale1.FontSize = 14;
    scale1.EdgeColor = 'none';

    dim =
[0.755528989838613,0.717241379310345,0.139270771069933,
0.177164367816092];
    rpmstr = {strcat(num2str(rpm(ii)),' RPM')};
    rpm_count =
annotation('textbox',dim,'String',rpmstr);
    rpm_count.FontSize = 30;
    rpm_count.EdgeColor = 'k';
    rpm_count.BackgroundColor = 'w';
    rpm_count.VerticalAlignment = 'Middle';
    rpm_count.HorizontalAlignment = 'Center';
```

```
    F(ii) = getframe(f2);
    last_frame = F(ii);
    close all
end

%SAVE to AVI
v = VideoWriter('SBNLoss_Congfig1.avi','Uncompressed
AVI');
v.FrameRate = 10;
open(v)
writeVideo(v,F);
close(v)
```

F.2.2 Sort_SBN_Data function

```
function [SBN] = Sort_SBN_Data(data)
%This function sorts the raw input LMS Test.Lab data
into usable variables
%for Run number kk

%Force
for kk = 4 % Input Run Number
    for ii = 1:5
        RunNum = (strcat('Run',num2str(kk)));
        OrderNum = (strcat('Order',num2str(9*ii)));

        Fx.(RunNum).Mnt710(:,ii) =
data.(RunNum).DF.(OrderNum).OrderSection.y_values.value
s(:,1);
        Fy.(RunNum).Mnt710(:,ii)  =
data.(RunNum).DF.(OrderNum).OrderSection.y_values.value
s(:,2);
        Fz.(RunNum).Mnt710(:,ii)  = -
(data.(RunNum).DF.(OrderNum).OrderSection.y_values.valu
es(:,3));

        Fx.(RunNum).Mnt1442(:,ii) =
data.(RunNum).DF.(OrderNum).OrderSection.y_values.value
s(:,4);
```

```
        Fy.(RunNum).Mnt1442(:,ii)  =
data.(RunNum).DF.(OrderNum).OrderSection.y_values.value
s(:,5);
        Fz.(RunNum).Mnt1442(:,ii)  = -
(data.(RunNum).DF.(OrderNum).OrderSection.y_values.valu
es(:,6));

        Fx.(RunNum).Mnt2130(:,ii) =
data.(RunNum).DF.(OrderNum).OrderSection.y_values.value
s(:,7);
        Fy.(RunNum).Mnt2130(:,ii)  =
data.(RunNum).DF.(OrderNum).OrderSection.y_values.value
s(:,8);
        Fz.(RunNum).Mnt2130(:,ii)  = -
(data.(RunNum).DF.(OrderNum).OrderSection.y_values.valu
es(:,9));
    end
end


%Velocity
for kk = 4
    for ii = 1:5
        RunNum = (strcat('Run',num2str(kk)));
        OrderNum = (strcat('Order',num2str(9*ii)));

        Vx.(RunNum).Mnt710(:,ii) =
data.(RunNum).Vel.(OrderNum).OrderSection.y_values.valu
es(:,1);
        Vy.(RunNum).Mnt710(:,ii)  =
data.(RunNum).Vel.(OrderNum).OrderSection.y_values.valu
es(:,2);
        Vz.(RunNum).Mnt710(:,ii)  =
data.(RunNum).Vel.(OrderNum).OrderSection.y_values.valu
es(:,3);

        Vx.(RunNum).Mnt1442(:,ii) =
data.(RunNum).Vel.(OrderNum).OrderSection.y_values.valu
es(:,4);
        Vy.(RunNum).Mnt1442(:,ii)  =
data.(RunNum).Vel.(OrderNum).OrderSection.y_values.valu
es(:,5);
```

```
        Vz.(RunNum).Mnt1442(:,ii)  =
data.(RunNum).Vel.(OrderNum).OrderSection.y_values.valu
es(:,6);

        Vx.(RunNum).Mnt2130(:,ii) =
data.(RunNum).Vel.(OrderNum).OrderSection.y_values.valu
es(:,7);
        Vy.(RunNum).Mnt2130(:,ii)  =
data.(RunNum).Vel.(OrderNum).OrderSection.y_values.valu
es(:,8);
        Vz.(RunNum).Mnt2130(:,ii)  =
data.(RunNum).Vel.(OrderNum).OrderSection.y_values.valu
es(:,9);
    end
end

Fr.Run4.Mnt710 =
sqrt(Fx.Run4.Mnt710.^2+Fy.Run4.Mnt710.^2+Fz.Run4.Mnt710
.^2);
Fr.Run4.Mnt1442 =
sqrt(Fx.Run4.Mnt1442.^2+Fy.Run4.Mnt1442.^2+Fz.Run4.Mnt1
442.^2);
Fr.Run4.Mnt2130 =
sqrt(Fx.Run4.Mnt2130.^2+Fy.Run4.Mnt2130.^2+Fz.Run4.Mnt2
130.^2);

Vr.Run4.Mnt710 =
sqrt(Vx.Run4.Mnt710.^2+Vy.Run4.Mnt710.^2+Vz.Run4.Mnt710
.^2);
Vr.Run4.Mnt1442 =
sqrt(Vx.Run4.Mnt1442.^2+Vy.Run4.Mnt1442.^2+Vz.Run4.Mnt1
442.^2);
Vr.Run4.Mnt2130 =
sqrt(Vx.Run4.Mnt2130.^2+Vy.Run4.Mnt2130.^2+Vz.Run4.Mnt2
130.^2);

SBN.Run4.Mnt710 = Fr.Run4.Mnt710.*Vr.Run4.Mnt710;
SBN.Run4.Mnt1442 = Fr.Run4.Mnt1442.*Vr.Run4.Mnt1442;
SBN.Run4.Mnt2130 = Fr.Run4.Mnt2130.*Vr.Run4.Mnt2130;
```

F.3 FRF using Modal Expansion and Order Synthesis

Order Based Modal Analysis should be performed in LMS Test.Lab. The OBMA results are input into 4 sheets of an excel file in a pre-processing routine as shown. The first sheet is for the mode shapes for all modes extracted using OBMA. Column A shows the numeric distance from the pump outlet of the measurement point. Column B shows the measurement point name. Column C shows the real part of the MODE 1 shape and Column D shows the imaginary part of the MODE 1 shape. The remaining OBMA mode shapes are formatted in the same way as Column C and D in successive columns. Row 1 is used for table headers and Column A should be sorted smallest to largest. This should be done for each order processed using OBMA. This information is found by right-clicking on OBMA processing folder and navigating to properties.

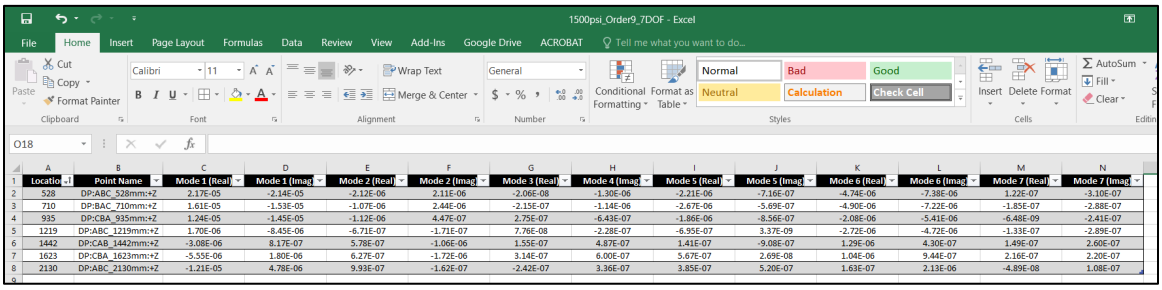

Locatio	Point Name	Mode 1 (Real)	Mode 1 (Imag)	Mode 2 (Real)	Mode 2 (Imag)	Mode 3 (Real)	Mode 4 (Imag	Mode 5 (Real	Mode 5 (Imag	Mode 6 (Real)	Mode 6 (Imag	Mode 7 (Real)	Mode 7 (Imag
528	DP:ABC_528mm:+Z	2.17E-05	-2.14E-05	-2.12E-06	2.11E-06	-2.06E-08	-1.30E-06	-2.21E-06	-7.16E-07	-4.74E-06	-7.38E-06	1.22E-07	-3.10E-07
710	DP:BAC_710mm:+Z	1.61E-05	-1.53E-05	-1.07E-06	2.44E-06	-2.15E-07	-1.14E-06	-2.67E-06	-5.69E-07	-4.90E-06	-7.22E-06	-1.85E-07	-2.88E-07
935	DP:CBA_935mm:+Z	1.24E-05	-1.45E-05	-1.12E-06	4.47E-07	2.75E-07	-6.43E-07	-1.86E-06	-8.56E-07	-2.08E-06	-5.41E-06	-6.48E-09	-2.41E-07
1219	DP:ABC_1219mm:+Z	1.70E-06	-8.45E-06	-6.71E-07	-1.71E-07	7.76E-08	-2.28E-07	-6.95E-07	3.37E-09	-2.72E-06	-4.72E-06	-1.33E-07	-2.89E-07
1442	DP:CAB_1442mm:+Z	-3.08E-06	8.17E-07	5.78E-07	-1.06E-06	1.55E-07	4.87E-07	1.41E-07	-9.08E-07	1.29E-06	4.30E-07	1.49E-07	2.60E-07
1623	DP:CBA_1623mm:+Z	-5.55E-06	1.80E-06	6.27E-07	-1.72E-06	3.14E-07	6.00E-07	5.67E-07	2.69E-08	1.04E-06	9.44E-07	2.16E-07	2.20E-07
2130	DP:ABC_2130mm:+Z	-1.21E-05	4.78E-06	9.93E-07	-1.62E-07	-2.42E-07	3.36E-07	3.85E-07	5.20E-07	1.63E-07	2.13E-06	-4.89E-08	1.08E-07

Figure 73: Sheet 1 OBMA Excel File Pre-Processing

Sheet 2 is for the complex reference factors formatted identically to Sheet 1. There should a reference factor for each mode for all reference locations. The pump outlet (0mm) was the reference location for the OBMA processing in this project.

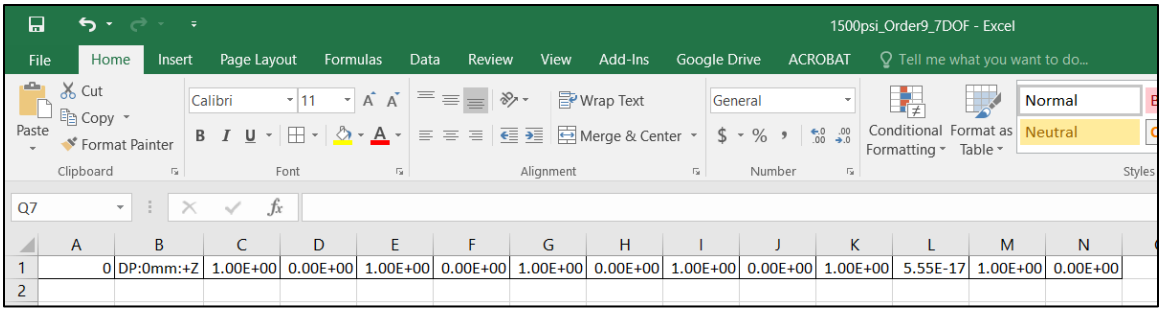

	A	B	C	D	E	F	G	H	I	J	K	L	M	N
1	0	DP:0mm:+Z	1.00E+00	0.00E+00	1.00E+00	0.00E+00	1.00E+00	0.00E+00	1.00E+00	0.00E+00	1.00E+00	5.55E-17	1.00E+00	0.00E+00
2														

Figure 74: Sheet 2 OBMA Excel File Pre-Processing

Sheet 3 Column A and Column B are identical to Sheet 1. Column C and Column D are the real and imaginary parts of the lower residual. Column E and Column F are the real and imaginary parts of the upper residual. It is important that Column A is sorted smallest to largest.

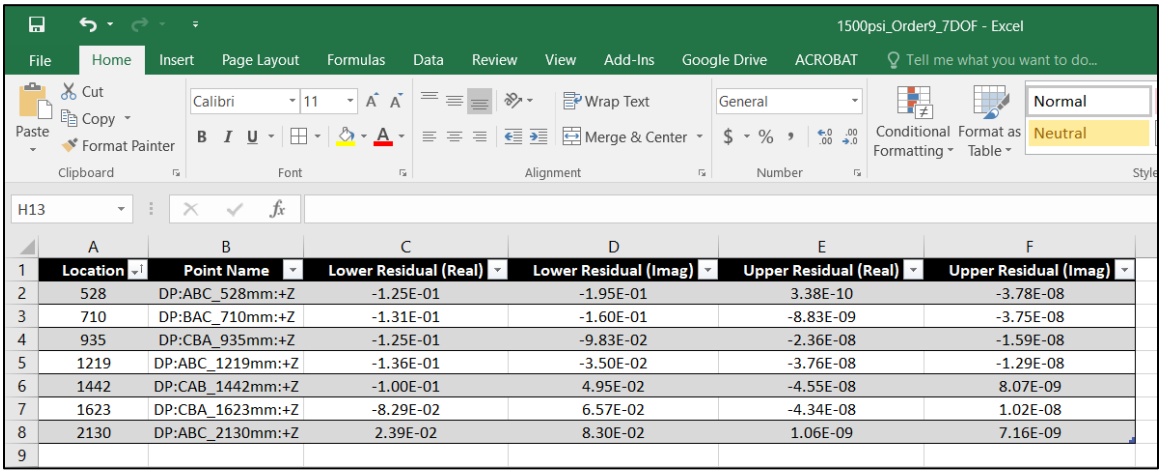

	A	B	C	D	E	F
1	Location	Point Name	Lower Residual (Real)	Lower Residual (Imag)	Upper Residual (Real)	Upper Residual (Imag)
2	528	DP:ABC_528mm:+Z	-1.25E-01	-1.95E-01	3.38E-10	-3.78E-08
3	710	DP:BAC_710mm:+Z	-1.31E-01	-1.60E-01	-8.83E-09	-3.75E-08
4	935	DP:CBA_935mm:+Z	-1.25E-01	-9.83E-02	-2.36E-08	-1.59E-08
5	1219	DP:ABC_1219mm:+Z	-1.36E-01	-3.50E-02	-3.76E-08	-1.29E-08
6	1442	DP:CAB_1442mm:+Z	-1.00E-01	4.95E-02	-4.55E-08	8.07E-09
7	1623	DP:CBA_1623mm:+Z	-8.29E-02	6.57E-02	-4.34E-08	1.02E-08
8	2130	DP:ABC_2130mm:+Z	2.39E-02	8.30E-02	1.06E-09	7.16E-09
9						

Figure 75: Sheet 3 OBMA Excel File Pre-Processing

Right click on the OBMA processing in LMS Test.Lab and navigate to the properties tab. Select ALL properties and copy and paste into cell A1 of sheet 4. It is important that the real part is in column M and the imaginary part is in Column L. Deleting the text so that Column M and L are numeric is necessary.

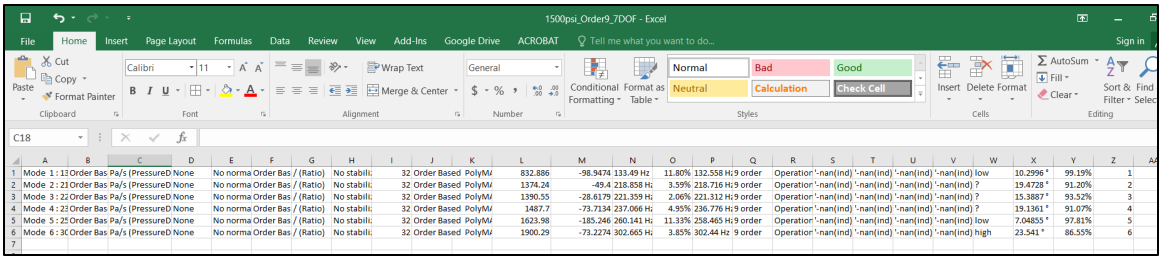

Figure 76: Sheet 4 OBMA Excel File Pre-Processing

The desired location for modal expansion is input as the exp_loc variable. The motor speed range for each order section should be updated appropriately. Only the 9th and 18th order FRF's were processed using this technique.

F.3.1 Modal Expansion FRF Processing

```
%Ben Kolb
%Dynamic Pressure at Expanded locations
% Requires modparam function, Expandshapes function,
SynthOrders function

clc
clear
close all

for jj = 1:2
%%%%%%%%%%%%%%%%%%%%%%%%%%%%%%%%%%%%%%%%%%%%%%%%%%%%%%%%%%%%
%%%%%%%%%%%%%%%%%%%%%%%%%%%%%%%%%%%%%%%%%%%%%%%%%%%%%%%%%%%%
%Exported Modal Data from LMS Test.Lab Order Bassed
Modal Analysis
    filename = '1500psi_Order9_7DOF.xlsx';
    if jj ==1
        filename = '1500psi_Order9_7DOF.xlsx';
        order = 9;
    else
        filename = '1500psi_Order18_7DOF.xlsx';
        order = 18;
    end
%INPUT the desired expansion location in terms of
distance from the pump outlet
```

```
    exp_loc = 1079;
%%%%%%%%%%%%%%%%%%%%%%%%%%%%%%%%%%%%%%%%%%%%%%%%%%%%%%%%%%%%
%%%%%%%%%%%%%%%%%%%%%%%%%%%%%%%%%%%%%%%%%%%%%%%%%%%%%%%%%%%%

%modparam function loads modal data from formatted
excel files
[shape,Ua,ref,pole,resid,master_dof] =
modparam(filename);

%Expandshapes function expands the mode shapes
[Un,T,LRn,URn,exp_dof] =
ExpandShapes(Ua,master_dof,exp_loc,resid);
%
%SynthOrders function sythesizes the orders using
expanded data sets
[SynthOrd,rpm,f] =
SynthOrders(Un,ref,pole,LRn,URn,order);
SO.(strcat('Order',num2str(order))) = SynthOrd(:,end);

%Plot Shapes
% [fig] = plotshapes(exp_dof,Un,order,U_7DOF);

%Generate the FRFs referencing measured pump outlet
pressure data
Meas_P0 = load('Measured_1500psi_P0.mat');
Meas_P0 = Meas_P0.OrderSection.y_values.values;

Pi = SynthOrd(:,end);
Pj = Meas_P0(:,1);
SynthFRF(:,jj) = Pi.*conj(Pj)./(Pj.*conj(Pj));
end

%Plotting Synthesized Orders
fig2 = figure(2);
semilogy(rpm/60*9,abs(SO.Order9),':b','Linewidth',2)
hold on
semilogy(rpm/60*18,abs(SO.Order18),':r','Linewidth',2)
legend('Synthesized 9th Order','Synthesized 18th
Order','Location','southoutside');
xlabel('Motor Speed (RPM)')
ylabel('Pressure (Pa)')
```

```
%Plotting FRF's from Synthesized Orders
fig3 = figure(3);
semilogy(rpm,abs(SynthFRF(:,1)),':b','LineWidth',2)
hold on
semilogy(rpm,abs(SynthFRF(:,2)),':r','LineWidth',2)
xlabel('Frequency (Hz)')
ylabel('Mag FRF (/)')
title(strcat('1500 psi :',num2str(exp_loc),'mm'))
legend('Synthesized 9th Order FRF','Synthesized 18th
Order FRF')

%Store and save FRF data in one variable
SynthFRF_Orders(:,1) = SynthFRF(:,1);
SynthFRF_Orders(:,2) = SynthFRF(:,2);
save('SynthFRF_1079mm','SynthFRF_Orders')
```

F.3.2 modparam function

```
function [shape,Ua,ref,pole,resid,master_dof] =
modparam(filename)
%THis function sorts the excel formatted shape data
into usable modal
%parameter variables for modal expansion processing

shape_data = xlsread(filename,1);
ref_data = xlsread(filename,2);
resid_data = xlsread(filename,3);
properties = xlsread(filename,4);

master_dof = shape_data(:,1);
shape_data = shape_data(:,3:end);
ref_data = ref_data(:,3:end);
resid_data = resid_data(:,3-1:end);

for ii = 1:size(shape_data,2)/2
    n = 2*ii-1;
    shape.(strcat('mode',num2str(ii))) =
shape_data(:,n) + 1j*shape_data(:,n+1);
    Ua(:,ii) = shape.(strcat('mode',num2str(ii)));
    ref(:,ii) =  ref_data(:,n) + 1j*ref_data(:,n+1);
```

```
    pole(:,ii) =  properties(ii,5) +
1j*properties(ii,4);
end
    resid.lower =  resid_data(:,2) +
1j*resid_data(:,3);
    resid.upper =  resid_data(:,4) +
1j*resid_data(:,5);
end
```

F.3.3 ExpandShapes function

```
function [Un,T,LRn,URn,exp_dof] =
ExpandShapes(Ua,master_dof,exp_loc,resid)
% This function interpolates the expanded locations
into the mode shapes, formulates the SEREP
%transformation matrix and expands the residuals

exp_dof = vertcat(master_dof,exp_loc);

for ii = 1:size(Ua,2)
    exp_shape =
interp1(master_dof,Ua(:,ii),exp_loc,'pchip');
    Un(:,ii) = vertcat(Ua(:,ii),exp_shape);
end

T = Un * pinv(Ua);

LRn = T*resid.lower;
URn = T*resid.upper;
```

F.3.4 SynthOrders function

```
function [SynthOrd,rpm,f] =
SynthOrders(Un,ref,pole,LRn,URn,order)
%This function synthesizes the orders from the expanded
modal parameters

rpm = 800:5:2345;
f = rpm./60*order;
w = 2*pi*f;
total = 0;
```

```
for ii = 1:size(Un,2)
part.(strcat('mode',num2str(ii))) =
Un(:,ii).*ref(:,ii)./(1j*w - pole(:,ii)) ...
    + conj(Un(:,ii)).*conj(ref(:,ii))./(1j*w -
conj(pole(:,ii)));
total = total + part.(strcat('mode',num2str(ii)));
end
Y = (1j*w).^4.*(total + LRn./(1j*w).^2 + URn);
SynthOrd = Y';
end
```

F.4 Energy Balancing

Energy balance processing requires the source flow ripple, measured outlet dynamic pressure, measured dynamic force and integrated measured acceleration from each of the first 5 order sections in separate .MAT files. A .mat file for the FRF generated using either equation (12) or the modal expansion processing is also required. A sortdata function reformats the raw imported .MAT files into usable variables and a Noise_Metrics function processes the variables into FBN, SBN and energy balance results.

F.4.1 Energy Balance Processing

```
clc
clear
close all

%Load Flow Ripple Order Sections
%UNITS: m^3/s
data.Qs.O9 = load('Qs_1500psi_Order9.mat');
data.Qs.O18 = load('Qs_1500psi_Order18.mat');
data.Qs.O27 = load('Qs_1500psi_Order27.mat');
data.Qs.O36 = load('Qs_1500psi_Order36.mat');
data.Qs.O45 = load('Qs_1500psi_Order45.mat');

%Load Measured FRF's for 710 mm and 1442 mm
%UNITS: Pa/Pa
```

```
data.MFRF.Mnt710 = load('FRF_710mm_BAC.mat');
data.MFRF.Mnt1442 = load('FRF_1442mm_CAB.mat');

% Load Pump Outlet Pressure
%UNITS: Pa
%Note: Data was collected with the wrong sensitvity,
the appropriate
%correction factor was applied
data.P0.Mnt710and1442.data =
load('DP_P0_710and1442.mat');

% Load Force Components At Mounts
%UNITS: N
data.Fx.Mnt710 = load('DF_710mm_X.mat');
data.Fy.Mnt710 = load('DF_710mm_Y.mat');
data.Fz.Mnt710 = load('DF_710mm_Z.mat');

data.Fx.Mnt1442 = load('DF_1442mm_X.mat');
data.Fy.Mnt1442 = load('DF_1442mm_Y.mat');
data.Fz.Mnt1442 = load('DF_1442mm_Z.mat');

% Load Velocity Components at Mounts
%Units: m/s
data.Vx.Mnt710 = load('Vel_710mm_X.mat');
data.Vy.Mnt710 = load('Vel_710mm_Y.mat');
data.Vz.Mnt710 = load('Vel_710mm_Z.mat');

data.Vx.Mnt1442 = load('Vel_1442mm_X.mat');
data.Vy.Mnt1442 = load('Vel_1442mm_Y.mat');
data.Vz.Mnt1442 = load('Vel_1442mm_Z.mat');

%Sort loaded data into Source Flow Ripple, FRFs, Outlet
pressures and mount
%forces and velocities
[Qs,MFRF,P0,Fx,Fy,Fz,Fr,Vx,Vy,Vz,Vr] = sortdata(data);

for ii = 1:2
PA.Mnt710(:,ii) =
P0.Mnt710Mnt1442(:,ii).*MFRF.Mnt710(:,ii).*0.0001979326
09;
```

```
PA.Mnt1442(:,ii) =
P0.Mnt710Mnt1442(:,ii).*MFRF.Mnt1442(:,ii).*0.000197932
609;
end

rpm = 800:5:2315;
%Solve for Source FBN, Local FBN and SBN, Energy
Balance and Force and
%Energy Transfer Functions
[FBNs,FBN,SBN,EB,FTF,ETF] =
Noise_Metrics(Qs,MFRF,P0,Fr,Vr);

%%

Mount1.Config1 = abs(sum(SBN.Mnt710,2));
Mount2.Config1 = abs(sum(SBN.Mnt1442,2));

EBCurve1 =
abs(sum(Qs(:,1:5),2).*sum(P0.Mnt710Mnt1442(:,1:5),2)) -
abs(sum(SBN.Mnt710(:,1:5),2));
EBCurve2 =
abs(sum(Qs(:,1:5),2).*sum(P0.Mnt710Mnt1442(:,1:5),2)) -
abs(sum(SBN.Mnt710(:,1:5),2)-
sum(SBN.Mnt1442(:,1:5),2));
FBNCurve1 =
sum(Qs(:,1:5),2).*((MFRF.Mnt710(:,1).*P0.Mnt710Mnt1442(
:,1)+MFRF.Mnt710(:,2).*P0.Mnt710Mnt1442(:,2)+MFRF.Mnt71
0(:,3).*P0.Mnt710Mnt1442(:,3)+MFRF.Mnt710(:,4).*P0.Mnt7
10Mnt1442(:,4)+MFRF.Mnt710(:,5).*P0.Mnt710Mnt1442(:,5))
);
FBNCurve2 =
sum(Qs(:,1:5),2).*((MFRF.Mnt1442(:,1).*P0.Mnt710Mnt1442
(:,1)+MFRF.Mnt1442(:,2).*P0.Mnt710Mnt1442(:,2)+MFRF.Mnt
1442(:,3).*P0.Mnt710Mnt1442(:,3)+MFRF.Mnt1442(:,4).*P0.
Mnt710Mnt1442(:,4)+MFRF.Mnt1442(:,5).*P0.Mnt710Mnt1442(
:,5)));
FBNs_Mnt710Mnt1442 =
sum(Qs(:,1:5),2).*sum(P0.Mnt710Mnt1442(:,1:5),2);

f3 = figure(3);
plot(rpm,abs(FBNs_Mnt710Mnt1442),'r','LineWidth',2)
hold on
```

```
plot(rpm,abs(FBNCurve1),'b','LineWidth',2)
plot(rpm,EBCurve1,'--k','LineWidth',2)
legend('Source FBN','FBN Prediction: Mount 1','Energy
Balance: Mount 1','Location','NorthWest')
axis([800 2340 0 60])
xlabel('Motor Speed (RPM)')
ylabel('Power (Watts)')
set(gca,'FontSize',20);
set(f3,'Position',[1,1,1128.8,308.8])

f4 = figure(4);

plot(rpm,abs(FBNs_Mnt710Mnt1442),'r','LineWidth',2)
hold on
plot(rpm,abs(FBNCurve2),'b','LineWidth',2)
plot(rpm,EBCurve2,'--k','LineWidth',2)

legend('Source FBN','FBN Prediction: Mount 2','Energy
Balance: Mount 2','Location','NorthWest')
axis([800 2340 0 60])
xlabel('Motor Speed (RPM)')
ylabel('Power (Watts)')
set(gca,'FontSize',20);
set(f4,'Position',[1,1,1128.8,308.8])
```

F.4.2 sortdata function

```
function [Qs,MFRF,P0,Fx,Fy,Fz,Fr,Vx,Vy,Vz,Vr] =
sortdata(data)

% This function takes the raw import order sections
from LMS Test.Lab and
% reformats to usable MATLAB variables

%Flow ripple dataconverted from liters/sec to m^3/s
Qs(:,1) = data.Qs.O9.Section(1:304)'/1000;
Qs(:,2) = data.Qs.O18.Section(1:304)'/1000;
Qs(:,3) = data.Qs.O27.Section(1:304)'/1000;
Qs(:,4) = data.Qs.O36.Section(1:304)'/1000;
Qs(:,5) = data.Qs.O45.Section(1:304)'/1000;
```

```
%Formatting measured FRF order sections from data
import
MFRF.Mnt710 =
data.MFRF.Mnt710.OrderSection.y_values.values(1:304,:);
MFRF.Mnt1442 =
data.MFRF.Mnt1442.OrderSection.y_values.values(1:304,:)
;

%Formatting measured outlet pressure order sections
from data import
P0.Mnt710Mnt1442 =
data.P0.Mnt710and1442.data.OrderSection.y_values.values
(1:304,:)*(0.1/(1.46778*10^-7));

%Sorting force and velocity data from data import and
forumulating
%resultant Fr and Vr
Fx.Mnt710 =
data.Fx.Mnt710.OrderSection.y_values.values(1:304,:);
Fy.Mnt710 =
data.Fy.Mnt710.OrderSection.y_values.values(1:304,:);
Fz.Mnt710 = -
(data.Fz.Mnt710.OrderSection.y_values.values(1:304,:));
%Data Collected in -Z

Fx.Mnt1442 =
data.Fx.Mnt1442.OrderSection.y_values.values(1:304,:);
Fy.Mnt1442 =
data.Fy.Mnt1442.OrderSection.y_values.values(1:304,:);
Fz.Mnt1442 = -
(data.Fz.Mnt1442.OrderSection.y_values.values(1:304,:))
; %Data Collected in -Z

Vx.Mnt710 =
data.Vx.Mnt710.OrderSection.y_values.values(1:304,:);
Vy.Mnt710 =
data.Vy.Mnt710.OrderSection.y_values.values(1:304,:);
Vz.Mnt710 =
data.Vz.Mnt710.OrderSection.y_values.values(1:304,:);

Vx.Mnt1442 =
data.Vx.Mnt1442.OrderSection.y_values.values(1:304,:);
```

```
Vy.Mnt1442 =
data.Vy.Mnt1442.OrderSection.y_values.values(1:304,:);
Vz.Mnt1442 =
data.Vz.Mnt1442.OrderSection.y_values.values(1:304,:);

Fr.Mnt710 = sqrt(Fx.Mnt710.^2 + Fy.Mnt710.^2 +
Fz.Mnt710.^2);
Fr.Mnt1442 = sqrt(Fx.Mnt1442.^2 + Fy.Mnt1442.^2 +
Fz.Mnt1442.^2);

Vr.Mnt710 = sqrt(Vx.Mnt710.^2 + Vy.Mnt710.^2 +
Vz.Mnt710.^2);
Vr.Mnt1442 = sqrt(Vx.Mnt1442.^2 + Vy.Mnt1442.^2 +
Vz.Mnt1442.^2);

end
```

F.4.3 Noise_Metrics Function

```
function [FBNs,FBN,SBN,EB,PA,FTF,ETF] =
Noise_Metrics(Qs,MFRF,P0,Fr,Vr)

%This function outputs Source FBN, Local FBN, Measured
SBN and Energy
%balance at each mount from the date sorted with the
sortdata function.
%Additionally the "fluid force" (mount pressure ripple
* cross sectional area), a force
%transfer function and an energy transfer function are
computed.

%Source Fluidborne Noise
for ii = 1:5
FBNs.Mnt710Mnt1442(:,ii) =
Qs(:,ii).*P0.Mnt710Mnt1442(:,ii);
end

%Local Mount Fluidborne Noise @ 710mm and @ 1442 mm
for ii = 1:2
FBN.Mnt710(:,ii) =
Qs(:,ii).*MFRF.Mnt710(:,ii).*P0.Mnt710Mnt1442(:,ii);
```

```
FBN.Mnt1442(:,ii) =
Qs(:,ii).*MFRF.Mnt1442(:,ii).*P0.Mnt710Mnt1442(:,ii);
end

%Local Structureborne Noise @ 710mm and @ 1442 mm
SBN.Mnt710 = Fr.Mnt710.*Vr.Mnt710;
SBN.Mnt1442 = Fr.Mnt1442.*Vr.Mnt1442;

%Energy Balance Methode Results @ 710mm and @ 1442 mm
for ii = 1:5
EB.Mnt710(:,ii) = FBNs.Mnt710Mnt1442(:,ii) -
SBN.Mnt710(:,ii);
EB.Mnt1442(:,ii) = FBNs.Mnt710Mnt1442(:,ii) -
SBN.Mnt710(:,ii) - SBN.Mnt1442(:,ii);
end

%Fluid Force  @ 710mm and @ 1442 mm
for ii = 1:2
PA.Mnt710(:,ii) =
.3067.*MFRF.Mnt710(:,ii).*P0.Mnt710Mnt1442(:,ii);
PA.Mnt1442(:,ii) =
.3067.*MFRF.Mnt1442(:,ii).*P0.Mnt710Mnt1442(:,ii);
end

% %Force and Energy Transfer Functions @ 710mm and @
1442 mm
 loc = [710,1442];
%
for ii = 1:2
    for kk = 1:2
        Gxf =
Fr.(strcat('Mnt',num2str(loc(kk))))(:,ii).*conj(PA.(str
cat('Mnt',num2str(loc(kk))))(:,ii));
        Gff =
PA.(strcat('Mnt',num2str(loc(kk))))(:,ii).*conj(PA.(str
cat('Mnt',num2str(loc(kk))))(:,ii));
        FTF.(strcat('Mnt',num2str(loc(kk))))(:,ii) =
Gxf./Gff;

        Gxf =
SBN.(strcat('Mnt',num2str(loc(kk))))(:,ii).*conj(FBN.(s
trcat('Mnt',num2str(loc(kk))))(:,ii));
```

```
        Gff =
FBN.(strcat('Mnt',num2str(loc(kk))))(:,ii).*conj(FBN.(s
trcat('Mnt',num2str(loc(kk))))(:,ii));
        ETF.(strcat('Mnt',num2str(loc(kk))))(:,ii) =
Gxf./Gff;
    end

end

end
```

G Copyright documentation

Michigan Tech

Ben Kolb <bskolb@mtu.edu>

Permissions Link Fix: Proc Instn Mech Engrs Vol 212, Issue 4
4 messages

Ben Kolb <bskolb@mtu.edu> Mon, Jan 14, 2019 at 11:59 AM
To: permissions@sagepub.com

Hello,

I am looking to receive permission to use Figure 1 in "A method to reduce noise in hydraulic systems by optimizing pipe clamp locations" by A H MKwong* and K A Edge. This figure is in Proceedings of the Institution of Mechanical Engineers Vol 212, Issue 4, 1998. This figure would be printed in my master's thesis at Michigan Technological University. The link to request permissions appears to be broken for this article. Could you please advise a fix or alternative?

Thank you and I look forward to hearing from you,

--
Ben Kolb
Michigan Technological University
Mechanical Engineering Graduate Research Assistant
M: (920) 676-1328

PermissionsUK <PermissionsUK@sagepub.com> Mon, Jan 14, 2019 at 2:14 PM
To: Ben Kolb <bskolb@mtu.edu>

Dear Ben Kolb,

Thank you for your email. I am pleased to report we can grant your request without a fee as part of your thesis.

Please accept this email as permission for your request as detailed below. Permission is granted for the life of the edition on a non-exclusive basis, in the English language, throughout the world in all formats provided full citation is made to the original SAGE publication.

The permission is subject to approval from any co-authors on the original project. Please note approval excludes any graphs, photos, excerpts, etc. which required permission from a separate copyright holder at the time of publication. If your material includes anything which was not your original work, please contact the rights holder for permission to reuse those items.

If you have any questions, or if we may be of further assistance, please let us know.

Best Wishes,

Craig Myles

on behalf of **SAGE Ltd. Permissions Team**

SAGE Publications Ltd

1 Oliver's Yard, 55 City Road

London, EC1Y 1SP

UK

www.sagepub.co.uk

From: Ben Kolb <bskolb@mtu.edu>
Sent: Monday, January 14, 2019 9:00 AM
To: permissions (US) <permissions@sagepub.com>
Subject: Permissions Link Fix: Proc Instn Mech Engrs Vol 212, Issue 4

[Quoted text hidden]

Ben Kolb <bskolb@mtu.edu> Mon, Jan 14, 2019 at 2:42 PM
To: PermissionsUK <PermissionsUK@sagepub.com>

Thank you Craig,

Could you also advise on permissions for Figure 1 in "Pressure pulsations in reciprocating pump piping systems. Part 2: experimental investigations and model validation" by Kevin Edge? This article is in Proceedings of the Institution of Mechanical Engineers Vol 211, Issue 3, 1997. This figure would also be printed in my master's thesis at Michigan Technological University.

Thank you,
Ben Kolb
[Quoted text hidden]

PermissionsUK <PermissionsUK@sagepub.com> Mon, Jan 14, 2019 at 2:44 PM
To: Ben Kolb <bskolb@mtu.edu>

Dear Ben,

Thank you for your reply, and we are happy to grant you permission for the reuse of Figure 1 from "Pressure pulsations in reciprocating pump piping systems. Part 2: experimental investigations and model validation" free-of-charge for reuse in your thesis, as well.

Please accept this email as permission for your request as detailed below. Permission is granted for the life of the edition on a non-exclusive basis, in the English language, throughout the world in all formats provided full citation is made to the original SAGE publication.

As a courtesy, we ask that you contact the author to let them know the content will be republished. Please note this approval excludes any content which requires additional permission from a separate copyright holder. If the SAGE material includes anything not '© the Author' or '© SAGE', please contact the rights holder for permission to reuse those items.

Best Wishes,

Craig Myles

on behalf of **SAGE Ltd. Permissions Team**

SAGE Publications Ltd

1 Oliver's Yard, 55 City Road

London, EC1Y 1SP

UK

www.sagepub.co.uk

From: Ben Kolb <bskolb@mtu.edu>
Sent: Monday, January 14, 2019 11:42 AM
To: PermissionsUK <PermissionsUK@sagepub.com>
Subject: Re: Permissions Link Fix: Proc Instn Mech Engrs Vol 212, Issue 4

[Quoted text hidden]